Philipps Universität Marburg

# Analysis of the Host Stress Response to Ebola Virus Infection and Generation of a Recombinant Marburg Virus Expressing EGFP to Study Viral Spread

**Dissertation zur Erlangung des**
**Doktorgrades der Naturwissenschaften**
**(Dr. rer. nat.)**


dem Fachbereich Biologie
der Philipps-Universität Marburg
vorgelegt von
**Kristina Maria Schmidt**
aus Haan
Marburg/Lahn, 2012

Vom Fachbereich Biologie der Philipps-Universität Marburg als Dissertation am _____ angenommen.

**Erstgutachter:** Prof. Dr. Renate Renkawitz-Pohl

**Zweitgutachter:** Prof. Dr. Elke Mühlberger

Tag der mündlichen Prüfung am _____ .

# Table of Contents

# 1. Zusammenfassung

Die hoch pathogenen Filoviren Ebola- (EBOV) und Marburg-Virus (MARV) sind Erreger eines hämorrhagisches Fiebers mit Lethalitätsraten von bis zu 90%. Bislang sind weder spezifische antivirale Medikamente noch eine Impfung für den Einsatz am Menschen verfügbar. Die hohe Sterblichkeitsrate sowie die fehlende Therapie und Prophylaxe bedingen, dass Filoviren als Erreger der höchsten biologischen Sicherheitsstufe (4) klassifiziert werden und somit eine Erforschung nur in Hochsicherheitslaboratorien erlaubt ist.

**Herstellung eines rekombinanten Marburg-Virus mit Fluoreszenzmarker**

Ziel dieses Projekts war die Herstellung eines rekombinanten MARV, welches das „enhanced green fluorescence protein“ (EGFP)-Gen von einer zusätzlichen, in das virale Genom eingefügten Transkriptionseinheit exprimiert. Viren, die fluoreszierende Proteine exprimieren, erleichtern die Untersuchung des viralen Vermehrungszyklus und sind wertvolle Hilfsmittel für das „Screenen“ von potentiellen antiviralen Medikamenten. Das EGFP-Gen wurde zwischen dem zweiten Gen des MARV-Genoms, dem VP35-Gen, und dem nachfolgenden VP40-Gen eingefügt. Das rekombinante Virus (rMARV-EGFP) wurde über ein cDNA-Zwischenprodukt in transfizierten Zellen generiert und anschliessend in „live-cell imaging“ Versuchen eingesetzt. Eine Expression von EGFP wurde 32 Stunden nach Infektion erstmals detektiert und eine Infektion von Nachbarzellen nach 55 Stunden. Im Vergleich zum rekombinanten Wildtyp-MARV wurde ein eingeschränktes virales Wachstum festgestellt. Dies ist wahrscheinlich auf die Insertion einer zusätzlichen Trankriptionseinheit zurückzuführen, da Gene, die hinter dem eingefügten EGFP-Gen liegen, weniger stark exprimiert wurden.

In filoviralen Infektionen können charakteristische virale Einschlusskörper (inclusion bodies) detektiert werden, die sich im Zytoplasma infizierter Zelle bilden. Initiiert wird die Bildung dieser Einchlusskörper durch die Akkumulation des viralen Nukleoproteins (NP). Immunfluoreszenzanalysen von Zellen, die mit rMARV-EGFP infiziert waren, zeigten eine Akkumulation des EGFP in viralen Einschlusskörpern. In Tansfektionsexperimenten wurde die Relokalisierung verschiedener Fluoreszenzproteine in filovirale Einschlusskörper untersucht. Dies zeigte, dass ektopisch exprimierte Fluoreszenzproteine sowohl mit MARV- als auch mit EBOV-spezifischen Einschlusskörpern colokalisierten. Des Weiteren konnte nachgewiesen werden, dass die Expression von NP in der Abwesenheit anderer viraler Proteine ausreichend für die Akkumulation von EGFP in den Einschlusskörpern ist. Im Gegensatz dazu akkumulierten ektopisch exprimierte GFP-Fusionsproteine, die ein zelluläres Lokalisierungssignal besitzen, nicht in MARV-spezifischen Einschlusskörpern. Dies lässt darauf schließen, dass ektopisch exprimierte Proteine unspezifisch in den viralen Einschlusskörpern akkumulieren, wenn sie kein Lokalisierungssignal besitzen. Durch Immunfluoreszenzanalysen konnte zudem gezeigt werden, dass die EGFP-Aggregate zwar durch die Autofluoreszenz detektiert werden konnten, aber nicht in der Antikörperfärbung sichtbar waren. Dies weist darauf hin, dass Antikörper nicht in der Lage sind, virale Einschlusskörper zu durchdringen.

**Die zelluläre Stressantwort in Ebola-Virus Infektion**

Ebola-Viren sind in der Lage, essentielle antivirale Signalwege der Interferon-induzierten Immunantwort zu hemmen. Im Rahmen dieser Arbeit wurde die Interaktion von EBOV mit einem weiteren antiviralen Abwehrmechanismus, der zellulären Stressantwort, untersucht. Exogen

induzierter Stress kann zur Aktivierung vier verschiedener Kinasen führen, die in aktivierter Form die α-Untereinheit des eukaryotischen Initiationsfaktors 2 (eIF2) phosphorylieren. Dies wiederum führt zu einer Hemmung der Proteinsynthese, welche mit der Bildung von cytoplasmatischen „stress granules“(SG) und „processing bodies“ (PB) einhergeht. Viren, die auf den zellulären Proteinsyntheseapparat angewiesen sind, haben vielseitige Abwehrstrategien gegen die zelluläre Stressantwort entwickelt. Im Folgenden wurde untersucht, wie EBOV mit SG und PB interagiert. Aufgrund der dynamischen Struktur von SG und PB wurden vorwiegend mikroskopische Analysen durchgeführt.

Zunächst wurde untersucht, ob filovirale Infektionen eine Stressantwort induzieren. Es konnte gezeigt werden, dass in EBOV-infizierten Zellen keine endogenen SG gebildet werden. Die Behandlung von EBOV-infizierten Zellen mit dem Stressinduktor Natriumarsenit (As) führte zur Bildung von SG, allerdings in einer geringeren Anzahl von infizierten Zellen, verglichen mit nicht infizierten, behandelten Zellen. Die Ergebnisse weisen auf eine Hemmung von SG in mit EBOV infizierten Zellen hin.

Zur besseren Visualisierung von SG wurde für die weiteren Untersuchungen eine Zelllinie verwendet, die das SG-Markerprotein „ras-GAP SH3 domain binding protein 1“ (G3BP) konstitutiv exprimiert. In mit EBOV infizierten, G3BP-exprimierenden Zellen wurden SG mit zwei verschiedenen Toxinen induziert, As und Hippuristanol (Hip). Während As die Phosphorylierung von eIF2α induziert, bewirkt Hip die Hemmung der eIF4A-abhängigen Translationsinitiation, ein Prozess, der unabhängig von der Phosphorylierung von eIF2α zu der Bildung von SG führt. SG-Bildung wurde durch beide Toxine in mit EBOV infizierten Zellen ausgelöst, eine Reduktion wurde allerdings nur für die Bildung von As-induzierten SG in mit EBOV infizierten Zellen beobachtet. Interessanterweise wurden zudem SG-ähnliche G3BP-EGFP-Aggregate in den viralen Einschlusskörpern beobachtet, die sowohl in behandelten als auch in nicht behandelten EBOV-infizierten Zellen auftraten. Es konnte weiterhin durch Transfektionsversuche gezeigt werden, dass die Bildung viraler Einschlusskörper, die durch die Expression von Nukleokapsidproteinen induziert wurde, nicht ausreichend war, um die Aggregation von G3BP-EGFP in den viralen Einschlusskörpern zu bewirken. Dies lässt darauf schließen, dass andere Faktoren, wie beispielsweise virale RNA, benötigt werden, um SG-Komponenten in die viralen Einschlusskörper zu rekrutieren. Diese Ergebnisse weisen auf eine Hemmung der zellulären Stressantwort durch EBOV hin, die auf der Inhibition der Bildung von SG und auf einer Sequestierung essentieller SG-Komponenten beruht.

Zur weiteren Charakterisierung der Inhibition von SG durch EBOV wurden in Transfektionsversuchen die RNA-bindenden EBOV Proteine NP, VP30 und VP35 einzeln exprimiert. Während VP30 mit SG kolokalisierte ohne diese zu beeinträchtigen, wurde für das dsRNA-bindende VP35 eine inhibierende Wirkung auf die Bildung von SG beobachtet. In Zellen, die VP30 oder VP35 gemeinsam mit NP exprimierten, wurden beide Proteine in die von NP induzierten Einschlusskörper rekrutiert, und die Kolokalisation mit SG war entweder stark reduziert oder nicht vorhanden. Dies wurde auch in mit EBOV infizierten Zellen beobachtet. Diese Ergebnisse lassen darauf schließen, dass VP30 und VP35 nur in ungebundener Form mit SG interagieren. Die Menge an freien VP30- und VP35-Proteinen in EBOV-infizierten Zellen ist wahrscheinlich zu gering, um in der Immunfluoreszenzanalyse detektiert zu werden.

Unter As-induzierten Stressbedingungen wird die „dsRNA dependent protein kinase“ (PKR) von dem zellulären Protein „PKR activating protein“ (PACT) aktiviert. Aktivierte PKR phosphoryliert

eIF2α, was zur Bildung von SG führt. Die Aktivierung von PKR durch dsRNA wird von dem EBOV-Protein VP35 effizient inhibiert. Im Rahmen dieser Arbeit konnte gezeigt werden, dass die As-induzierte Aktivierung von PKR nicht von EBOV inhibiert werden kann. Fabrozzi et al. (2011) konnten bereits eine Bindung zwischen VP35 und PACT in nicht gestressten Zellen nachweisen. In dieser Arbeit wurde diese Bindung durch Coimmunpräzipitationsanalysen bestätigt und zudem gezeigt, dass in mit As behandelten Zellen VP35 nicht in der Lage ist an PACT zu binden. Dies könnte eine Bindung von PACT an PKR ermöglichen und damit zu der beobachteten Aktivierung von PKR führen. Die Aktivierung von PKR in mit EBOV infizierten Zellen nach As-Behandlung könnte auch die Bildung von SG in diesen Zellen erklären. Aus der beobachteten Reduktion von As-induzierten SG in EBOV-infizierten Zellen wird geschlossen, dass VP35 SG-Komponenten inhibiert oder relokalisiert. Dies scheint mit der Expressionsrate von VP35 zusammenzuhängen.

Zur weiteren Charakterisierung der zellularen Stressantwort wurde die Rolle von PB in EBOV infizierten Zellen näher untersucht. Hierzu wurde eine Zelllinie verwendet, die das PB-Markerprotein „mRNA-decapping enzyme 1A" (DCP1a) exprimiert. Eine Rekrutierung von As-induzierten PB an die viralen Einschlusskörper, die aber nicht zu einer Kolokalisation führte, konnte in EBOV infizierten Zellen beobachtet werden. Diese wurde auf die von NP initiierte Bildung von Einschlusskörpern zurueckgefuehrt. Expressionsstudien zeigten, dass PB mit VP35 kolokalisierten, aber nicht mit VP30 oder NP. Des Weiteren konnte gezeigt werden, dass in Zellen, in denen es zu einer durch VP35 bedingten Hemmung der SG-Bildung kam, die entstandenen, diffusen G3BP-EGFP-Aggregate nicht nur mit VP35 kolokalisierten, sondern auch mit PB interagierten. Dies weist darauf hin, dass VP35 mit SG- und PB-Komponenten interagiert und diese verbindet.

Zusammengefasst zeigen die Ergebnisse dieser Arbeit, dass EBOV Mechanismen zur Kontrolle der antiviralen zellulären Stressantwort entwickelt hat, in denen VP35 eine wichtige Rolle spielt, da es mit Komponenten von SG und PB interagiert. Des Weiteren scheint die Bindung zwischen VP35 und PACT eine wichtige Rolle in der Kontrolle von PKR zu spielen.

# 2. Summary

Ebola virus (EBOV) and Marburg virus (MARV) belong to the filovirus family and cause outbreaks with case fatality rates up to 90%. Currently there is no approved vaccine or antiviral treatment available. Therefore filoviruses are classified as priority A select agents, which can only be handled in high containment biosafety level 4 laboratories.

**Generation of an infectious Marburg virus clone expressing EGFP**

The generation of recombinant viruses expressing enhanced green fluorescent protein (EGFP) has significantly improved the study of their replication cycle and opened up the possibility for the rapid screening of antiviral drugs. The goal of this part of the work was to generate a recombinant MARV expressing EGFP from an additional transcription unit inserted between the second and third genes, encoding VP35 and VP40, respectively. The recombinant MARV containing the EGFP gene (rMARV-EGFP) was successfully rescued and used in live-cell imaging to follow viral spread in real time, revealing EGFP expression at 32 hours post infection (hpi), and infection of neighboring cells at 55 hpi. A slight growth restriction of rMARV-EGFP compared to the wt rMARV was observed which might be due to the additional gene insertion.

During filovirus infection characteristic viral inclusions are formed in the cytoplasm of infected cells, induced by self-aggregation of the nucleoprotein (NP). Immunofluorescence analysis of rMARV-EGFP-infected cells revealed an accumulation of EGFP in these viral inclusions. This was reproduced by transient expression of both EGFP and other fluorescent proteins (FPs) along with filovirus nucleocapsid proteins, which further showed that NP-induced inclusion formation was sufficient for the recruitment. In contrast, ectopic GFP fusion proteins containing a localization signal were not relocated into inclusions formed by MARV NP and VP35. Taken together, the observed relocalization of ectopically expressed, untagged FPs suggests an unspecific recruitment to the viral inclusions based on a weak interaction. Interestingly, EGFP aggregates observed by autofluorescence were undetected by antibody-based immunofluorescence. This indicates that antibodies might not be able to penetrate viral inclusions.

**Cellular stress response to Ebola virus infection**

EBOV is known to antagonize various antiviral signaling pathways including the interferon response. Here, the interaction of EBOV with another host antiviral defense mechanism, the cellular stress response, was analyzed. During environmental stress a small range of kinases phosphorylate the eukaryotic initiation factor 2α (eIF2α), which plays a central role in the control of translational arrest. Cellular stress is also accompanied by the formation of cytoplasmic stress granules (SGs) and processing bodies (PBs) containing stalled messenger ribonucleoprotein bodies. Since viruses depend on the cellular translation apparatus for viral protein synthesis, many viruses have evolved strategies to antagonize cellular stress response mechanisms. Here we demonstrate that EBOV interferes with the cellular stress response. Since, SGs and PBs are highly dynamic structures, which cannot be isolated from cells, most of the studies presented here were performed by microscopic analysis. Formation of endogenous SGs was not observed in EBOV-infected cells, suggesting that filovirus infection per se does not induce a stress response. This raised the question of whether SG formation is actively inhibited in EBOV-infected cells. The oxidative stressor sodium arsenite (As) induces eIF2α phosphorylation and SG formation. After As-

treatment, SGs formed in EBOV-infected cells, albeit in fewer cells compared to non-infected cells, indicating that EBOV is able to inhibit As-induced SG formation to a certain level.

For better visualization SG formation was further analyzed in U2OS cells expressing an EGFP-tagged SG maker protein, ras-GAP SH3 domain binding protein 1 (G3BP). In EBOV-infected G3BP-EGFP-expressing cells, SG formation was induced by As and Hippuristanol (Hip). Hip leads to SG formation by inhibiting eIF4A-dependent translation initiation, a process, which does not involve phosphorylation of eIF2α. In some EBOV-infected cells treated with As, G3BP-EGFP was diffusely distributed and SG formation was impaired. This was not seen in Hip-treated cells, suggesting that EBOV inhibits SG formation to a certain level in response to phospho-eIF2α-mediated stress. This inhibition seemed to be dependent on the size of the viral inclusions, suggesting that the level of viral protein expression is important for the inhibition.

Intriguingly, G3BP-EGFP SG-like aggregates were observed within the viral inclusions in unstressed and in stressed EBOV-infected cells. Transient expression of viral nucleocapsid proteins leading to inclusion formation was not sufficient for the aggregation of G3BP granules inside the inclusions, suggesting that other viral components, including the viral RNA, are needed to sequester SG components in the inclusions. Together this data suggest a mechanism of EBOV to interfere with SGs by sequestering SG components in the viral inclusions.

To further understand how EBOV interacts with SGs, the EBOV RNA-binding proteins NP, VP30, and VP35 were individually examined for their ability to interact with SGs. While VP30 colocalized with SGs without affecting their structure, the double-strand (ds) RNA-binding protein VP35 inhibited SG formation induced by phospho-eIF2α-mediated stress when expressed at high levels. However, when VP30 and VP35 were coexpressed with NP, both proteins were relocated into NP-derived viral inclusions and colocalization with SGs was strongly reduced or absent, which was also observed in EBOV-infected G3BP-EGFP cells. This indicates that only free VP35 and VP30 are able to colocalize with SGs and that both proteins are preferentially relocated to viral inclusions. It is conceivable that the amount of free VP35 and VP30 in infected cells is too low to be detected by IFA.

In As-treated cells the dsRNA-dependent protein kinase (PKR) is activated by the cellular protein, PKR activating protein (PACT). Activated PKR phosphorylates eIF2α, inducing SG formation. In EBOV-infected cells, activation of PKR by dsRNA has been shown to be efficiently inhibited by VP35. Our data revealed that EBOV was not able to block As-induced PKR activation. This indicates that PKR activation by PACT cannot be antagonized by VP35. Previous studies have reported that VP35 binds to PACT in unstressed cells (Fabozzi et al., 2011) Here we show that the VP35-PACT interaction was disrupted in stressed cells. This indicates that VP35 loses the ability to sequester PACT from binding to PKR, such that PKR can be activated. This further explains the presence of SGs in EBOV-infected cells but the questions remains, how eIF2α-induced SG formation is inhibited in EBOV-infected and VP35 expressing cells? Possible mechanisms include the inhibitory function of VP35 on SG formation or the sequestering of SG components.

To analyze the role of PBs in EBOV infection, a U2OS cell line expressing the PB marker protein mRNA-decapping enzyme 1A (DCP1a) fused to mRFP was used. In EBOV-infected cells, As-induced PBs were observed to surround viral inclusions, suggesting a recruitment of PBs. In transient transfection experiments, PBs colocalized with VP35 but not with VP30 or NP. Expression of VP35 in U2OS cells containing both G3BP-EGFP and DCP1a-mRFP resulted in diffusely aggregated SGs that colocalized with VP35 and intermingled with PBs. This suggests that

VP35 interacts and links constituents of PBs and SGs. The results indicate that EBOV exhibits antiviral control strategies at the level of the host stress response, where VP35 functions as a key player, since it directly interacts with cellular stress components of both SGs and PBs. Furthermore, the binding between VP35 and PACT seems to play an important role in the control of PKR.

# 3. Introduction

## 3.1. Taxonomy

Ebolaviruses and Marburgviruses constitute the family *Filoviridae* in the order Mononegavirales. Members of this order are characterized by their non-segmented, single-stranded (ss) RNA genomes of negative polarity and include the virus families *Filoviridae*, *Rhabdoviridae*, *Paramyxoviridae* and *Bornaviridae* (Fig. 1). Phylogenetic analysis of their genomes shows that filoviruses are closely related to the paramyxoviruses in the order *Mononegavirales* and particularly to the human respiratory syncytial virus (RSV) (Muhlberger et al., 1992; Sanchez et al., 1992) .

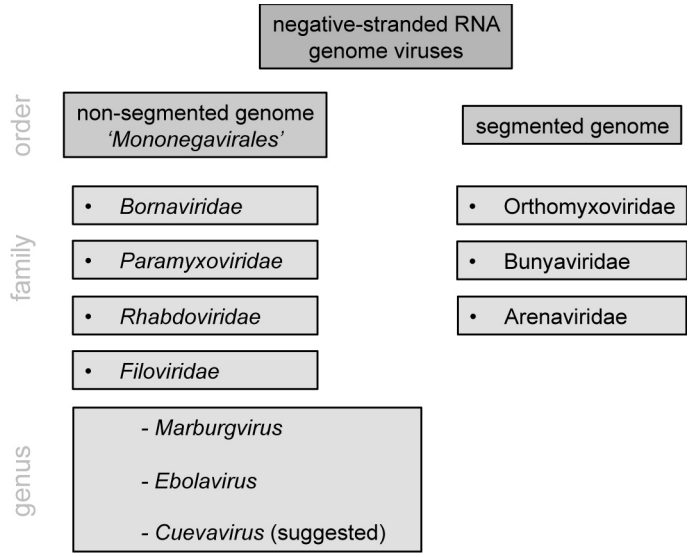


*Fig 1.: Taxonomy of single-stranded negative-sense RNA viruses.*

Marburgvirus isolates show a genome sequence variability of 21% and are therefore classified as a single species *Marburg marburgvirus*. Ebolaviruses are divided into five species on the basis of differences in gene and genome sequence, pathogenicity, geographic origin and occurrence, and in antigenicity. The five species are: *Sudan ebolavirus* (virus: Sudan virus (SEBOV)), *Zaire ebolavirus* (virus: Ebola virus (EBOV)), *Thaï forest ebolavirus* (virus: Thaï Forest virus (TAFV)), *Bundibugyo ebolavirus* (virus: Bundibugyo virus (BDBV)) (Kuhn et al., 2010), *Reston ebolavirus* (virus: Reston virus (RESTV)), all of which have a genome sequence homology of 60-70%.

## 3.2. Epidemiology

The first cases of filovirus infections were reported in 1967 following human outbreaks of acute hemorrhagic fever in the cities of Marburg and Frankfurt in Germany and Belgrade in the former Yugoslavia (Martini and Siegert, 1971; Slenczka, 1999). Initial infections occurred in persons working with blood, organs or tissue cell cultures from infected African green monkeys (*Cercopithecus aethiops*) that had been imported from Uganda. The pathogen was named Marburg virus (MARV) after the city with the most initial cases and where much of the initial research of the virus was performed, which included the first isolation of a filovirus. Reported

MARV outbreaks have resulted in case fatality rates of between 21-91% and are shown in Figure 2.

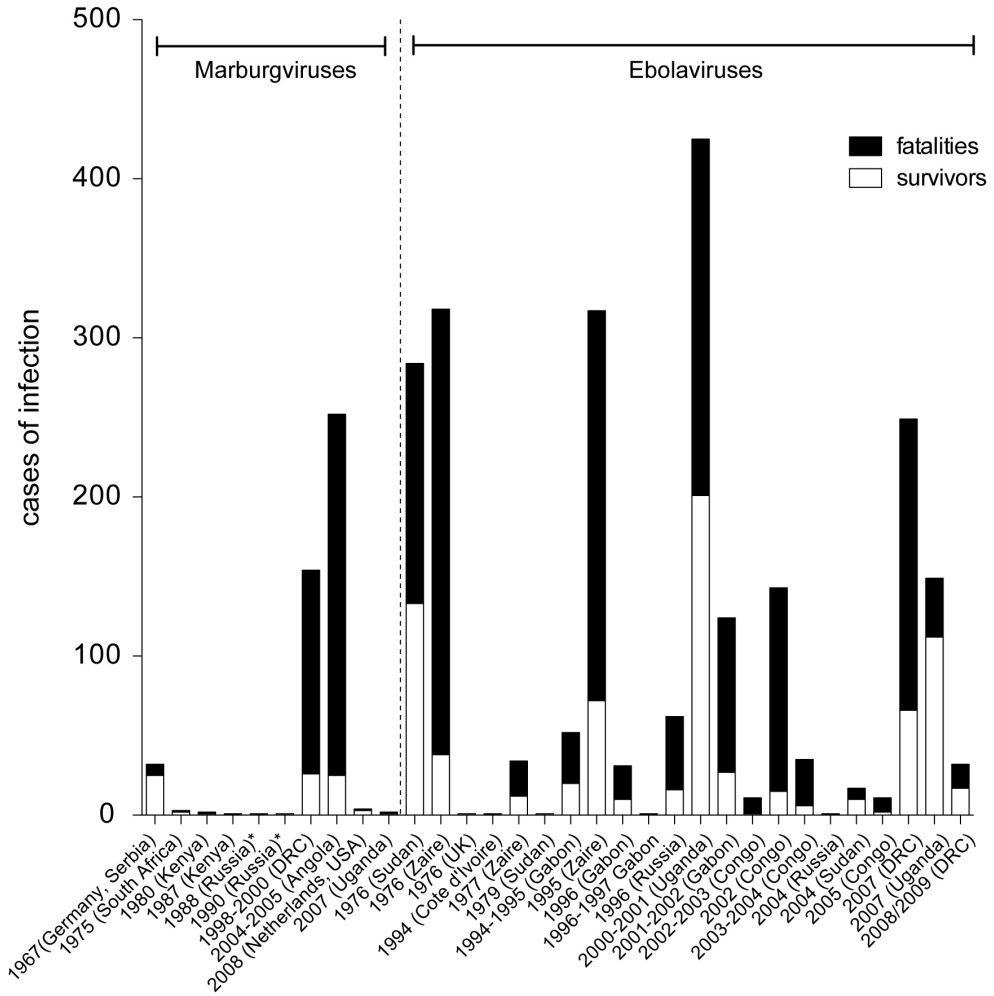


*Fig. 2: Overview of cases of infection during filovirus outbreaks. Case fatality rates for Marburgvirus and Ebolavirus outbreaks.*

Similar cases of hemorrhagic fever were reported in 1976 with outbreaks occurring in two locations: southern Sudan and shortly thereafter in northern Zaire (now the Democratic Republic of the Congo, DRC). The causative agents isolated from patients in both outbreaks were named Ebolaviruses after a river in northwestern DRC. The two epidemics were caused by two different species, later named *Sudan ebolavirus* and *Zaire ebolavirus*. Case fatality rates from reported outbreaks have been between 80-90% for EBOV and 50-55% for SEBOV (Fig. 2). The *Thaï forest ebolavirus* species (formally named *Cote d'Ivoire ebolavirus*) was discovered in 1994 when virus was isolated from an infected ethnologist who had performed a necropsy on a chimpanzee in the Thaï forest reserve in Cote d'Ivoire, Africa. *Bundibugyo ebolavirus*, the most recently added species to the genus *Ebolavirus* (Kuhn et al., 2010), has a reported fatality rates of 36% since its discovery in the 2007 outbreak in Uganda (Fig. 2) (Towner et al., 2008).

The only known ebolavirus species discovered outside of Africa, *Reston ebolavirus,* was identified in 1989 in Reston, VA, USA (Fig. 3). RESTV-infected Cynomolgus monkeys (*Macaca fascicularis*) were imported from the Philippines (Fig. 3), where the virus was found to be endemic. It represents

the only species in the genus *Ebolavirus* with no reported lethal human infections. Although it has caused deadly outbreaks in nonhuman primates and domestic pig populations, it is not certain if these animals died from additional infections with other viruses.

Aside from *Reston ebolavirus,* filoviruses are endemic in Central Africa in an area that lies approximately between the 10$^{th}$ parallel north and south of the Equator as indicated by the locations of known outbreaks (see Fig. 3). The natural reservoir for filoviruses remains to be identified but infectious marburgvirus has been isolated from Egyptian fruit bats (*Rousettus aegyptiacus*) and infectious Reston virus has been isolated from domestic pigs (*Sus scrofa*).

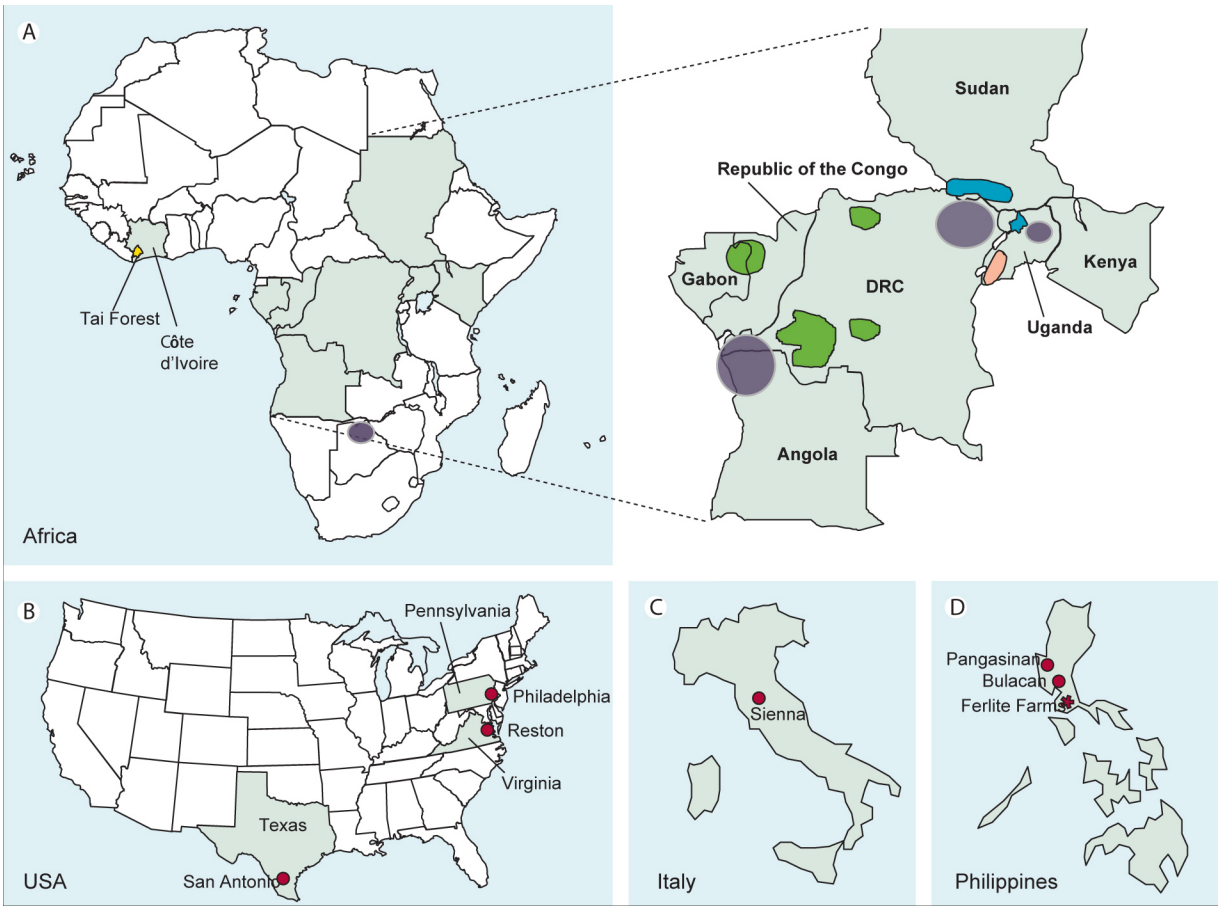


*Fig. 3: Overview of filovirus outbreaks. MARV outbreaks occurred in Angola, DRC, Uganda and Zimbabwe (A, purple). Outbreaks of the different Ebolaviruses occurred in Sudan and Uganda (A, Sudan ebolavirus; blue), DRC, Republic of Congo, Gabon (A, Zaire ebolavirus; green), Cote d'Ivoire (A, Thai Forest ebolavirus; yellow), USA, Italy and the Philippines (B-D, Reston ebolavirus; red), Uganda (A, Bundibugyo ebolavirus; cream) (modified from (Feldmann and Geisbert, 2011) .*

Work with filoviruses is restricted to high-containment Biosafety Level 4 (BSL-4) laboratories due to the lack of an approved vaccine or treatment, the high lethality, and the risk of potential transmission via aerosols (CDC, DHHS, and NIH. 2009). Filoviruses are classified as Category A Bioterrorism Select Agents by the Centers for Disease Control and Prevention (CDC) for their potential threat to public health and safety. The National Institute of Allergy and Infectious Diseases (NIAID) further classified them as Category A Priority Pathogens and the World Health Organization (WHO) as Risk Group 4 agents.

## 3.3. Pathogenesis

Filoviruses are mainly transmitted through direct contact with body fluids of infected patients or animals. Viruses enter the body through small lesions in the skin or mucosal skin. Early target cells are macrophages, monocytes, and dendritic cells (Ryabchikova et al., 1996; Geisbert et al., 2003). It is assumed that virus spread occurs from the initial infection site via the primary target cells to the local lymph nodes and through the blood to the liver and spleen. Viral particles are likely distributed systemically throughout the body by the lymphatic system (reviewed in (Feldmann and Geisbert, 2011). Symptomatic manifestation of the disease starts after an incubation time of 2-21 days with sudden onset of unspecific flu-like symptoms. In the acute phase of the disease, hemorrhages develop in the mucosal epithelia of the intestinal tract, lungs, and mouth, due to the increased permeability of the endothelium (Martini, 1973; Bwaka et al., 1999; Slenczka, 1999). Viral replication is very efficient; at two days following the onset of symptoms, viral titers in the blood of infected patients with a fatal outcome of the disease were higher than $10^8$ virus particles / ml (Towner et al., 2004). In fatal cases the adaptive immune response is severely inhibited and dysregulated, which might influence the outcome of the disease (Baize et al., 1999; Bradfute et al., 2008). Massive apoptosis of non-infected lymphocytes might play a role in filovirus pathogenesis (Baize et al., 1999). In addition, it has been shown that filoviruses encodes several proteins that actively inhibit the innate immune response (Basler et al., 2000; 2003; REID et al., 2005; Cardenas et al., 2006; Prins et al., 2009; Valmas et al., 2010). Patients with a fatal course of infection succumb to infection six to sixteen days after the appearance of the first symptoms of hemorrhagic fever.

## 3.4. Morphology and genome structure

Filovirus particles have a characteristic filamentous shape that gave the virus family its name. Virions appear as branched, circular, U or 6-shaped and long filamentous forms, which vary in length from 974-1086 nm but sustain a constant diameter of 80 nm (Fig. 4A).

The filamentous enveloped particles contain a negative-sense, ssRNA genome. The 19 kilobases genome is flanked by non-coding 3' *leader* and 5' *trailer* sequences and contains seven viral genes. The open reading frames (ORFs) are flanked by nontranslated regions and separated by highly variable intergenic regions (IRs) of varying lengths (Fig. 4C). The *leader* and *trailer* are non-transcribed regions and contain the replication and transcription promoters as well as the signals for encapsidation of the genome.

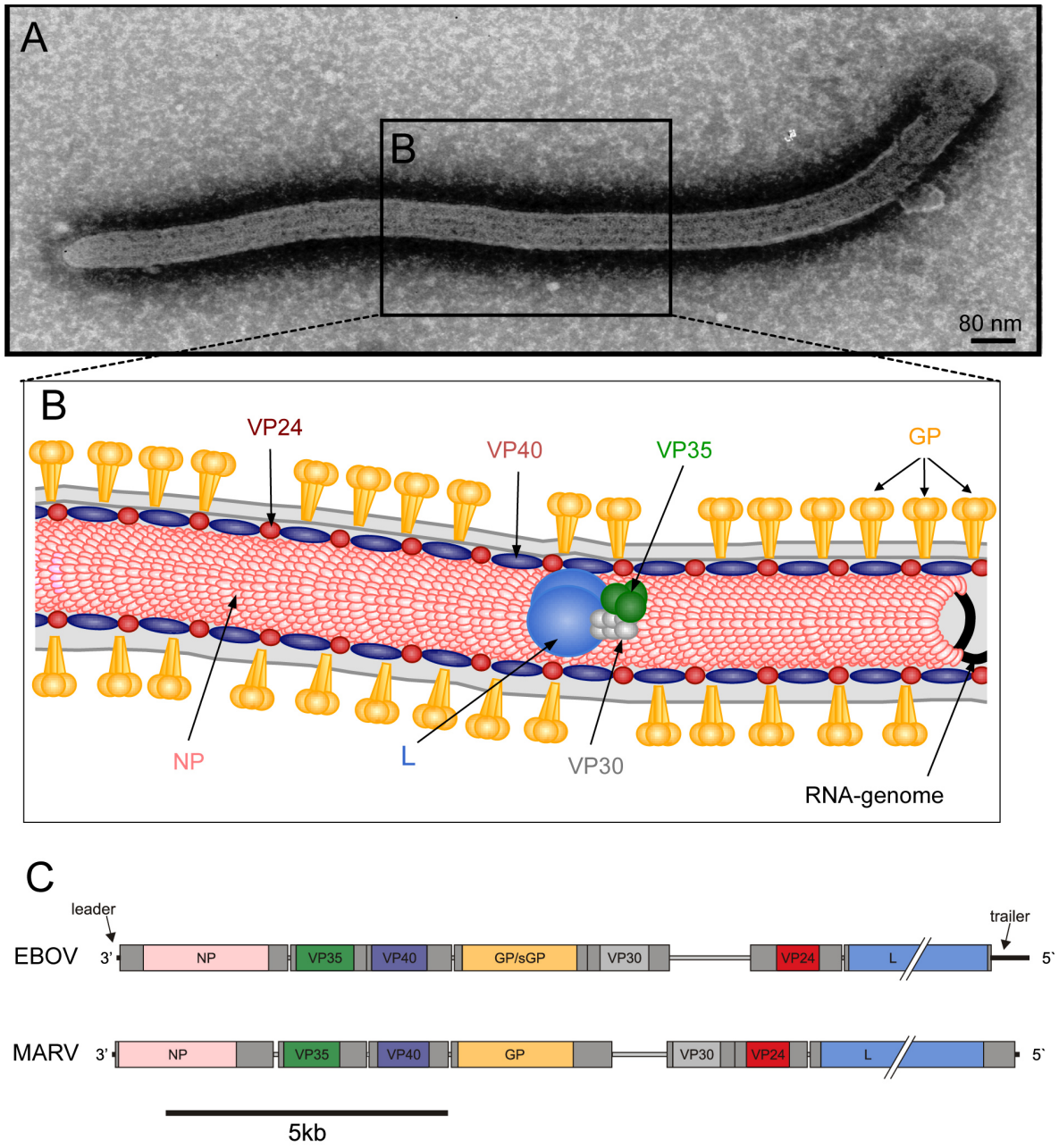


*Fig. 4: Schematic of the filovirus morphology and genome structure.*

The viral proteins encoded on the viral genome include the nucleoprotein (NP), the polymerase cofactor viral protein (VP) 35, the matrix protein VP40, the surface glycoprotein GP, the transcription initiation factor VP30, the minor matrix protein VP24 and the RNA-dependent RNA polymerase, L (Fig. 4B and C). Encapsidation of the viral RNA by the nucleocapsid (NC) proteins (detailed below) protects it from both RNase degradation and detection by the host immune response. Genomic and antigenomic RNA are both encapsidated by the NC proteins and serve as the template for viral RNA synthesis. In contrast, the viral mRNAs are not encapsidated (Muhlberger et al., 1998; 1998).

NP encapsidates the viral genome and antigenome, which protects the RNA from RNases (see Replication and transcription). In addition, NP is important for the viral NC and inclusion formation.

Helical NP-structures formed by expression of NP associated with non-viral RNA, which is not protected from RNase digestion (Noda et al., 2010). The NCs form a helical structure consisting of genomic RNA and tightly associated proteins that are essential for replication and transcription of the viral genome. The NC is formed by NP, which interacts with VP35, VP30, and the polymerase L, either directly or via a linker protein.

In infected cells, these interactions redirect all four NC proteins into cytoplasmic aggregates, described in more detail below. The membrane-associated VP24 protein has also been shown to be required for structured NC assembly (Huang et al., 2002; Mateo et al., 2011).

### 3.4.1 Viral inclusion bodies and nucleocapsids

Following infection of the cell, viral inclusions are formed in the cytoplasm. These cytoplasmic viral inclusions are thought to be active sites of viral replication and assembly of newly synthesized NCs. The first morphological sign of viral inclusion formation observed by electron microscopy (EM) analysis appears as high-density granular material in the cytoplasm that contains RNA and viral proteins at 9 hours post infection (hpi) with EBOV and 12 hpi with MARV (Ryabchikova and Price, 2004). Later, highly organized tubular structures with an average diameter of 50 nm can be detected, which are thought to represent the newly synthesized viral NCs (Ryabchikova and Price, 2004; Noda et al., 2006; Olejnik et al., 2011)). By immunofluorescence microscopy viral inclusions appear as large aggregates in the cytoplasm of filovirus-infected cells (Becker et al., 1998; Schmidt et al., 2011) (Fig. 5A). These inclusions look similar to those formed in cells expressing NP alone due to self-assembly. However, these inclusions are more pronounced when VP35 is coexpressed (Fig. 5A).

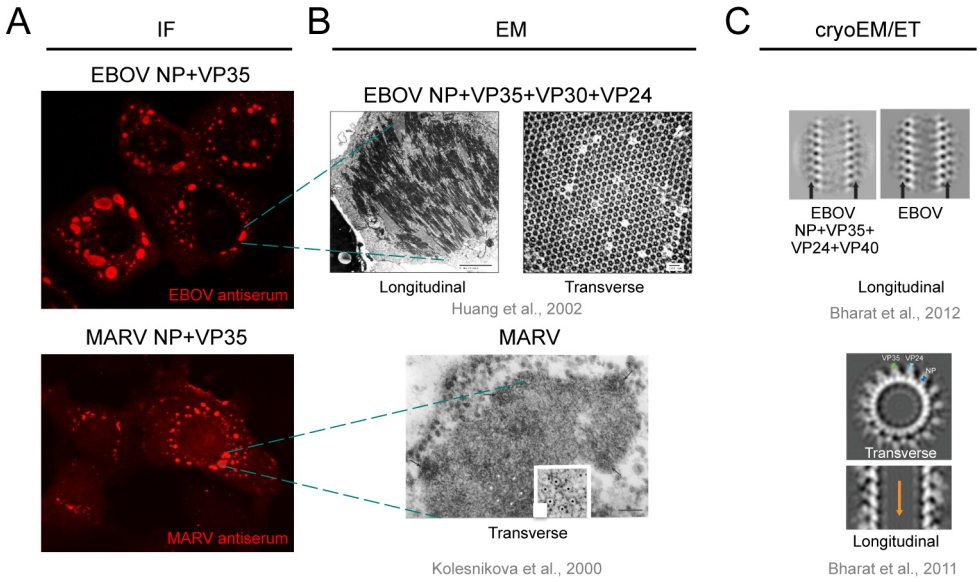


*Fig. 5: Filoviral NC formation. (A) Immunofluorescence (IF) analysis of EBOV and MARV inclusions formed by NP and VP35. (B) Electron microscopy (EM) analysis of EBOV and MARV inclusions. EBOV: Expression of the viral proteins NP, VP35, VP30, and VP24 in transfected HEK293T cells (Huang et al., 2002). MARV: viral inclusion in MARV-infected Vero cells (Kolesnikova et al., 2000). (C) Cryo EM and electron tomography (ET) of EBOV and MARV NC conformation. EBOV: Transfection of viral proteins NP, VP35, VP24, VP40 (Bharat et al., 2012). MARV-infected Vero cells (Bharat et al., 2011).*

EBOV NP, expressed in the absence of other viral proteins, forms loose coil-like helices of approximately 20 nm in diameter that are morphologically distinct from authentic NCs as shown by CryoEM (Noda et al., 2006; Watanabe et al., 2007; Bharat et al., 2012). The NP helices serve as the core for the formation of NC-like structures (Watanabe et al., 2007). EM studies further revealed that expression of EBOV NP, VP24 and VP35 results in the formation of highly structured NC-like helices of approximately 50nm in diameter that are morphologically indistinguishable from the NCs observed in EBOV-infected cells (Fig. 5B) (Huang et al., 2002; Noda et al., 2006). These three proteins are sufficient and essential for the structure of the NC-like helices whereas viral RNA is not essential for this process. The NC-like structures are transported to the plasma membrane where virus budding occurs upon coexpression of VP40. It is believed that VP40 interacts with NP and recruits the NC-like structures to the cell membrane during virus budding to form virus-like particles (VLPs). VLPs containing the NC helices (formed by the four viral proteins NP, VP24, VP35 and VP40) and EBOV virions have been shown to be indistinguishable in structure, symmetry and flexibility (Fig.5C) (Bharat et al., 2012).

Detailed cryo-electron tomography (cryo-ET) analysis revealed the conformation of MARV NCs (Bharat et al., 2011). Core-conserved truncated versions of MARV NP (390 N-terminal residues) formed helices closely matching the helical parameters of viral NCs (e.g. innermost density, diameter, hand, and pitch) and assembled in the absence of any other viral proteins.

## 3.5. Replication and transcription

After entry into the cell, filoviral NCs are released into the cytoplasm of the infected cell where transcription and replication of the viral RNA genome takes place (Fig. 6). NP, VP35, L, and VP30 form the polymerase complex needed for both viral transcription and replication. The polymerase complex transcribes the encapsidated negative-sense RNA genome, leading to monocistronic mRNAs. These mRNAs are co-transcriptionally capped and polyadenylated and subsequently translated by the cellular translation machinery (Fig. 6). It is believed that during transcription, the polymerase complex only has access to the promoter located in the *leader* region of the viral genome but frequently detaches from the template primarily at the gene borders. Consequently, genes located closer to the 3’ end *leader* region of the genome are transcribed at a higher frequency than the genes located at the 5’ end, which leads to an mRNA-gradient.

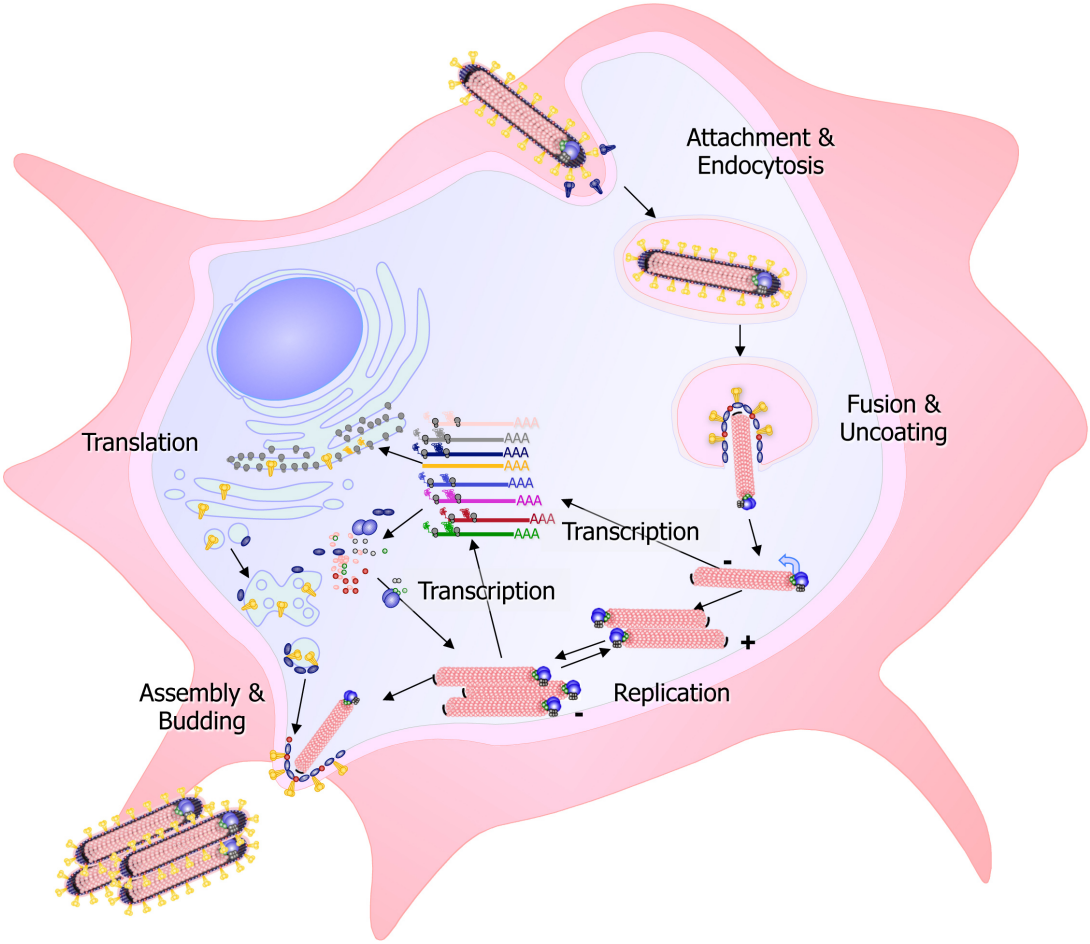


*Fig. 6: Schematic of the filoviral replication and transcription cycle. Courtesy of Dr. K. Brauburger published in Olejnik et al., 2011.*

During replication, the genomic RNA serves as the template for the production of positive-sense antigenomes, which are complementary to the genomes. The antigenomes, encapsidated by the nucleocapsid proteins, are used as templates for genome synthesis (Fig. 6) (for review see (Mühlberger, 2007)). For EBOV it has been shown that VP40 and VP24 inhibit transcription and replication (Watanabe et al., 2007; Hoenen et al., 2010). This suggests that maturation of the NCs negatively regulates viral replication.

## 3.6. Rescue system for full-length recombinant MARV

Rescue systems allow for the generation of full-length recombinant infectious viruses entirely from cDNA plasmids. This technic can be used to rescue viruses expressing fluorescence maker proteins. These recombinant viruses can then be used as tools to study viral replication cycles and open up the possibility for rapid screening assays. Since, it is not possible to introduce specific mutations directly into the viral RNA genome , it has to be reverse transcribed into cDNA first. The cDNA allows mutations to be made and additional genes to be inserted into the genome (e.g. enhanced green fluorescence protein (EGFP); described in the results). The recombinant cDNA of the MARV full-length antigenome was cloned into a plasmid under the control of the T7 RNA polymerase promoter (Enterlein et al., 2006), and the NC genes are each also under the control of

the T7 RNA polymerase promoter. BSR-T7 hamster cells constitutively expressing the T7 RNA polymerase are transfected with the plasmid containing the MARV full-length cDNA along with the plasmids encoding the four NC protein genes (Fig. 7). To increase the amount of T7 RNA polymerase, a plasmid encoding the DNA-dependent T7 RNA polymerase is transfected along with the other plasmids. Using the transfected plasmids as templates, the T7 RNA polymerase synthesizes an ssRNA representing the viral antigenome and the mRNAs of the NC protein genes. Subsequent translation occurs by the host protein synthesis machinery. MARV full-length antigenomes are then replicated by the NC proteins, which results in the generation of the negative-sense genome. In turn, the genome serves as a template for RNA replication and transcription, leading to viral mRNA production and subsequent protein synthesis. Finally, the genome is packaged by the viral proteins and released from the cell as mature infectious particles during the budding process.

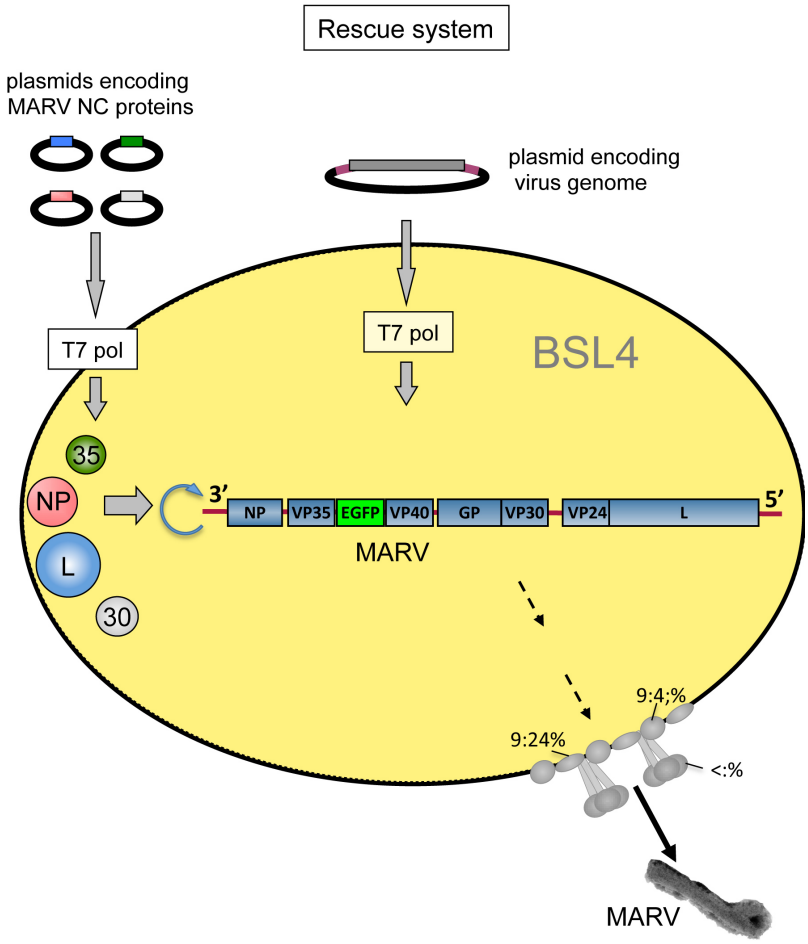


*Fig. 7: The recombinant MARV rescue system. Filovirus-permissive cells are transfected with plasmids encoding the four nucleocapsid proteins along with a plasmid encoding full-length MARV cDNA cloned under the control of the T7 RNA polymerase promoter. Replication of the antigenome by the NC proteins results in the negative-sense genome. The genome serves as a template for replication and transcription, leading to viral mRNA production and subsequent protein synthesis. This leads to assembly and release of mature infectious viral particles from the cell. GP: Glycoprotein; VP24: Viral protein 24; L: RNA-dependent RNA polymerase; NP: Nucleoprotein; VP35: Viral protein 35; VP30: Viral protein 30; T7 pol: T7 RNA polymerase.*

## 3.7. Stress response and mRNA silencing

Virus infections induce stress responses at multiple levels since host cell processes are interrupted or co-opted. When cells are exposed to various types of environmental stress, translational initiation is reprogrammed to a state of global translational arrest of housekeeping transcripts. This process is accompanied by the formation of distinct cytoplasmic structures known as stress granules (SGs) and an increased number of processing bodies (PBs) (Fig. 8). Both SGs and PBs are multicomponent, compositionally related messenger ribonucleoprotein (mRNP) complexes. They cooperatively regulate translation and decay of mRNAs. SGs are compartments of translationally silenced mRNPs. In contrast to SGs, PBs not only store mRNAs for subsequent translation (Brengues et al., 2005) but also facilitate their degradation (Sheth and Parker, 2003; Cougot et al., 2004).

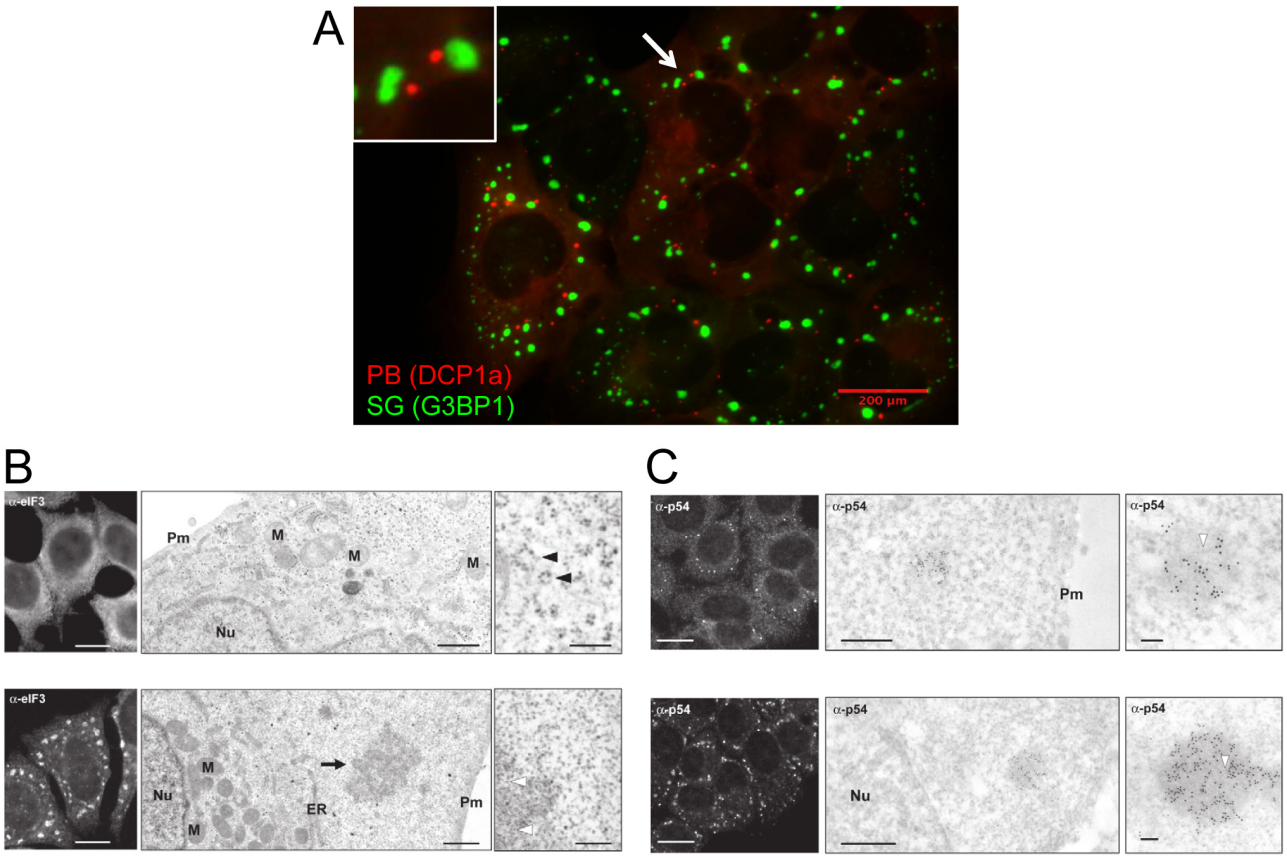


Souquere et al., 2009 Souquere et al., 2009

*Fig. 8: SGs and PBs in microscopic analyses. (A) U2OS cell line constitutively expressing tagged proteins, ras-GAP SH3 domain binding protein 1 (G3BP1)-EGFP and mRNA-decapping enzyme 1A (DCP1a)-mRFP, which constitute marker proteins for SGs and PBs, respectively. Both tagged proteins (G3BP and DCP1a) exhibited very similar behavior to their endogenous counterparts in the parental U2OS cells (Kedersha et al., 2008). The stable cell line was treated with sodium arsenite (As), which induces oxidative stress. G3BP-containing SGs (green) and DCP1a-containing PBs (red) can be observed in the cytoplasm of As-treated cells. (B and C) SG (B) and PB (C) formation in the cytoplasm of HeLa cells in non-treated cells (upper panels) and As-treated cells (lower panels). Analyzed by immunofluorescence staining using an antibody-detecting eukaryotic initiation factor (eIF) 3 (SGs) and p54 (PBs) and by EM (from (Souquere et al., 2009). Pm: plasma membrane; M: mitochondrion; Nu: nucleus. Scale bars: (A) 200 µm (B) 10 µm, 1 µm and 200 nm for left, middle and right (C) 10 mm, 500 nm and 100 nm for left, middle and right panels, respectively.*

### 3.7.1 Stress granule assembly

SGs were first described in tomato cell lines submitted to heat shock (Nover et al., 1983; 1989). EM analyses showed that SGs do not have membranes, and their typical dimensions are 1 - 2 µm (Souquere et al., 2009) (Fig. 8B). Based on immunofluorescence analysis of SG components, SGs are defined as macromolecular aggregates of stalled 48S pre-initiation complexes that form in response to stress (Kedersha et al., 1999). Initiation pathways leading to SG formation are shown in Figure 9.

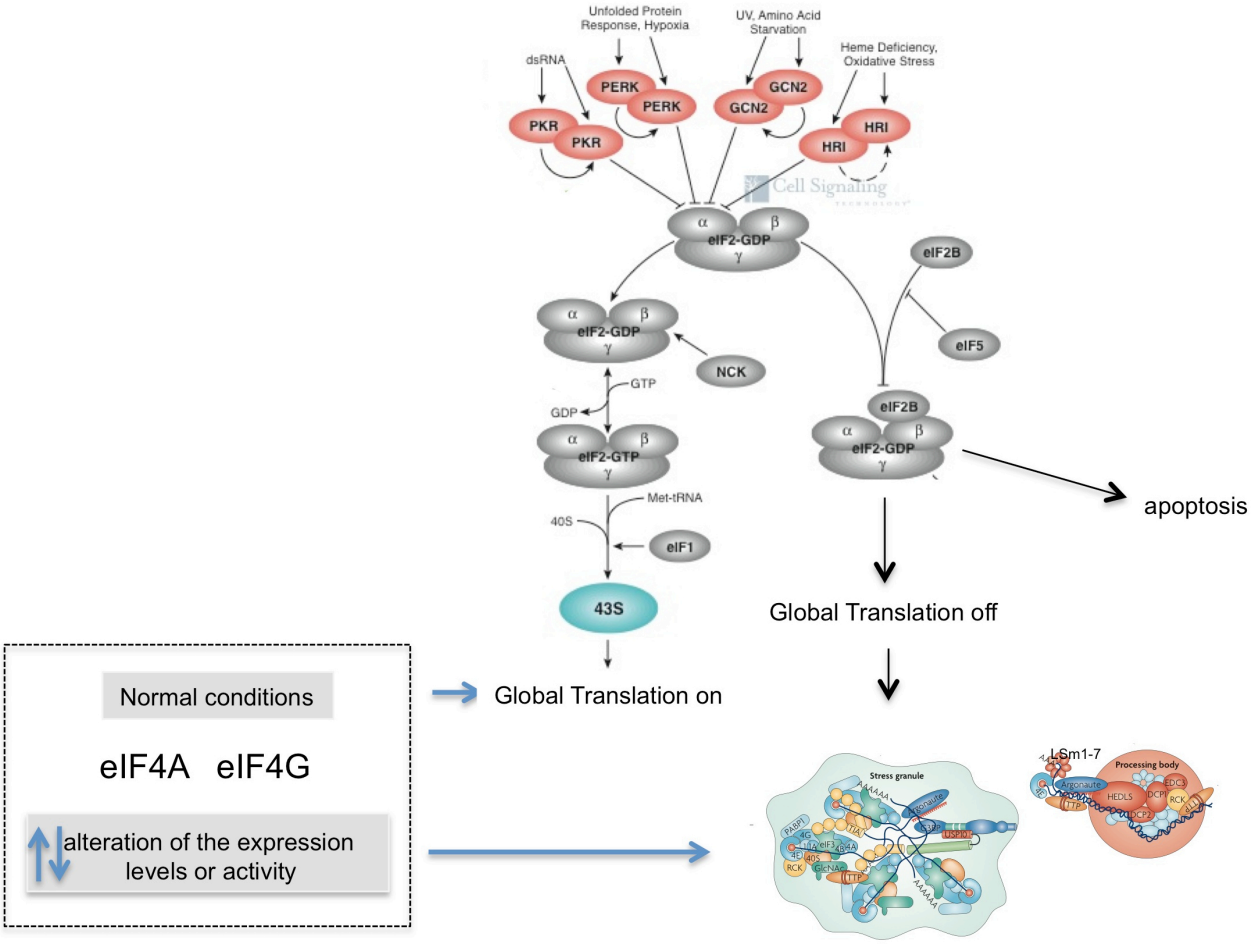


*Fig. 9: Pathways of SG formation initiation. The best-known pathway for SG formation initiates with the phosphorylation of the heterotrimeric eIF2 at its alpha (α) subunit on serine residue 51. The α subunit is the target of a family of four serine or threonine kinases that regulate protein synthesis in response to their activation by different forms of environmental stress. The double-stranded (ds) RNA-dependent protein kinase (PKR) is a component of the interferon (IFN) response and is commonly activated by RNA viruses producing dsRNA as RNA replication intermediates (Maggi et al., 2000). PKR also senses heat, ultraviolet (UV) irradiation and oxidative stress (Williams, 2001). In addition, overexpressed PKR is a potent inducer of apoptotic cell death (Gil and Esteban, 2000). PKR-like endoplasmic reticulum (ER) kinase (PERK) is activated by ER stress caused by unfolded proteins in the ER (Shi et al., 1998; Harding et al., 1999; Harding, Novoa, Zhang, Zeng, Wek, Schapira, and Ron, 2000; Harding, Zhang, Bertolotti, Zeng, and Ron, 2000). General control non-derepressible-2 (GCN2) senses amino acid or serum starvation and UV irradiation (Berlanga et al., 1999). GCN2 is not commonly linked to virus infection, although it has been shown that GCN2 is activated upon binding to Sindbis virus genomic RNA (Berlanga et al., 2006). Heme-regulated inhibitor (HRI) monitors changes in the availability of heme during erythrocyte differentiation and is activated under conditions of oxidative stress as well as heat shock (Han et al., 2001; Lu and Chen, 2002). Phosphorylation of eIF2α by each of these kinases increases the affinity of eIF2 for eIF2B, and thereby prevents the exchange of GDP for GTP. By functioning as a competitive inhibitor of eIF2B, phospho-*

*eIF2α reduces the availability of the eIF2-GTP-tRNA$^{Met}$ ternary complex, preventing the assembly of the 48S pre-initiation complex (Srivastava et al., 1998). A phospho-eIF2α-independent stimulus leading to the formation of SGs has been observed by the inhibition of the translation initiation factors eIF4G and eIF4A (Bordeleau et al., 2006; Mazroui et al., 2006). Both factors belong to the eIF4F protein complex composed of three subunits: eIF4E, the cap binding protein; eIF4A, a bidirectional ATP-dependent RNA helicase and eIF4G, a modular scaffolding protein that binds eIF4E, eIF4A, eIF3 and PABP1. Under normal conditions the mRNA 5' cap structure (m7GpppN, where N is any nucleotide) interacts with eIF4F. Simultaneous interactions between eIF4G, eIF4E and PABP1 circularize mRNA and promote translation initiation (Tarun and Sachs, 1996; Imataka et al., 1998; Kahvejian et al., 2005) Modified from Cell Signaling and Kedersha..*

When the stalled initiation complex is assembled at the 5' end of polysomal mRNA, actively translating ribosomes detach from the transcript, resulting in polysome disassembly. Detachment of ribosomes from mRNA transcripts induces actively organized assembly of SGs, containing stalled mRNAs in mRNP complexes (Fig. 10) (Kedersha et al., 1999; 2005) (Wek et al., 2006). The SG assembly process is mediated by self-aggregation and the RNA binding ability of the translational silencer T cell-activated intracellular antigen (TIA) -1 and TIAR due to their prion-related domain (Kedersha et al., 2002; Gilks et al., 2004). G3BP1 also contains a self-interacting and RNA binding domains and contributes to SG formation (Tourrière, 2003).

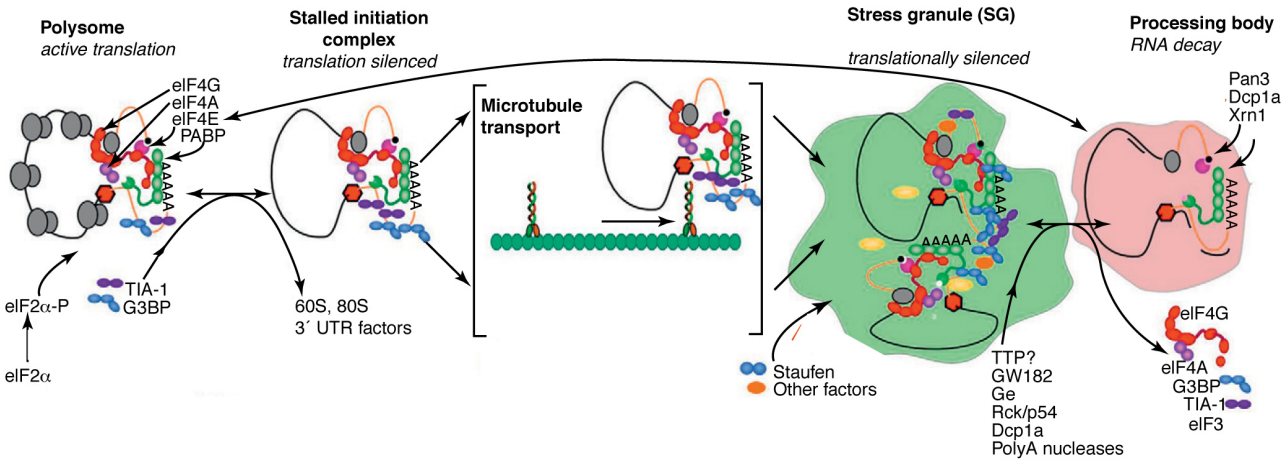


*Fig. 10: Formation of SGs and PBs. Modified from White et al., 2012.*

In the work presented here cellular stress was chemically induced by sodium arsenite (As), which causes oxidative stress that leads to the phosphorylation of eIF2α through the kinases HRI and PKR (McEwen, 2005; Daher et al., 2009)(see 3.7.5 PKR and PACT).

To induce stress independently of eIF2α phosphorylation, hippuristanol (Hip) was used. Hip is a small molecule, discovered by Jerry Pelletier (Bordeleau et al., 2006) that was isolated from the coral *Isis hippuris*. The compound is a selective inhibitor of eIF4A RNA binding activity. eIF4A is a DEAD-box RNA helicase that is thought to unwind local secondary structures in the 5' untranslated region of the mRNA to facilitate access of the 43S ribosome complex to the mRNA. As a component of the eIF4F complex eIF4A is required for recruitment of the ribosomes to cellular and many viral mRNAs (review see (Rogers et al., 2002)). Therefore Hip specifically inhibits eukaryotic cap-dependent translational initiation and it can be used to distinguish between modes of eIF4A/cap-dependent and independent, such as internal ribosomal entry sites (IRES) translational initiation.

Depending on their induction, SGs can consist of different components. The major components are a non-canonical, translationally silent 48S pre-initiation complex that includes the small (40S) ribosomal subunit and a number of early transcription initiation factors such as eIF3, eIF4A, eIF4E, and eIFG. SGs also contain mRNAs and a set of RNA binding proteins (RNA-BP) such as TIA-1, poly (A)-binding protein 1 (PABP1), human antigen R (HuR) and G3BP1 (Kedersha et al., 1999; 2005; Mazroui et al., 2006). RNA-BPs regulate mRNA stability, structure and function of transcripts as well as translation initiation or silencing. SGs do not contain eIF2 ternary complex and the large ribosomal subunit (Kedersha and Anderson, 2002).

### 3.7.2 Processing body assembly

Mammalian PBs, like SGs, are dynamic structures constitutively present in the cytoplasm of cells. Their number and size increase during stress (Kedersha et al., 2005; Teixeira et al., 2005) and with the amount of mRNA to degrade (e.g. accumulation of mRNA by blocking mRNA decay or inhibition of translational initiation)(Sheth and Parker, 2003; Cougot et al., 2004; Andrei, 2005; Brengues et al., 2005; Wilczynska, 2005) Conversely, blocking transcription, deadenylation of mRNAs or translational elongation decreases the size and number of PBs (Sheth and Parker, 2003; Cougot et al., 2004). The size of PBs ranges between 100-300 nm in mammalian cells (Eystathioy et al., 2002; Yang, 2004). Despite the fact that PB assembly is dependent on RNA (Cougot et al., 2004; Teixeira et al., 2005) the recruitment of mRNAs to PBs is not simply the consequence of not being translated, but rather the effect of an active silencing mechanism. Interrupting mRNA translation, which results in mRNAs accumulating in the cytoplasm only induces PB formation in the presence of active RNA interference (RNAi) or miRNA silencing pathways (Eulalio et al., 2007).

In eukaryotes, mRNA degradation is regulated by two major mechanisms. One involves the multisubunit exosome, where transcripts are degraded by 3’ to 5’ exonucleases (for review see (van Hoof and Parker, 1999) The second mechanism involves PBs, which control mRNA turnover by the 5’ to 3’ mRNA decay machinery. PBs contain enzymes catalyzing decapping, deadenylation and 5’ to 3’ degradation such as the decapping complex DCP1/DCP2 and its cofactors LSm1-7, Rck/p54, Hedls/GE-1 (human enhancer of decapping large subunit, also known as GE-1) and the exonuclease, Xrn1. The 5’ cap is then irreversibly removed by a decapping complex and the mRNA is degraded by the 5’ to 3’ exonuclease Xrn1 (for review see (Eulalio et al., 2007).

Proteins that function in posttranscriptional gene silencing are also localized in PBs. These include (i) proteins involved in nonsense-mediated mRNA decay (NMD) e.g. the Upf complex, which degrades mRNAs harboring premature termination codons (Sheth and Parker, 2006); (ii) proteins targeting AU-rich element (ARE)-containing mRNAs for decay such as tristetraprolin (TTP) and butyrate response factor 1 (BRF1) which both deliver ARE-containing mRNAs to PBs and TTP also enhances decapping of target RNAs (Franks and Lykke-Andersen, 2007); (iii) proteins involved in RNA interference which silences mRNAs targeted by microRNAs (miRNAs) or small interfering RNAs (siRNAs) including Argonaute (Ago) proteins which are part of the RNA-induced silencing complex (RISC) (Jakymiw et al., 2005; Liu, 2006). Notably, ribosomal proteins and proteins involved in translation initiation are absent in PBs with the exception of the cap-binding protein eIF4E and its binding partner eIF4E-transporter (eIF4E-T) (Andrei, 2005; Brengues et al., 2005;

Kedersha et al., 2005; Teixeira et al., 2005), suggesting that mRNPs must be free of ribosomes and eIFs to assemble into PBs.

### 3.7.3 Interplay of SGs and PBs

SGs and PBs are highly dynamic structures of constant mRNP exchange, which has made it impossible to isolate them (Mollet et al., 2008). Microscopy analysis is currently the most suitable method to study these structures. So far it is not known if SGs and PBs exchange mRNPs or other components. However, actively forming SGs are frequently observed next to pre-existing PBs. Further contacts can also be established after SG assembly (Fig. 8) (Kedersha et al., 2005; Mollet et al., 2008). Live-cell imaging has shown that the interactions between SGs and PBs are dynamic and transient (Kedersha et al., 2005; Wilczynska, 2005). Little is known about the mechanism of this interaction. Some RNA-BPs including TTP and BRF1 are present in both SG and PBs and their overexpression promotes and stabilizes the association between SGs and PBs ((Kedersha et al., 2005). Live-cell imaging has revealed a dynamic association between poly-C binding protein 2 (PCBP2)-enriched PBs and SGs (Fujimura et al., 2008). A dynamic movement of Ago2 to newly assembled SGs in addition to PBs was detected by establishing a stably expressing EGFP-Ago2 cell line (Leung et al., 2006). Further, miRNA was required for Ago2 localization to SGs but not to PBs. Fluorescence recovery after photobleaching (FRAP) experiments have revealed that many components such as TTP, TIA and G3BP1 cycle rapidly in and out of either PBs or SGs whereas others such as DCP1a and Fas-activated serine/threonine phosphatase (FAST) are more static (Kedersha et al., 2005; Fujimura et al., 2008). However, EM analyses have revealed discrete morphological structures for adjacent SGs and PBs, which do not intermingle (Souquere et al., 2009). In mammals, SGs and PBs contain many of the same proteins, in particular translational repressors such as Ago2, TTP, BRF-1 (Wilczynska, 2005; Yang, 2006; Yang and Bloch, 2007) and the transcriptional regulator PCBP2 (Fujimura et al., 2008) a facilitator of IRES-mediated translation of both viral and cellular transcripts (Bedard et al., 2004).

### 3.7.4 Viruses and cellular stress response

In general, manipulation of SG formation has been described for a number of RNA viruses, especially viruses containing either a positive-sense ssRNA genome or a dsRNA genome. Viruses exhibit special strategies such as compartmentalization of their replication machinery in order to shield viral RNA from recognition by the innate immune system upon release into the cytoplasm.

For some RNA viruses it has been shown that SG formation is induced upon entry but then inhibited at later stages of infection. Mammalian orthoreoviruses, which belong to the dsRNA viruses, and Semliki Forest virus, which belongs to the positive-sense RNA alphavirus family, induce SG formation in an early stage of infection by inducing eIF2α phosphorylation (McInerney et al., 2005; Qin et al., 2009). The induction of SG formation in an eIF2-independent manner has been reported for Poliovirus, another positive-sense RNA virus (Mazroui et al., 2006; White et al., 2007). In each of these cases it has been suggested that increased viral replication and subsequent viral protein synthesis is linked to SG inhibition. Poliovirus synthesizes different proteases, that mediate cleavage of crucial components needed for SG formation e.g. G3BP1 and eIF4G subunits (Gradi et al., 1998; White et al., 2007).

Inhibition of SG formation during infection has been observed for segmented negative-sense RNA viruses including Junin virus and Influenza A virus. Both viruses block eIF2α phosphorylation either directly or upstream in the signaling process (Khaperskyy et al., 2011; Linero et al., 2011). For Influenza A virus, it has been shown that the viral protein NS1, a known type I IFN antagonist, inhibits PKR activation (Khaperskyy et al., 2011).

Recent publications suggest that RSV, a negative-sense RNA virus closely related to filoviruses, modulates SG function to maximize replication efficiency. However, there are conflicting data on the ability of RSV to induce SGs formation in infected cells (Hanley et al., 2010; Lindquist et al., 2010; 2011).

### 3.7.5 PKR and PACT

IFN-induced PKR is part of the innate immune response and crucial for establishing an antiviral state in the host cell. The best-studied activator of PKR is dsRNA, which plays a major role in activating PKR during viral infections (Hovanessian, 1989; Meurs et al., 1990). Endogenous PKR is constitutively expressed in low amounts and mostly monomeric and inactive. Activation of PKR leads to its autophosphorylation and subsequently to phosphorylation of its substrate eIF2α, leading to translational arrest (see 3.7.1 SG assembly). In addition to its central role in the antiviral response, PKR has been implicated in signal transduction pathways triggered by extracellular stress (see 3.7.1 SG assembly), specific cytokines, growth factors and dsRNA-induced pathways in the inflammatory response (Williams, 1999). Recently it has been reported that PKR can be activated independently of dsRNA by binding to PKR-activating protein (PACT) (Fig. 11). Activation of PKR by PACT requires exposure of cells to extracellular stress including As treatment, treatment with other stressors such as actinomycin D or hydrogen peroxide, andthe withdrawal of growth factors (Patel, 2000; Peters et al., 2001). Unlike PKR, PACT is not regulated by IFN or dsRNA (Peters et al., 2001).

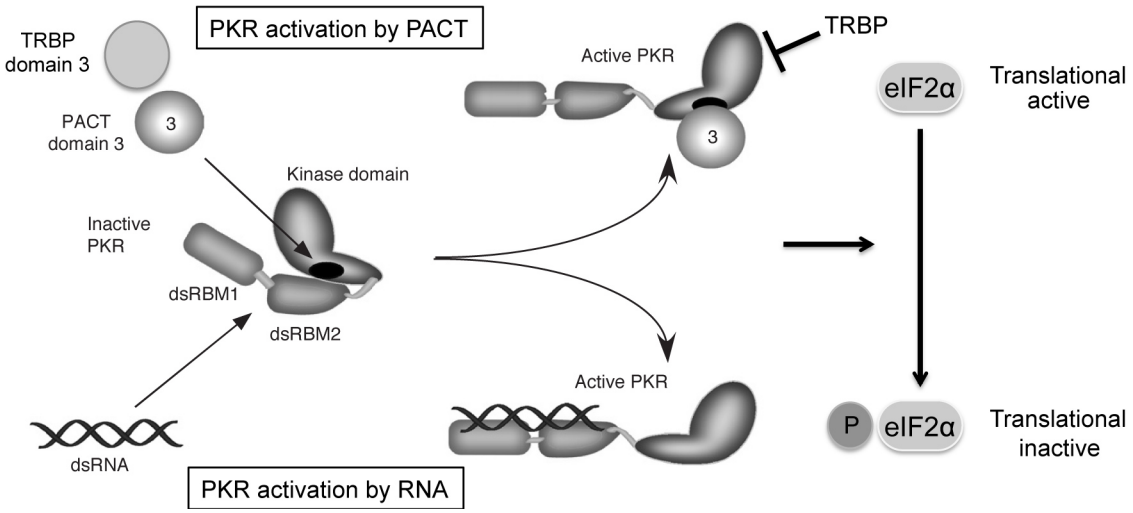


*Fig. 11: Model for PKR activation by PACT or dsRNA. In non-stressed cells PACT and TRBP form heterodimers. This interaction dissociates upon treatment with different extracellular stresses such as As (Daher et al., 2009). In cells exposed to As stress, PACT is phosphorylated at serine residues Ser246 and Ser287 in domain 3 of PACT (recently referred to as the Medipal domain) (Peters et al., 2006). The Ser246 residue is constitutively phosphorylated in cells,*

*whereas Ser287 is phosphorylated following the application of stress. However, phosphorylation of Ser287 did not take place, in the absence of phosphorylated Ser246, indicating that the constitutive phosphorylation is a requirement for Ser287 phosphorylation. Phosphorylation of PACT decreases its interaction with TRBP thereby facilitating its binding to PKR with increased affinity (Singh et al., 2011). dsRBM=dsRNA binding domain. Modified from Sen and Peters, 2007*

Considering the critical role of PKR in cellular metabolism, cells have developed mechanisms to regulate its activity. Transactivation-responsive (TAR) RNA-binding protein (TRBP) controls the PACT-induced activation of PKR and has an opposite role, since direct binding of TRBP to PKR prevents PKR autophosphorylation (Benkirane et al., 1997; Gupta, 2003). TRBP was discovered due to its high affinity to TAR, an RNA hairpin formed by the HIV genome. PACT and TRBP have 40% identity at the amino acid level and show a high degree of structural similarity (Patel and Sen, 1998). Both proteins contain three copies of dsRNA-binding motifs. The two N-terminal copies are capable of binding dsRNA and the third C-terminal copy does not bind dsRNA but mediates protein-protein interaction with several proteins. For PACT-TRBP interaction all three dsRNA-binding motifs are required (Laraki et al., 2008). Thus, TRBP regulates the activation of PKR by controlling PACTs accessibility to PKR and its inhibitory effect on PKR activation.

Both, PACT and TRBP interact with Dicer together with the Argonaute proteins in the RISC complex. RISC is the effector complex that incorporates and processes miRNA and siRNA precursors. miRNAs and siRNAs are derived from hairpin- or dsRNA precursors, respectively, and facilitate the silencing process called RNA interference (RNAi). PACT and TRBP depletion leads to inhibition of miRNA-mediated gene silencing (Kok et al., 2007).

## 3.8. EBOV RNA-binding proteins

EBOV is known to antagonize crucial pathways in the interferon-induced innate immune response. Translational arrest in response to cellular stress leads to the formation of cytoplasmic SGs and PBs. Since filoviruses depend on the cellular translation apparatus for viral protein synthesis, this this represents an important antiviral defense mechanism. EBOV RNA-binding proteins, which are potentially involved in the antiviral stress response mediated by the formation of SGs and PBs, are described in the following section.

### 3.8.1 Inhibition of dsRNA-mediated cellular responses by VP35

The multifunctional EBOV VP35 plays an essential role in viral replication and is a structural component for virus assembly. In addition, VP35 contributes to filoviral immune modulation by impairing the host innate immune response. VP35 has been identified as a very efficient type I IFN antagonist (Basler et al., 2003; Hartman et al., 2004; Cardenas et al., 2006) (see Fig. 13). IFN antagonism is mediated by a C-terminal interferon inhibitory domain (IID), which contains a dsRNA-binding domain (Fig. 12).

| | |
|---|---|
| **ZEBOV VP35wt** | **305 - R A C Q K S L R - 312** |
| **ZEBOV VP35_3A** | **305 - A A C Q A S L A - 312** |

*Fig. 12: VP35 IID domain.*

VP35IID was also shown to inhibit PKR-mediated shut down of the host translational machinery (Feng et al., 2006; Schumann et al., 2009). IID contains a cluster of basic amino acids involved in

dsRNA binding. When three of the basic amino acids were substituted to alanine (R305A, K309A and R312A) (VP35-3A) dsRNA binding as well as dsRNA-binding-mediated IFN inhibition were abolished (Hartman et al., 2004; Leung et al., 2009; Zhu et al., 2012). Most importantly, VP35-3A is not able to antagonize PKR and subsequently eIF2α phosphorylation (Schumann et al., 2009).

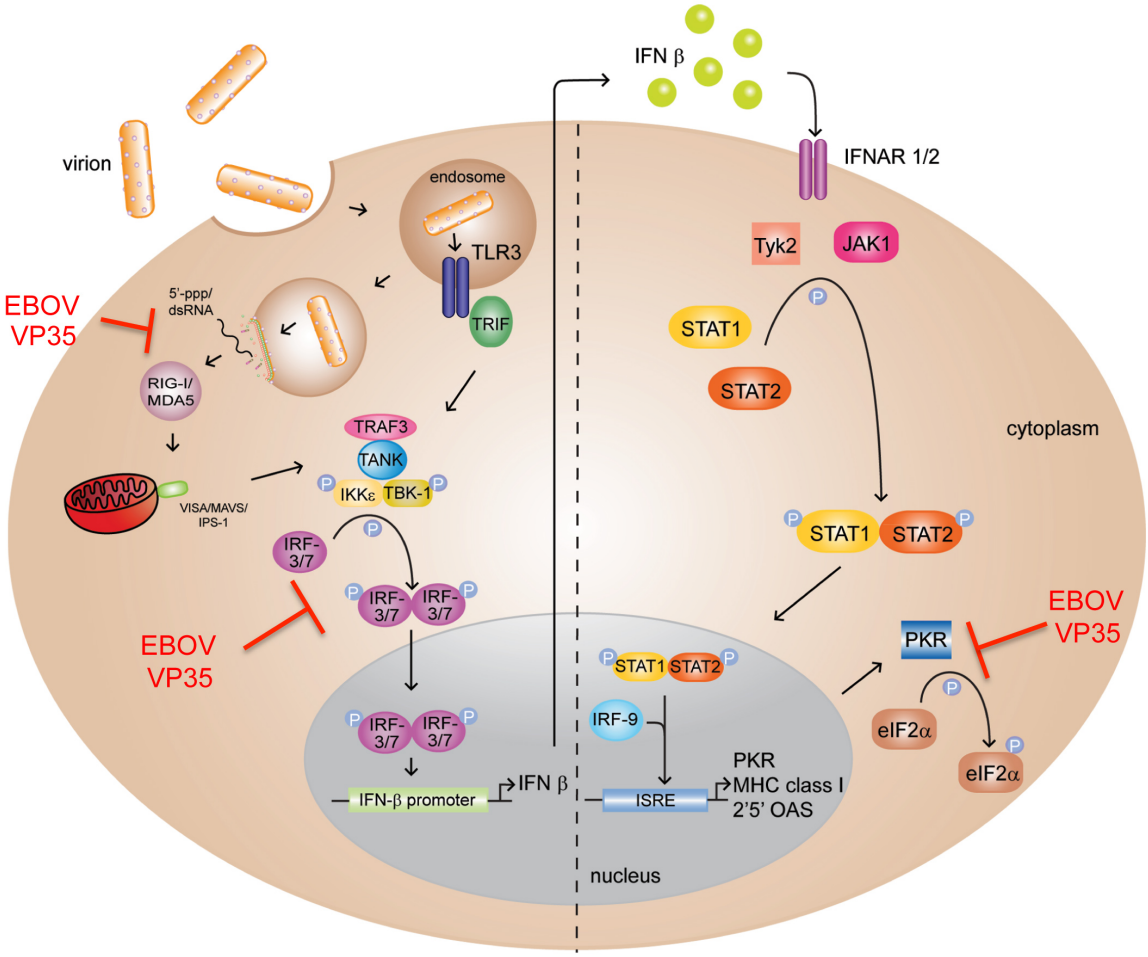


*Fig. 13: Inhibition of the type I IFN response by EBOV VP35. Transfected filoviral 5'triphosphate ends of the genomic RNA can be recognized by RIG-I (Habjan et al., 2008). Activated RIG-I triggers a signal transduction cascade leading to the type I IFN response. EBOV VP35 is able to block the induction of the type I IFN response via RIG-I (Cardenas et al., 2006). VP35 antagonizes the phosphorylation of interferon regulatory factor (IRF) -3/7 by interacting with TBK-1 and IKKε kinase domains. Phosphorylation of IRF3/7 by TBK-1/IKKε leads to the dimerization and translocation of IRF3/7 into the nucleus where it activates the IFN-β promoter (Basler et al., 2003). VP35 also promotes SUMOylation of IRF-7, repressing IFN gene transcription (Chang et al., 2009) and antagonizes PKR activation (Feng et al., 2006; Schumann et al., 2009). Modified from Leung et al., 2010.*

Furthermore, the dsRNA-binding activity of VP35IID suppresses the host RNAi pathway (Haasnoot et al., 2007; Zhu et al., 2012). More recent studies showed that VP35 interacts with Dicer constituents, TRBP and PACT (Fabozzi et al., 2011). Therefore, VP35 potentially targets both the RNAi- and PKR-related functions of TRBP and PACT.

### 3.8.2 RNA-binding proteins VP30

In contrast to VP35, VP30 and NP are not known to interact with the host immune response. They are both part of the RNA replication and transcription competent NC (see above: 3.4 Morphology and genome structure; 3.5 Replication and transcription) and have been shown to be able to bind RNA.

For VP30, ssRNA-binding activity by an arginine-rich region in the N-terminus has been reported but the function of this is not known (John et al., 2007). Phosphorylation of VP30 negatively regulates its transcriptional activity but increases its interaction with NP (Modrof et al., 2002; Martínez et al., 2008; 2011). The N-terminus of VP30 contains a zinc $(Zn)^{2+}$-binding Cys3-His (CCCH Zn-finger) motif that is required for efficient viral transcription (Weik et al., 2002; Modrof et al., 2003). Interestingly, many cellular RNA-BPs that accumulate in SGs also contain this unconventional CCCH Zn-finger motif. This motif allows them to interact with and regulate the stability of ARE-containing mRNAs, such as interleukin-6 and other cytokines (see above: 3.7.2 PB assembly). In addition, VP30 interacts with Dicer and with TRBP in the presence of siRNA (Fabozzi et al., 2011). The function of this interaction is not known.

## 3.9. Outline and goals

**Part I: The goal of the work in part I was to generation and characterize a recombinant Marburg virus expressing EGFP. To achieve this goal, the following strategy was used:**

1. The cloning strategy was designed for the generation of a cDNA clone encoding the recombinant MARV expressing EGFP (rMARV-EGFP) with consideration of the positioning of the EGFP ORF near the 3' end of the viral genome was to maximize the number of EGFP transcripts and thereby increase the sensitivity for virus detection. The cloning steps were verified on cDNA level by sequencing analysis and the genomic viral RNA level by RNA isolation and analysis.

2. The viral protein expression and growth kinetics of rMARV-EGFP were characterized and compared to the wildtype recombinant MARV.

3. Live-cell imaging was used to analyze the spread of rMARV-EGFP in infected cells.

4. The data received from live cell imaging analysis of rMARV-EGFP revealed an EGFP aggregation at the sites of viral inclusion formation. To further characterize this EGFP aggregates, immunofluorescence analysis was used to study the relocalization of several fluorescence proteins to MARV, EBOV and RESTV inclusions.

**Part II: Filoviruses depend on the cellular translation apparatus for viral protein synthesis. It has been shown that EBOV antagonizes crucial pathways in the IFN-induced innate immune response. However, it is not known whether EBOV influences the host stress response mediated by the formation of SGs. The host stress response to EBOV infection was investigated considering the following aims:**

1. It was analyzed by immunofluorescence analysis if SG formation is induced in EBOV-infected cells.

2. To investigate if EBOV is able to interfere with the cellular stress response, EBOV-infected cells were treated with exogenous stress inducers and the formation of SG was analyzed.

3. Our data revealed that stress-induced SG formation is reduced in EBOV-infected cells. To identify the viral component(s) interfering with the cellular stress reponse, EBOV RNA-binding proteins NP, VP30, and VP35 were analyzed for their ability to alter a stress-induced SG formation.

4. It was examined if EBOV infection affects the stress-induced phosphorylation of PKR and eIF2α, which results in translational arrest and the formation of SGs and PBs. PKR is an important kinase for sensing viral infection. Phosphorylation of PKR and its substrate eIF2α have been shown to be suppressed in EBOV VP35 expressing cells (Hartman et al., 2004; Feng et al., 2006; Schumann et al., 2009).

5. During cellular stress the activation of PKR is induced by PACT (Patel and Sen, 1998). Since, PACT has been show to interact with EBOV VP35 in non-stressed cells (Fabozzi et al., 2011), it was analyzed if VP35 and PACT still bind during cellular stress, which suggests a possible mechanism for the stress-induced activation of PKR in EBOV infection.

6. PB formation in EBOV infection was analyzed together with a potential interaction with EBOV RNA-binding proteins. PBs are part of the stress-induced translational arrest, which in contrast to SGs, can also facilitate mRNA degradation.

# 4. Material and Methods

## 4.1. Equipment/Appliances

| | |
|---|---|
| Cell culture incubator | Thermo Scientific |
| Gel Doc 2000 | BIO RAD |
| Thermostat 5320 | Eppendorf AG |
| Thermomixer 5436 | Eppendorf AG |
| Horizontal shaker 3018 | Gesellschaft für Labortechnik mbH |
| Fastblot Whatman | Biometra |
| Zeiss Axiovert 200 M inverted microscope | Zeiss |
| Zeiss LSM5 Pascal confocal microscope | Zeiss |
| Zeiss LSM710 confocal microscope | Zeiss |
| Miniprotean 3 Western Blot chambers | BIO RAD |

## 4.2. Consumables

| | |
|---|---|
| 10 cm dish (cell culture) | Sarstedt |
| 10 cm dish (bacteria) | Sarstedt |
| 6- and 24-well plates | Sarstedt |
| Blotting paper (Whatman 3MM) | Whatman |
| Cryo vials | Coring |
| Screw cap 1.5 ml vials | Sarstedt |
| Polystyrene tube 5 ml, round bottom | Falcon |
| PCR tubes 0.2 ml | Fischer |
| Tubes 1.5 ml | Sarstedt |
| Tubes 15 ml | Falcon |
| Tubes 50 ml | Falcon |
| Parafilm | Pechney Plastic Packaging |
| Immobilon$^{TM}$ P Membran | Millipore |
| Pipette tips (different sizes, filter and non-filter) | Denville |
| Serological pipettes (1 – 25 ml) | Sarstedt |
| Cell culture flasks (25 $cm^2$, 75 $cm^2$, 175 $cm^2$) | Sarstedt |
| GIBCO Leibovitz's L-15 Medium | Invitrogen |

### Chemicals and reagents

| | |
|---|---|
| *Trans*IT-LT1 | Mirus |
| FuGeneHD | Roche |
| Paraformaldehyde (PFA) 32% | Electron Microscopy Sciences |
| TRIZOL | Invitrogen |
| Glycine | Boston Bioproducts |
| Triton X -100 | Boston Bioproducts |
| Laemmli 2x (S3401) | Sigma |
| NP40 | IGEPAL |
| Sodium Chloride (NaCl) | Boston Bioproducts |
| HEPES (1M) | Lonza |
| Protease Inhibitor Cocktail (P2714-1BTL) | Sigma |
| Perce Protein A/G Agarose (20422) | Thermo Scientific |
| Needle: pink 18G1 ½ 305196, brown sub Q 305115 | BD Bioscience, USA |
| Cell lysis buffer | Invitrogen |
| Calyculin A | Cell Signaling |
| Dithiothreitol (DTT) | Fluka Analytical |
| Protein marker: dual color (161-0374) | BioRad |
| PageRuler prestained protein ladder | Fermentas |
| Stripping buffer | GM Biosciences |
| Dulbecco's modified Eagle medium (DMEM) | Lonza |
| PBS | Lonza |
| BSA | Atlanta Biologicals |
| SDS | Boston Bioproducts |
| Ethanol (EtOH) | Pharma |
| TAE (10x) | Boston Bioproducts |
| Tween 20 | Boston Bioproducts |

## 4.3. Kits and Buffer

### Kits

| | |
|---|---|
| CalPhos$^{TM}$ mammalian Transfection Kit | Clonetech, USA |

| | |
|---|---|
| (631312) | |
| OneStep RT-PCR | Qiagen, Germany |
| QIAFilter DNA plasmid | Qiagen, Germany |
| QIAquick PCR purification Kit | Qiagen, Germany |
| QIAquick Gel extraction Kit | Qiagen, Germany |

Kits were used according to the suppliers' protocols if not otherwise indicated.

**Buffer**

**Buffer for immunofluorescence analysis**

| | |
|---|---|
| Blocking reagent | 20 g BSA |
| | 2 ml Tween 20 |
| | 30 ml Glycerin |
| | 5 ml $NaN_3$ (10 % solution) |
| | add 1 liter PBS |
| | → filter |
| Glycine solution (0.1 M) | 3.75 g Glycine |
| | add 500 ml $ddH_2O$ |
| Triton solution (0.1%) | 0.1 ml Triton X-100 |
| | add 100 ml PBS |

**Buffer for Western blot analysis**

| | |
|---|---|
| 10% SDS | 50 g SDS |
| | 500 ml $H_2O$ |
| SDS sample buffer (2x) | 20 ml Glycerin (50 %) |
| | 5 ml DTT (1M) |
| | 10 ml SDS (10 %) |
| | 4.5 ml Tris-HCl (1 M, pH 6,8) |
| | 1 spatula tip of Bromophenol blue |
| RIPA buffer | 20 mM Tris-HCl, pH 7.5 |
| | 150 mM NaCl |
| | 10 mM EDTA |
| | 0.1% (w/v) SDS |
| | 1% (v/v) Triton X100 |
| | 1% (v/v) deoxycholate |

| | |
|---|---|
| | 10 mM iodacetamide |
| 1.5 M Tris pH 8.8 (SDS separation gel) | 181.71 g Tris |
| | add 1 liter dd$H_2O$ |
| | → adjust to pH 8.8 |
| 1.5 M Tris pH 6.8 (SDS stacking gel) | 181.71 g Tris |
| | add 1 liter dd$H_2O$ |
| | → adjust to pH 6.8 |
| Protein runnning buffer for SDS-PAGE (10x) | 10 g SDS |
| | 30 g Tris |
| | 144 g Glycine |
| | add 1 liter dd$H_2O$ |
| Western blot Anode buffer I | 36,34 g Tris |
| | 200 ml EtOH |
| | add 1 liter $H_20$ |
| Western blot Anode buffer II | 3.03 g Tris |
| | 200 ml EtOH |
| | add 1 liter $H_20$ |
| Western blot cathode buffer | 5,25 g 6-Aminocaproic acid |
| | 3,03 g Tris 200 ml EtOH |
| | add 1 liter $H_20$ |

**Buffer for Coimmunoprecipitation**

| | | |
|---|---|---|
| NP40 cell lysis buffer | 50mM HEPES pH 7.4 | 25 ml (1 M) |
| | 150mM NaCl | 30 ml (2.5 M) |
| | 1% NP40 | 5 ml |
| | | add 500 ml dd$H_2O$ |
| NaCl | 2.5M | 73.05 g |
| | | add 500 ml $H_2O$ |

## 4.4. Plasmids and Nucleic acids

**Plasmids**

| | |
|---|---|
| pMARV (+) (vector: Bluescript) | Enterlein et al., 2006 |
| pMBG-Apa/Sac (vector: Bluescript) | Enterlein et al., 2006 |
| pTM1- MARV NP | Mühlberger lab |

| | |
|---|---|
| pTM1- MARV VP35 | Mühlberger lab |
| pTM1- MARV L | Mühlberger lab |
| pTM1- MARV VP30 | Mühlberger lab |
| pCAGGS-T7 (RNA-dependent DNA T7 polymerase) | Mühlberger lab |
| pCAGGS-MARV NP | Mühlberger lab |
| pCAGGS- MARV VP35 | Mühlberger lab |
| pCAGGS-RESTV NP | Mühlberger lab |
| pCAGGS-RESTV VP35 | Mühlberger lab |
| pCAGGS-EGFP | Mühlberger lab |
| pGFP-250 | Garcia-Mata et al., 1999 |
| pGFP-p50 dynamitin | kindly provided by R. B. Vallee |
| pCAGGS-EBOV NP | Mühlberger lab |
| pCAGGS-EBOV VP30 | Mühlberger lab |
| pcDNA3.1-EBOV $VP35_{HA}$ | Mühlberger lab |
| pCK-$PACT_{Flag}$ | Kindly provided by N. Kim (Lee et al., 2006) |
| pcDNA3- EBOV VP35-$3A_{HA}$ | Mühlberger lab |
| pCAGGS-VP24 EBOV | Mühlberger lab |
| pCAGGS-GP EBOV | Mühlberger lab |

**Generated plasmids**

| | |
|---|---|
| rMARV-EGFP (vector: Bluescript) | Schmidt et al., 2011 |
| rMARV-EGFP-KanR (vector: Bluescript) | |
| rMARV-AvrII (vector: Bluescript) | |
| rMARV-AvrII-KanR (vector: Bluescript) | |
| pMBG-Apa/Sac-AvrII (vector: Bluescript) | |

**Primer**

| | |
|---|---|
| #2070 EGFP-fwd 1 | GCAAGGGCGAGGAGCTGTTCACCGGG |
| #2071 EGFP-rev 1 | GCGGTTCACCAGGGTGTCGCCCTCG |
| # 867 EGFP | CAC CCA GTC CGC CCT GAG CAA AGA C |
| #122 MARV VP40 NTR | GGA CAA TTT AAG TAA CAA TTA A |

## 4.5. Enzymes and antibodies

### Restriction enzymes

| | |
|---|---|
| AvrII | NEB |
| ApaI | NEB |
| SacI | NEB |
| Eco47III (AfeI) | Fermentas |

### Primary antibodies

| | |
|---|---|
| eIF3eta (N-20) goat | Santa Cruz Biotechnology |
| HuR mouse | Santa Cruz Biotechnology |
| phospho-PKR (pT446) Rabbit (1120-1) | Epitomics |
| PKR mouse | BD Bioscience |
| eIF2α mouse | Biosource |
| phospho-eIF2α rabbit | Biosource |
| β-actin | Abcam |
| GFP B-2 | Santa Cruz Biotechnology |
| HA.11 Clone 16B12 mouse (Monoclonal) | Covance |
| Flag M2 mouse | Sigma |
| | |
| rabbit anti-NC MARV antiserum | Mühlberger lab |
| goat anti-MARV antiserum | Mühlberger lab |
| goat anti-EBOV antiserum, cross-reacts with RESTV NP | Mühlberger lab |
| mouse anti-EBOV VP35 | Kindly provided by C. Basler |
| mouse anti-EBOV NP | Mühlberger lab |
| rabbit anti-EBOV VP30 | Mühlberger lab |

### Secondary antibodies

| | |
|---|---|
| IRDye800-conjugated donkey anti-mouse | Rockland |
| Cy3 donkey anti-rabbit | Dianova |
| FITC donkey anti-mouse | Dianova |

| | |
|---|---|
| Alexa Fluor 647 donkey anti-rabbit | Invitrogen |
| Alexa Fluor 647 goat anti-mouse *highly cross-adsorbed* | Invitrogen |
| Alexa Fluor 594 donkey anti-goat | Invitrogen |
| Alexa Fluor 594 anti-mouse | Invitrogen |
| DyLight 594 donkey anti-rabbit | Jackson ImmunoResearch |
| Alexa Fluor 568 donkey anti-rabbit | Invitrogen |
| Alexa Fluor 488 chicken anti-mouse | Invitrogen |
| Alexa Fluor 488 goat anti-rabbit | Invitrogen |
| Alexa Fluor 350 donkey anti-rabbit | Invitrogen |

## 4.6. Cells and Viruses

**Prokaryotic cell lines**

| | |
|---|---|
| NEB-10 beta competent *E.coli* (C3019) | NEB |
| NEB turbo competent *E.coli* | NEB |

**Eukaryotic cell lines**

| | |
|---|---|
| HEK293T cells | Mühlberger lab |
| HeLa cells | Mühlberger lab |
| Human epithelial osteosarcoma (U2OS) cells | ATCC #HTB-96 |
| U2OS-derived stable cell lines: U2OS G3BP-EGFP and U2OS DCP1a-mRFP | Kindley provided by N. Kedersha Harvard Medical School (Kedersha et al, 2008) |
| Human fibro sarcoma (HT-1080) | Mühlberger lab |
| African green monkey (*Cercopithecus aethiops)* Vero E6 cells (organ: kidney) | ATCC #CRL-1586 |

Eukaryotic cell lines were maintained in Dulbecco's modified Eagle medium (DMEM) supplemented with penicillin (P) (50 units/ml), streptomycin (S) (50 mg/ml), L-glutamine (L-Gln) and 10% (v/v) fetal calf serum (FCS).

**Viruses**

| | |
|---|---|
| *Marburg marburgvirus* (Musoke) | Institute for Virology, Marburg |
| *Zaire ebolavirus* (Mayinga isolate) | Center of Diseases Control (CDC), Atlanta |
| *Zaire ebolavirus* (Kikwit 95 isolate) | NIAID, Rocky Mountain Laboratories, (Hamilton) |

## 4.7. Virus work performed under BSL 4 conditions

The work was performed under Biosafety level (BSL) 4 conditions at the facilities of the Philips University Marburg, Germany and at the National Institute of Allergy and Infectious Disease (NIAID), Rocky Mountain Laboratories, USA. All virus work was performed in a Biosafety Cabinet (BSC) inside the BSL 4 laboratory.

### 4.7.1 Infection of cells with Ebola virus and Marbrug virus

The infection of cells with *Zaire ebolavirus* (EBOV) (Kikwit isolate, $3x10^6$ plaque forming units (PFU)/ml) or recombinant EBOV-EGFP ($1x10^7$ PFU/ml) at a multiplicity of infection (MOI) of 1 was performed at the BSL 4 facility of the NIAID, USA. The infection of cells with recombinant Marburg virus (recMARV) or rMARV-EGFP at different MOI (as indicated) was performed by Dr. Schümann at the BSL 4 facility of the Philips University Marburg, Germany.

For infection, the medium of the cells was removed and cells were inoculated with 0.5 ml virus, diluted in DMEM supplemented with 2% FCS and incubated for 1 hour at 37 C in a cell incubator. After the incubation time the inoculum was replaced by fresh DMEM supplemented with 2% FCS. At indicated days post infection (dpi) cells were inactivated according to the following protocol and brought out of the BSL 4 facility.

### 4.7.2 Propagation and isolation of Ebola virus

Virus stocks were generated for EBOV. 30 – 50% confluent Vero E6 cells, seeded in 175 $cm^2$ cell culture flasks were inoculated with 10 ml of a 1:10 dilution of EBOV in DMEM (2% FCS) and incubated for 1 hour at 37 C (see infection). After the incubation time, 35 ml DMEM (2% FCS) were added and the cells were incubated at 37°C until a cytopathic effect (CPE) was visible (3 – 6 days). The virus containing supernatant fluid was then transferred to 50 ml Falcon tubes and centrifuged at 5000 rpm for 10 minutes at 4°C, in order to remove cell debris. The supernatant containing isolated virus was either stored at 4°C for experiments or further purified and concentrated by ultracentrifugation (see 4.7.3).

### 4.7.3 Purification and concentration of Ebola virus stocks via ultracentrifugation

Ultracentrifugation was used to concentrate EBOV. Loading and unloading of the aerosol tight ultracentrifugation buckets takes place in the BSC. 25 ml supernatant of isolated virus was pipetted in each polyallomer ultracentrifugation tube. 5 ml of a 20 % sucrose solution (w/v) was pipetted carefully along the wall of the ultracentrifugation tube to underlay the supernatant. Each tube was then filled with additional 5 ml of supernatant up to ~ 1 cm underneath the rim of the polyallomer tube. All tubes were balanced to less than 0.08 g difference between the tubes using a precision scale. The tubes were loaded into the buckets, which are aerosol tight. Then the buckets are placed in the rotor and centrifuged at 25000 rpm for 2 hours at 4°C (Beckmann Ultracentrifuge). After unloading, the supernatant was removed and each concentrated virus pellet was

resuspended in 0.5 ml PBS. Aliquots were frozen at -80°C and then placed in liquid nitrogen for long-term storage.

### 4.7.4 Determination of virus titer by $TCID_{50}$

EBOV titer was determined by using the Tissue Culture Infectious $Dose_{50}$ ($TCID_{50}$) assay. This endpoint dilution assay quantifies the amount of virus required to produce a CPE in 50% of the infected samples. $5x10^3$ Vero E6 cells were seeded in 180 µl DMEM (2 % FCS) per well of a 96 well plates and infected at a confluence of 30 – 50%. For infection, the medium of the first column was replaced by 200 µl of the first virus dilution (dilution 1:1000). Then 20 µl of each well in the first column was pipetted to the next column and resuspended with the 180 µl medium in each well of the second column. Fresh tips were used for each column to avoid a carry-over of virus at the tip. Diluted virus was used in the first four rows and two rows of cells were uninfected and used as control. The dilutions were between $10^{-3}$ and $10^{-10}$. The 96-well plate is incubated at 37°C and monitored daily by brightfield microscopy until a pronounced CPE is visible (minimum of 7 days). TCID50 was evaluated for the wells showing a CPE and the titer was determined by using the Spermann-Kärber method (Hierholzer and Killington, 1996)

## 4.8. Propagation, isolation and preparation of nucleic acids

Recombinant plasmid DNA was propagated by DNA transformation in Z-competent bacteria (NEB-10 beta competent *E.coli* or NEB turbo competent *E.coli*). Transformation was performed according to the manufacture's protocol. After bacteria propagation, DNA was isolated form the bacteria culture and purified.

**Plasmid preparation**

5 ml (small scale) or 150 ml (large scale) bacteria culture transformed with recombinant plasmid DNA was incubated over night at 37°C in a bacteria shaker (~200 rpm). Plasmid DNA preparations were performed according to the manufacture's protocols (Qiagen Miniprep and QIAfilter).

**TRIZOL RNA isolation**

Total RNA form rMARV-EGFP infected cells and supernatant were isolated using TRIZOL reagent according to the manufacture's recommendation. The isolated 20 µl RNA was amplified by reverse transcription-PCR.

**Reverse transcription-PCR (RT-PCR)**

RT-PCR is a two-step process in which a specific primer binds to an RNA template flanking the region of interest. This region is reverse transcribed to DNA and them amplified. The 20 µl RNA was denatured at 65°C for 10 minutes and then immediately transferred and incubated on ice. 2 µl RNA was used for the reverse transcription using the OneStep RT-PCR kit from Qiagen. The kit has the advantage that the reverse transcription and the PCR are carried out sequentially in one process. RT-PCR was carried out according to manufacture's standard protocol.

## 4.9. Transfection of eukaryotic cell lines

### 4.9.1 Lipid based transfection

For immunofluorescence analysis, cells were grown on glass coverslips in 6-well plates and transfected using FuGeneHD (HT1080) and *Trans*IT-LT1 (U2OS cells) according to the supplier's protocols.

### 4.9.2 Calcium-phosphate transfection

HEK293T cells were seeded in a 10cm-dish and transfected at a 60% confluence.

Transfection procedure using the CalPhos$^{TM}$ mammalian Transfection Kit:

x µl (24 µg) DNA

62 µl Calcium - solution

Add 500ul $H_2O$

$H_2O$ and DNA were pipetted in a 1.5 ml tube. 62 µl of Calcium solution was added, each sample was vortexed immediately.

The 2x HEPES buffered saline (HBS) was distributed into 500 µl aliquots in sterile 5 ml polystyrene tubes. During vortexing, the Calcium-DNA-$H_2O$ mix was added drop wise into the swirling 2x HBS and then incubated for 20 minutes at room temperature. After the incubation period a sample containing a total volume of 1 ml was pipetted drop wise on the HEK293T cells in 15ml 10% FCS DMEM supplemented with L-GLN and P/S. After an incubation period of 24 hours the DMEM medium was exchanged. At 48h post transfection the samples were harvested.

## 4.10. Analysis of proteins

### 4.10.1 Coimmunoprecipitation (CoIP)

Harvesting of transfected samples (transfection see above 4.9.2):

1. 4x 10 cm dishes each: 12 µg pCAGGS-EGFP + 12 µg pcDNA3.1-EBOV-VP35$_{HA}$

2. 4x 10 cm dishes each: 12ug pCAGGS-EGFP + 12 µg pCK-PACT$_{Flag}$

3. 4x 10 cm dishes each: 12 µg pcDNA3.1-EBOV-VP35$_{HA}$ + 12 µg pCK-PACT$_{Flag}$

Transfection (1. – 3.), which was performed in duplicate, were either treated with 2 mM As or left untreated and incubated for 30 minutes at 37°C. In addition, two sets (minus and plus As) were transfected. One was used for a pull-down using antibodies directed against the HA-tag and one was used with antibodies directed against the Flag-tag (see below). Cells were harvested for coimmunoprecipitation.

*Preparation*: The protein A/G-coupled agarose beads are stored in an Ethanol solution. Therefore they must be washed after removal of the Ethanol. 500 µl aliquots of the protein A/G- coupled beads are washed twice in 1000 µl of NP40 buffer plus protease inhibitor cocktail (PI) (dilution 1:500) by vortexing and centrifugation at full speed in a tabletop centrifuge for 20 seconds to pellet the beads. The second time the liquid above was removed, the volume of the beads was estimated in order to add the same volume of NP40 buffer plus protease inhibitor cocktail (dilution 1:500), resulting in a 50% slurry of beads which can be stored at 4°C.

HEK293T cells (samples 1. – 3.) were harvested on ice. Adherent cells were detached by gently pipetting down using 10 ml ice-cold PBS, then transferred to a 15 ml tube. The 15 ml tubes were centrifuged at 1000 rpm for 5 minutes at 4°C. The supernatant was discarded and the cell pellet was resuspended in 0.5 ml ice-cold PBS, transferred to 1.5 ml tubes and centrifuged at 13000 rpm in a tabletop centrifuge for 1 minute at 4°C. The supernatant was discarded and the cells were lysed by adding 1 ml of NP40 buffer plus PI (dilution 1:500). This was mixed by vortexing vigorously for 45 seconds. Cell lysate was then centrifuged at 13000 rpm for 20-30 minutes in a pre-cooled tabletop centrifuge and transferred to a new 1.5 ml tube on ice. An aliquot of 50 µl from the whole cell lysate (WCL) was removed and mixed with 50ul of 2-fold Laemmli loading buffer for Western blot analysis.

Binding of antibodies:

The remaining 950 µl of cell lysate was processed for CoIP by adding 2 µl of either a mouse anti-Flag antibody or a mouse anti-HA antibody and incubated in an overhead rotator at 4°C over night.

Binding of protein A/G-coupled beads:

40 µl of the 50% slurry of beads (see above: preparations) were pipetted into the cell lysate on ice and incubated overhead rotating for 2 hours at 4°C. In order to keep the 50% slurry from separating, it must be vortexed before pipetting to each sample.

CoIP:

After the incubation CoIP samples were washed with 1ml NP40 buffer plus PI (dilution 1:500) on ice. Each sample was vortexed vigorously for 30 seconds and subsequently the beads were pelleted by centrifugation in a tabletop centrifuge at 13,000 rpm for 20 seconds. The supernatant was removed by using a needle (pink, 18G1 ½ 305196 BD), except for a small volume, which was left to not accidently discard the beads.

After the last washing step all supernatant was removed using a needle (brown, Q 305115 BD), which is small enough to not let any beads through. All remaining liquid was removed from the beads by holding the needle in the middle of the beads and moving it around. The beads dry and turn white. Then 40 µl of the 2-fold Laemmli loading buffer was added to the CoIP samples. The CoIP samples and the WCL samples were incubated at 95C for 5 minutes, then vortexed for 2 seconds and centrifuged in a tabletop centrifuge at full speed for 1 minute. All supernatant of the CoIP samples was transferred to a new 1.5 ml tube. The CoIP samples were subsequently subjected to Western blot analysis

## 4.11. Western blot analysis of infected and transfected samples

### Harvesting of whole-cell lysates of EBOV infected cells

Whole-cell lysates of infected samples were prepared. Cells in a 6 well plate were scraped off into a 50 µl cell lysis buffer, transferred to a 1.5ml tube, and incubated for 20 minutes on ice. PI and the serine/threonine phosphatase inhibitor Calyculin A (0.1 µM) were added to cell lysis buffer prior to incubation. During the incubation, samples were mixed by vortexing. After the incubation, cells were centrifuged at 14,000 rpm for 10 minutes at 4°C. The supernatant was transferred to a fresh 1.5 ml tube. EBOV-infected samples were mixed with 50 µl 2x SDS sample buffer and boiled for 10 minutes before the samples were brought out for Western blot analysis.

### Electrophoresis of proteins

Binding of SDS to proteins results in a negative charged denatured protein - SDS complex. Proteins of different molecular weight can be separated by SDS-polyacrylamide gel electrophoresis (SDS-PAGE).

| | Stacking gel | Separation gel | |
|---|---|---|---|
| | 4% | 10% | 12% |
| 1.5 M Tris pH 8.8 | | 2.5 ml | 2.5 ml |
| 1.5 M Tris pH 6.8 | 1.25 ml | | |
| H2O | 2.9 ml | 4.0 ml | 3.3 ml |
| Polyacrylamide | 750 µl | 3.3 ml | 4 ml |
| 10 % APS | 50 µl | 100 µl | 100 µl |
| TEMED | 5 µl | 5 µl | 5 µl |

Table 1: SDS-gel components

SDS gels were loaded with samples and run at 140-180 V.

### Western blot analysis

The proteins run in an SDS-PAGE were transferred to a membrane for specific detection using antibodies directed against the protein of interest. The membrane was activated by 1 minute incubation in 100% MeOH and then incubated in Anode buffer II until the blot was assembled. Whatman papers were soaked in either Anode buffer I, II, or Cathode buffer and the blot was assembled in the blotting chamber as shown in Figure 14. Transfer by blotting is done by 30 V for 30 minutes (fast blot).

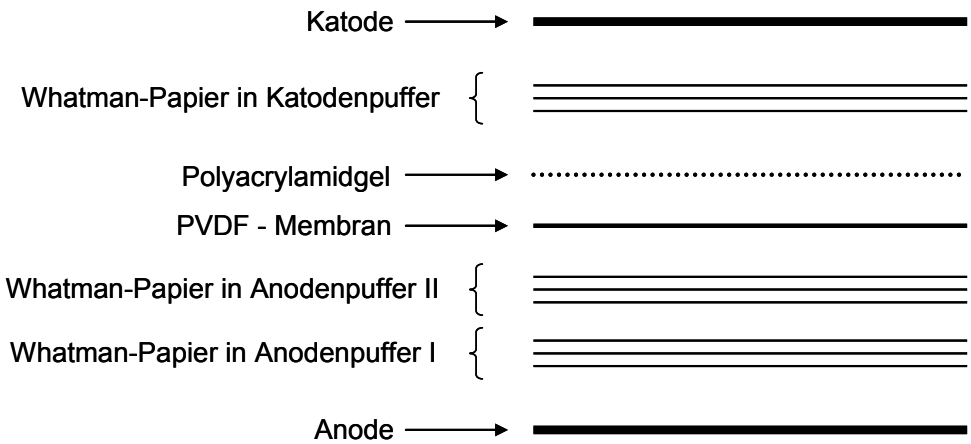


*Fig. 14: Western blot set up.*

After blotting, blots were incubated in 5% milk powder for 1 hour and then detected by specific antibodies targeting the protein of interest. In between antibody incubations blots were washed 3 times in TBS supplemented with Tween for 5 minutes.

Western blot detection was done with horseradish peroxidase-conjugated secondary antibody using an enhanced chemiluminescence detection reagent kit (Pierce) according to the manufacturer's protocol.

## 4.12. Immunofluorescence analysis of infected and transfected samples

At indicated days post infection (dpi) or post transfection (dpt) cells were treated with As or Hip (concentration indicated) for 30 minutes at 37°C or left untreated. Virus-infected cells were fixed and inactivated for 1 day with 4% PFA (v/v) at 4°C or room temperature. To assure proper inactivation the glass cover slips were transferred to a 24 well plate containing fresh 4% PFA (v/v) and incubated for another day before being brought out of the BSL 4 facility. After the inactivation period, cells were subjected to immunofluorescence analysis. Transfected cells were fixed in 4% PFA (v/v) for 20 minutes to 1 hour and subjected to immunofluorescence analysis. Permeabilization was either done by acetone/methanol treatment for 5 min at -20°C or by treatment with 0.1% (v/v) Triton X100 for 5 min at room temperature. Primary antibodies were diluted (as indicated) in 25 µl of blocking reagent and cells on glass cover slips were placed upside down in the antibody dilution and incubated for 1 hour (or as indicated) in a wet chamber at room temperature. After the incubation, the cells were washed 3 times with PBS and the secondary antibody incubation was performed in the same manner as the primary. After incubation of the secondary antibodies, the cells were washed 3 times for 10 minutes and mounted with mounting solution on glass slides.

All immunofluorescence analysis imaging was performed using a Zeiss Axiovert 200 M inverted microscope at a magnification of 63x (or as indicated).

# 5. Results

## 5.1. Generation of a recombinant Marburg virus clone expressing EGFP

The rMARV-EGFP infection experiments in this part of the results section were performed in collaboration with Dr. M. Schümann at the University of Marburg, Germany and resulted in a publication (Schmidt et al., 2011).

The aim of this work was to generate a recombinant Marburg virus (rMARV) containing an additional transcription unit (ATU) expressing EGFP that allows for the visualization of MARV spread in infected cells by fluorescent microscopy.

### 5.1.1 Cloning and characterization of the rMARV expressing EGFP

The following cloning strategy was used for generating the rMARV, which contains an ATU expressing EGFP.

The EGFP ORF was inserted into the intergenic region between the second and the third gene, encoding VP35 and VP40, respectively (Fig. 15). The rationale for positioning of the EGFP ORF near the 3' end of the viral genome was to maximize the number of EGFP transcripts and thereby increase the sensitivity for virus detection. At the same time, the ratio of the proteins NP and VP35 (first and second gene in the MARV genome) was not altered because it is known to be critical for the replication efficiency in the MARV minigenome system (Muhlberger et al., 1998). To keep the protein ratio in balance, EGFP was inserted at the third position instead of the second.

The pMARV(+) plasmid containing the full-length anti-genomic cDNA of MARV strain Musoke (described in (Enterlein et al., 2006; 2009)) was used as a template. First, an additional restriction site, AvrII, was inserted into the intergenic region (IR) between the second and the third genes (Fig 15). The intergenic region spanning 5 nts (CTATG) was mutated by in vitro mutagenesis, generating the AvrII restriction site (CCTAGG; inserted or substituted nts are underlined). Mutagenesis of the 22,152 kb pMARV(+) plasmid is both difficult and error prone due to its large size. Therefore, a shuttle plasmid containing only a part of the MARV genome was used for

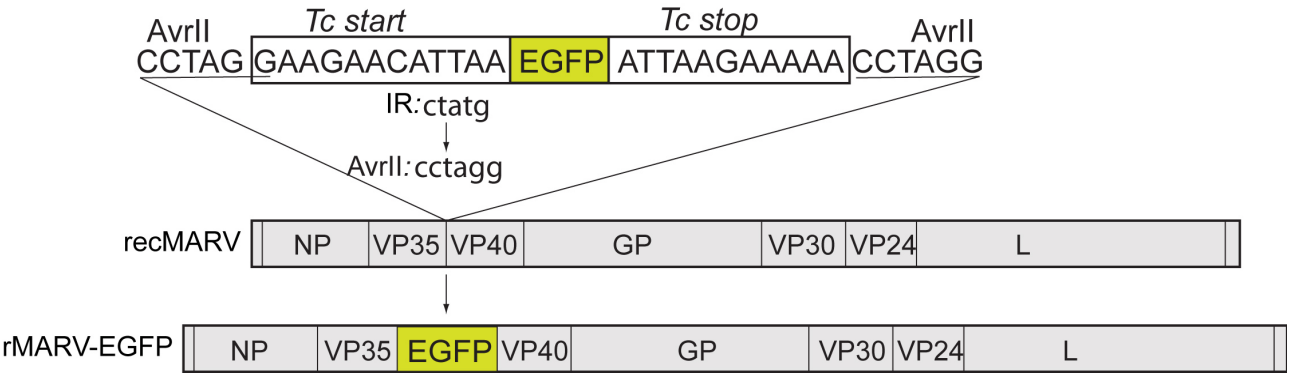


*Fig. 15: Scheme of rMARV-EGFP genome. The EGFP coding sequence is flanked by conserved MARV transcription start and stop signals. The EGFP ORF was inserted between the VP35 and VP40 gene via a newly created AvrII restriction site within the intergenic region (IR). The intergenic region spanning 5 nts (CTATG) was altered to CCTAGG.*

insertion of the AvrII recognition site. This pMBG-Apa/Sac plasmid (described in (Enterlein et al., 2006)) contains a part of the MARV Musoke genome, spanning nucleotides 3919-8991 (GenBank accession number DQ217792). This region includes the 3' end of the VP35 gene, the complete VP40 and GP genes, and the 5' end of the VP30 gene. Following the insertion of the AvrII site, the mutated region was cut out of the shuttle plasmid using the enzymes ApaI and SacI, which are also present in pMARV(+). This cloning step turned out to be highly inefficient. In order to increase efficiency and to successfully select for positive bacteria clones containing the mutated pMARV(+) plasmid including the AvrII site, a kanamycin antibiotic resistance gene (KanR) was inserted into the AvrII site of the pMBG-Apa/Sac-AvrII shuttle construct. The resulting plasmid pMBG-Apa/Sac-AvrII-KanR allowed the insertion of the AvrII site into the pMARV(+) using the restriction enzymes ApaI and SacI. The kanamycin resistance gene was removed from the rMARV-AvrII-KanR cDNA clone by digestion with the AvrII enzyme and subsequent re-ligation. The AvrII site within the MARV full-length cDNA clone (rMARV-AvrII) was then used to insert the ATU consisting of the EGFP ORF flanked by conserved MARV transcription-start and -stop signals (Fig. 15) and AvrII sites. Since this cloning step turned out to be very inefficient as well, the clone selection approach described above was used again. The EGFP gene contains a unique restriction site, which is not present in the rMARV-AvrII clone. This restriction site, *Eco47III*, was used to insert the KanR gene with flanking *Eco47III* sites into the EGFP ORF. Then, the EGFP-KanR construct, flanked by *AvrII* sites was cut using the *AvrII* restriction enzyme and ligated into the rMARV-AvrII plasmid cut with *AvrII*. The rMARV cDNA clone containing EGFP (rMARV-EGFP-KanR) was successfully selected taking advantage of the kanamycin resistance. Finally, the KanR gene was removed by digesting with *Eco47III* and re-ligating the rMARV-EGFP cDNA construct.

**Detection of recombinant genomes in supernatants and cell lysates of rMARV-EGFP-infected Vero E6 cells by reverse transcription PCR**

The rMARV containing the EGFP gene (rMARV-EGFP) was successfully rescued by Dr. Olga Dolnik under BSL 4 conditions at the Philips University Marburg. To verify stable integration of the EGFP gene in the viral genome, total RNA isolated from the supernatant of rMARV-EGFP infected Vero E6 cells was harvested. The isolated RNA was subjected to reverse transcription-PCR using primers flanking a 362 bp PCR fragment of the EGFP gene (#2070, #2071, for sequence see material and methods) (Fig. 16).

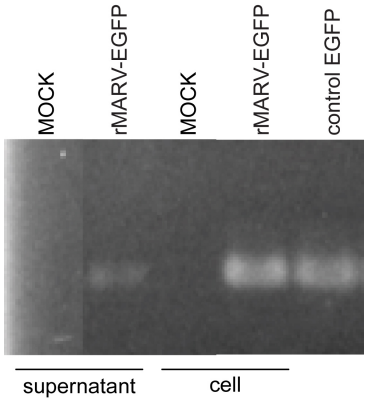


*Fig. 16: rMARV-EGFP cDNA confirming EGFP insertion. Vero E6 cells were infected with rMARV-EGFP and total RNA was isolated from cells and supernatants at 6 days post infection (dpi) using TRIZOL reagent. Cellular RNA from Vero E6 cells transiently expressing EGFP was used as a positive control. Total RNA was isolated and subjected to reverse transcription-PCR. cDNA was the separated on a 1% agarose gel and visualized using ethidiumbromide.*

RT-PCR was performed using primers binding in the EGFP ORF. Amplification of the PCR fragment confirmed that the rMARV-EGFP genome contains the inserted foreign gene (Fig. 16). Integration of EGFP in the MARV genome was also confirmed by sequencing the rMARV-EGFP plasmid DNA (#867, #122, primer sequences in material and methods).

Expression of EGFP in cells infected with rMARV-EGFP was analyzed by fluorescence microscopy (Fig. 17).

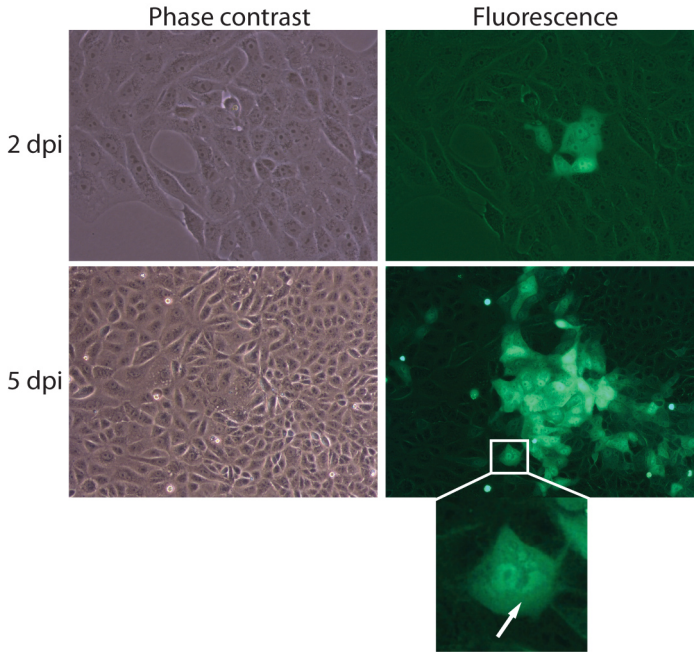


*Fig.17: Fluorescence microscopy of rMARV-EGFP-infected cells. $10^5$ Vero E6 cells were infected with rMARV-EGFP at a multiplicity of infection (MOI) of 0.05 in a 6-well plate. Living cells were analyzed by phase contrast and fluorescence microscopy. Images were collected at 2 and 5 dpi. Bottom panel shows rMARV-EGFP-infected cell at higher magnification. Aggregates of EGFP are indicated by an arrow. Images were taken by Dr. M. Schümann.*

Living cells were monitored for EGFP expression. Foci formation of green fluorescent cells was initiated at 1-2 dpi without inducing visible cytopathic effects (CPE). The initial signs of CPE were observed at 5 dpi, when EGFP was detected in clusters of infected cells (Fig. 17). These data show that rMARV-EGFP productively infects susceptible cells and can be used as a sensitive marker to visualize virus spread over time. It was observed that the EGFP was not only homogeneously distributed in the cytoplasm of the cells but also formed aggregates (Fig. 17, arrow).

### Comparison of progeny production of recombinant wild-type MARV and rMARV-EGFP

To assess the replication efficiency of rMARV-EGFP compared to recombinant wild-type virus (recMARV; described in (Enterlein et al., 2006; Yi et al., 2011), foci of infected cells were counted by fluorescence microscopy (Fig. 18). Progeny virus production of rMARV-EGFP was approximately four-fold reduced compared to wild-type virus, indicating a growth restriction of the EGFP-expressing recombinant virus.

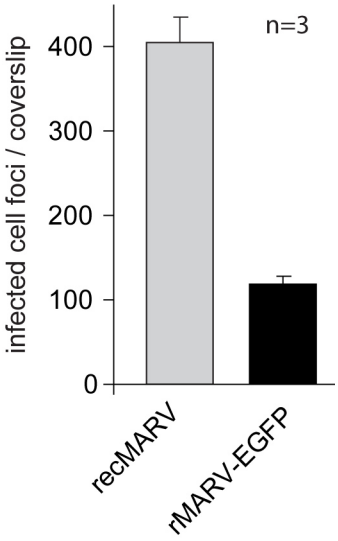


*Fig. 18: Virus titration performed by counting foci of infected cells. Supernatants of Vero E6 cells infected with recMARV or rMARV-EGFP (MOI=0.05) were collected at 6 dpi and used for infection of Vero E6 cells seeded on coverslips. At 2 dpi, cells were subjected to immunofluorescence analysis. Supernatants collected at 2 and 6 dpi, were purified by low-speed centrifugation, and 500 µl of the supernatants were used for infection of $10^5$ Vero E6 cells per well of a 6-well plate. At 2 dpi cells were fixed in 4% (w/v) paraformaldehyde for at least 24 hours, permeabilized with a mixture of acetone and methanol (1:1, v/v) for 5 min at -20°C, and incubated in blocking solution (10% (v/v) FCS in PBS++) for 10 min. Staining of infected cells was performed using an antiserum directed against MARV-specific nucleocapsid proteins (anti-NC antiserum) and an Alexa Fluor 568-conjugated donkey anti-rabbit secondary antibody. Foci of infected cells were counted by UV fluorescence microscopy. The experiment was performed in triplicate by Dr. M. Schümann. The bars represent mean values including standard deviations.*

To further address the growth restriction shown for rMARV-EGFP, the protein expression of both viruses was compared. The viral genes of the detected proteins were located either before or after the EGFP-insertion (Fig. 19).

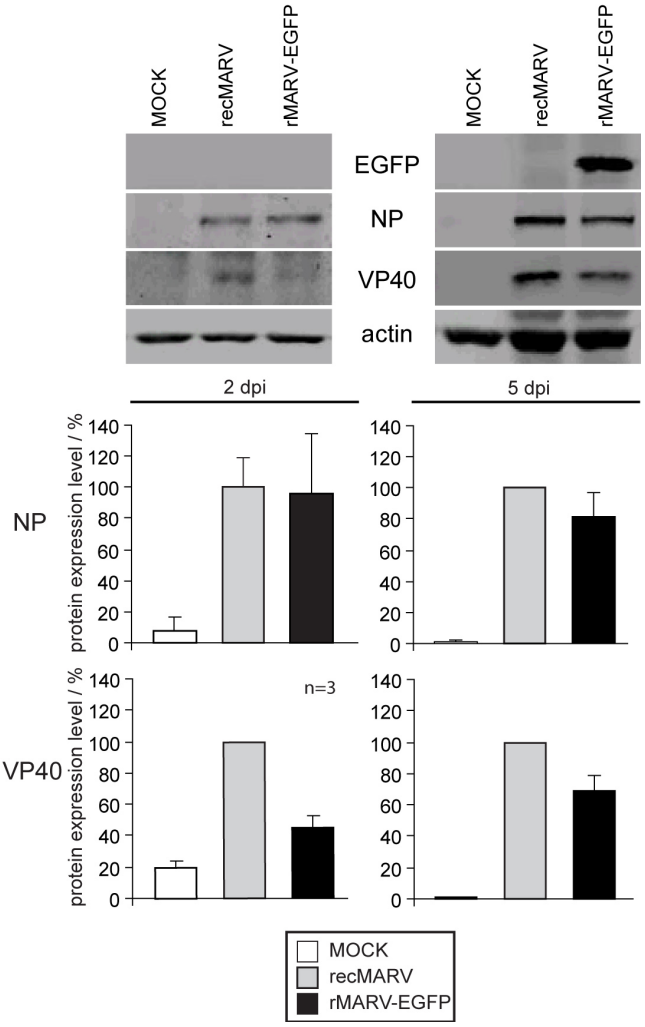

*Fig. 19: Quantitative Western blot analysis of virus protein and EGFP levels in Vero E6 cells infected with wild-type recMARV or rMARV-EGFP. Vero E6 cells were infected as described in Fig. 17. At 2 and 5 dpi, cells were scraped into 200 µl RIPA buffer and transferred to tubes containing 100 µl 4x protein loading buffer, boiled for 10 minutes and subjected to Western blot analysis. For Western blot analysis mouse monoclonal antibodies directed against EGFP (B-2; 1:5000 dilution), MARV NP (1:5000 dilution), MARV VP40 (1:1000 or 1:5000 dilution), and β-actin (1:10000 dilution) were used. IRDye800-conjugated donkey anti-mouse antibody was used as secondary antibody (1:10000 dilution). The intensity of the protein bands was quantified using an Odyssey imaging system (LI-COR) and standardized to β-actin. Assays were performed in triplicate by Dr. M. Schümann. Standard deviations are shown.*

While viral proteins could be readily detected at 2 dpi, EGFP accumulated to detectable levels only at 5 dpi, which might be due to differences in the sensitivity of the antibodies used (Fig. 19). NP levels were similar between recMARV and rMARV-EGFP at all time points, whereas VP40 levels were reduced in rMARV-EGFP-infected cells at 2 dpi and to a lesser extent at 5 dpi. Since the EGFP gene is located downstream of NP and upstream of VP40 gene (Fig. 19), the reduced VP40 expression in rMARV-EGFP indicates that the presence of the ATU causes a decrease in downstream protein expression, which might explain the slightly growth-restricted phenotype of rMARV-EGFP.

**Cell-to-cell spread of MARV-EGFP observed in live-cell imaging of infected cells**

Live-cell imaging was used to visualize the spread of rMARV-EGFP in cell culture. VeroE6 cells were infected with rMARV-EGFP and the cell monolayer was analyzed by collecting EGFP fluorescence and phase contrast photomicrographs. Photomicrographs of 25 different positions were captured every hour from 1 hpi for a period of 9 days ((Schmidt et al., 2011, supplementary movie; Ward et al., 2011). Single infected cells expressing EGFP were observed at 26 hpi. In most of the infectious centers, EGFP expression in neighboring cells was detected 20-30 hours later with a mean value of 24.6 hours, which correlates with the MARV Musoke replication cycle of approximately 21 hours (Muhlberger, 2004). However, in some infectious centers, EGFP expression in surrounding cells was observed as late as 48 hpi. Intriguingly, even late in infection, EGFP fluorescence was not homogenously distributed throughout the monolayer but restricted to individual foci, suggesting that virus spread occurred rather by direct cell-to-cell contact than by release of viral particles. Typically, individual infected cells were observed early in infection and later on the infection spread to cells in close proximity to the primarily infected cell (Fig. 20 and (Schmidt et al., 2011, supplementary movie). In addition, virus spread was promoted by viral replication in actively dividing cells (Fig. 20A and (Schmidt et al., 2011, supplementary movie).

After the first signs of CPE appeared at 5 dpi, the cell monolayer began to disintegrate at 6-7 dpi, followed by cell rounding and blebbing of EGFP-expressing cells, which correlates with impending cell death (Fig. 20B, arrows).

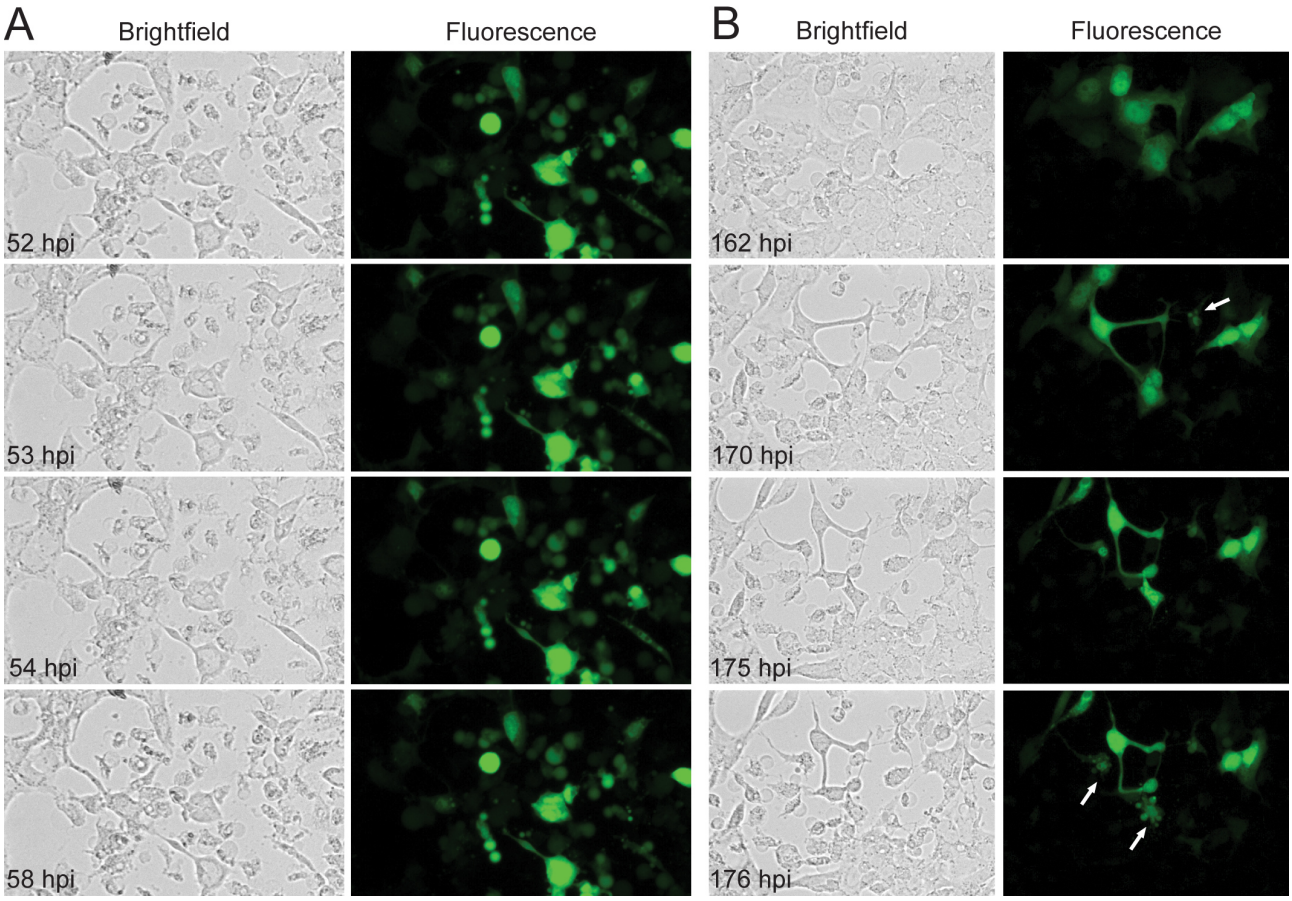


*Fig. 20: Time-lapse fluorescent microscopy of rMARV-EGFP spread. Vero E6 cells were infected with rMARV-EGFP at an MOI of 0.05 in a µ-Dish$^{35mm}$. At 1 hour post infection (hpi), the inoculum was replaced by GIBCO Leibovitz's L-15 Medium containing 20% (v/v) FCS. EGFP fluorescence and phase contrast images were captured every hour for a period of 9 days by an inverted fluorescence microscope (DM16000B Leica). (A) Cell division of infected cells. (B) Cytopathic effects at late stages of infection. Blebbing cells are indicated by arrows. Time points pi, when images were taken, are indicated. Images were taken with a 20x objective. Time-lapse experiment was performed by Dr. M. Schümann.*

rMARV-EGFP was successfully rescued and can be used as a tool for live cell imaging, allowing the investigation of intracellular dynamic processes during the course of infection. It also provides a fast and quantitative readout for antiviral drug screening assays and virus-spread studies.

### 5.1.2 EGFP accumulates in nucleocapsid protein-derived inclusion bodies

**EGFP accumulation during rMARV-EGFP infection**

Higher magnification of cells infected with rMARV-EGFP revealed that EGFP was not only homogenously distributed in the nucleus and in the cytoplasm, but was also observed in intracytoplasmic aggregates (see Fig. 17). Since MARV infection leads to the formation of inclusions in infected cells, we examined if the EGFP aggregates were colocalized with NC-derived inclusions. Therefore, at 2 and 5 dpi, rMARV-EGFP-infected cells were examined by indirect immunofluorescence using anti-NC antiserum recognizing the nucleocapsid proteins. EGFP autofluorescence was assessed in parallel.

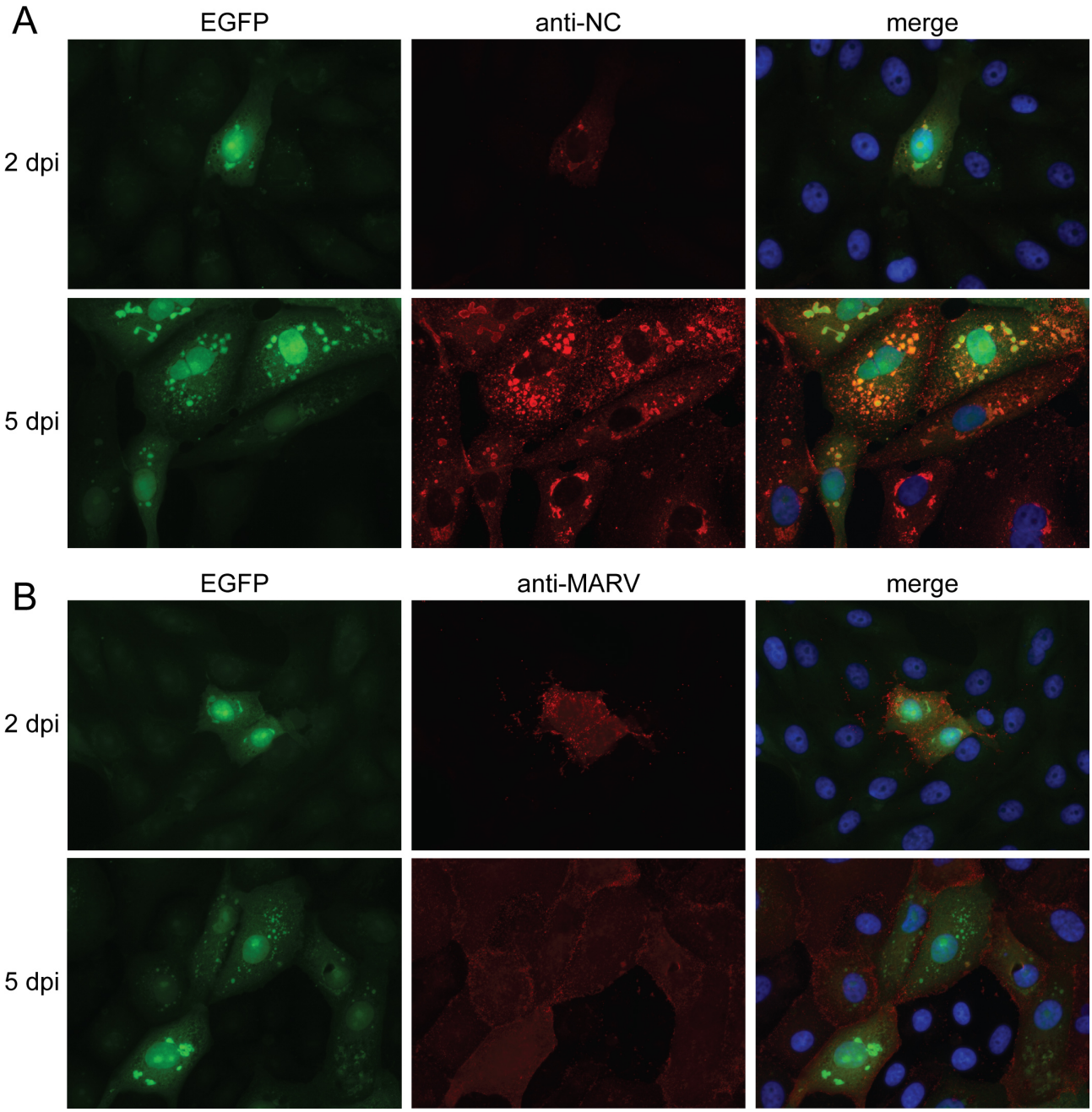


*Fig.21: Fluorescence microscopy analysis of EGFP and immunohistochemically labeled viral proteins in rMARV-EGFP-infected cells. Vero E6 cells were infected with rMARV-EGFP and subjected to immunofluorescence analysis at 2 and 5 dpi. Antibodies are directed against intracellular viral proteins (upper panels) or viral surface proteins (lower panels). $10^5$ Vero E6 cells per well of a 6-well plate were infected with rMARV-EGFP at a MOI of 0.05. At 2 and 5 dpi, cells were fixed in 4% (w/v) paraformaldehyde for at least 24 hours, permeabilized with a mixture of acetone and methanol (1:1, v/v) for 5 min at -20°C, and incubated in blocking solution (10% (v/v) FCS in PBS++) for 10 min. (A) As primary antibody, a rabbit antiserum directed against the nucleocapsid complex of MARV (anti-NC antiserum; 1:100) was used and a Alexa Fluor 568-conjugated donkey anti-rabbit secondary antibody (1:500 dilution). (B) A goat anti-MARV antiserum (1:500 dilution) was used, visualized by using a donkey anti-goat Alexa Fluor 594-labeled antibody (1:500 dilution). In addition, the cells were stained with 100 ng/ml 4'-6-diamidino-2-phenylindole (DAPI) for 10 min. Immunofluorescence was performed by Dr. M. Schümann.*

Cytoplasmic EGFP aggregates colocalized with MARV-induced inclusions (Fig. 21A). Interestingly, immunofluorescence analysis revealed infected cells that were stained with the virus-specific

antiserum but lacked detectable EGFP expression at 5 dpi, indicating that immunodetection using virus-specific antibodies is more sensitive than EGFP detection. To exclude the possibility of “cross-talk” or non-specific binding of antibodies, rMARV-EGFP-infected cells were stained with a goat anti-MARV antiserum that predominantly recognizes the MARV surface protein GP. Surface staining of infected cells was observed with the GP-specific antibody (Fig. 21B). However, green fluorescent inclusions were also visible (Fig. 21B).

**EGFP accumulates in nucleocapsid protein-derived inclusion bodies**

To further investigate the nature of the EGFP-positive viral inclusions, EGFP expression was monitored by live cell imaging in the absence or presence of MARV nucleocapsid proteins NP and VP35. U2OS cells were used for the transfection experiments because these cells are large and flat, resulting in high-quality images. U2OS cells were transfected with 500 ng or 50 ng EGFP expression plasmids along with plasmids encoding MARV NP and VP35 genes. When 50 ng of EGFP plasmid was used for transfection, EGFP accumulated in the nucleus but was also observed in the cytoplasm of transfected cells, where it was concentrated in inclusion-like aggregates surrounded by homogenously distributed protein (Fig. 22).

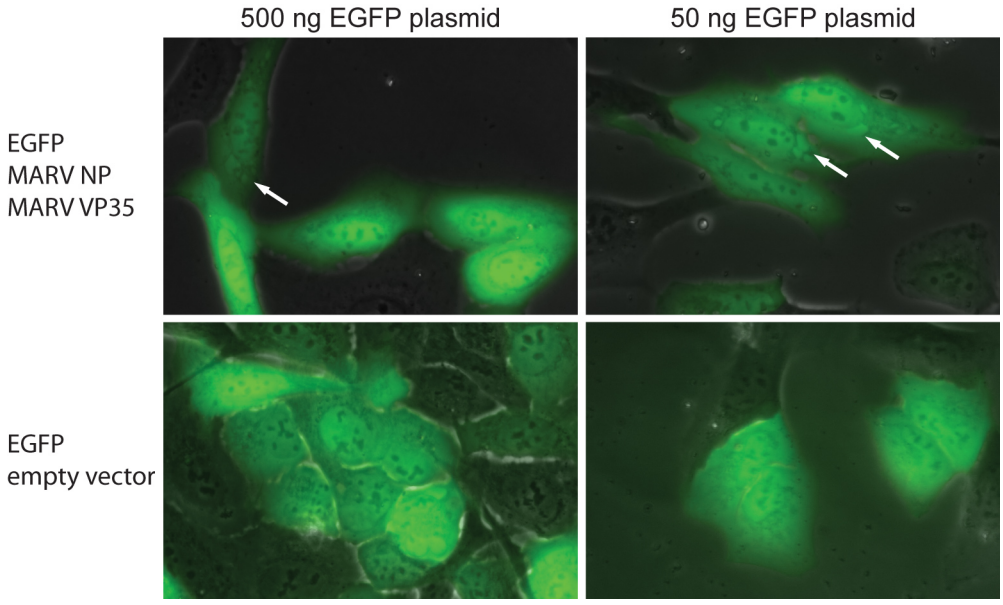


*Fig. 22: Live-cell imaging of EGFP colocalization with MARV inclusions formed by NP and VP35. U2OS cells were transfected with an EGFP expression construct alone or together with 500 ng plasmids DNA encoding MARV NP and MARV VP35, as indicated. EGFP autofluorescence is shown in green. Intracytoplasmic EGFP aggregates are indicated by arrows. Zeiss Axiovert 200 M inverted microscope was used for live-cell imaging of the transfected cells. Images were taken with a 40x objective.*

Cells in which EGFP was not concentrated in intracytoplasmic inclusions were also observed. However, since it was not possible to verify the expression of the nucleocapsid proteins in the live-cell imaging studies, it is not clear if these cells expressed NP and VP35. When 500 ng of EGFP plasmid was used for transfection, it was difficult to distinguish between concentrated EGFP and homogeneously distributed EGFP due to the high intensity of overexpressed EGFP. Inclusions

were only observed in a few cells with lower EGFP expression (Fig. 22). EGFP inclusions were not detected in cells expressing EGFP in the absence of NP and VP35 (Fig. 22, bottom panels).

### Driving force for EGFP relocalization

Next, the distribution of EGFP in transfected cells was analyzed by indirect immunofluorescence. Since aggregated EGFP could not be differentiated from the homogenous non-specific distribution when 500 ng EGFP plasmid was used for transfection, U2OS cells were transfected with 50 ng EGFP plasmid along with plasmids for NP and VP35 (Fig. 23A). As shown in the upper panels of Fig. 23A, EGFP was distributed in a punctate pattern and colocalized with intracytoplasmic nucleocapsid inclusions. Interestingly, the amount of intracytoplasmic homogenously distributed EGFP was reduced compared to the live-cell imaging data, which might be due to fixation and/or permeabilization effects, or due to the fact that EGFP is constantly being formed in the live cells, leading to limited bleaching. To exclude the possibility of antibody cross-reactivity, antibody staining was omitted. Fluorescence analysis revealed that EGFP was distributed in large cytoplasmic aggregates (Fig. 23A). In contrast, EGFP was homogenously distributed when expressed in the absence of NP and VP35 (Fig. 23A). Additionally, MARV NP and VP35 were individually expressed along with EGFP (Fig. 23B). NP-induced inclusion formation was sufficient for the relocalization and aggregation of EGFP. While EGFP colocalized with NP inclusions, it was homogeneously distributed in cells coexpressing VP35 and EGFP (Fig. 23B). Although the expression of VP35 in the absence of NP does not lead to inclusion formation, some VP35 aggregates were observed in cells expressing VP35 and EGFP. Interestingly EGFP did not colocalize with these aggregates (Fig. 23B).

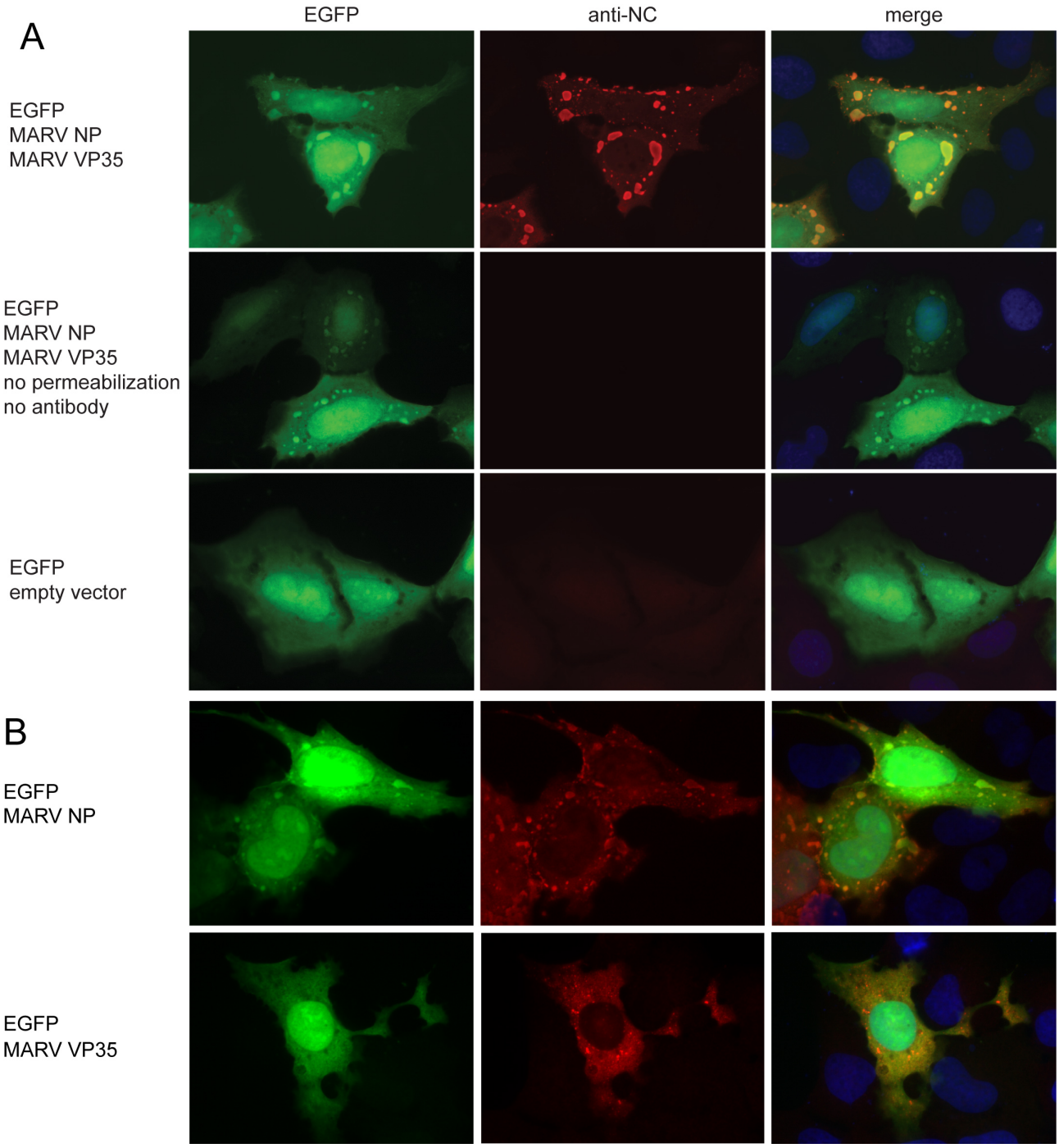


*Fig. 23: EGFP relocalization to MARV NP-derived inclusions. A. U2OS cells transfected with 50 ng EGFP plasmid along with 500 ng NP and 500 ng of VP35 plasmid. Cells were stained using a rabbit antiserum directed against the nucleocapsid complex of MARV (anti-NC antiserum; 1:100) or a goat anti-MARV antiserum (1:500 dilution). Antibody binding was visualized by using Alexa Fluor 568-conjugated donkey anti-rabbit secondary antibody (1:500) and donkey anti-goat Alexa Fluor 594-labeled antibody (dilution 1:500).* B. *U2OS cells transfected with 50 ng EGFP plasmid along with 500 ng of either NP or VP35 plasmid. Rabbit anti-NC antiserum (see A) and anti-rabbit Dylight 594-labed secondary antibody (dilution 1:100) were used for staining. U2OS cells were stained with 100 ng/ml 4'-6-diamidino-2-phenylindole (*DAPI) for 10 min (A and B).

### EBOV inclusion formation and EGFP

Next we addressed the question if the observed relocalization of EGFP in virus-derived inclusions was specific for MARV or could also be observed with other filovirus species. Therefore, EGFP was coexpressed with either *Reston ebolavirus* (RESTV) or EBOV NP and VP35 proteins. EGFP colocalized with both EBOV and RESTV inclusions (Fig. 24A), demonstrating that EGFP accumulation in inclusion bodies is not restricted to MARV. These observations were additionally verified in samples infected with a rEBOV expressing EGFP from an ATU between the first and the second gene in the viral genome (rEBOV-EGFP, kindly provided by H. Ebihara, published in (Ebihara et al., 2007)). EGFP expressed in rEBOV-EGFP-infected cells also colocalized with the viral inclusions (Fig. 24B). These data demonstrate that EGFP accumulation in inclusion bodies is not restricted to MARV but occurs irrespective of filoviral species.

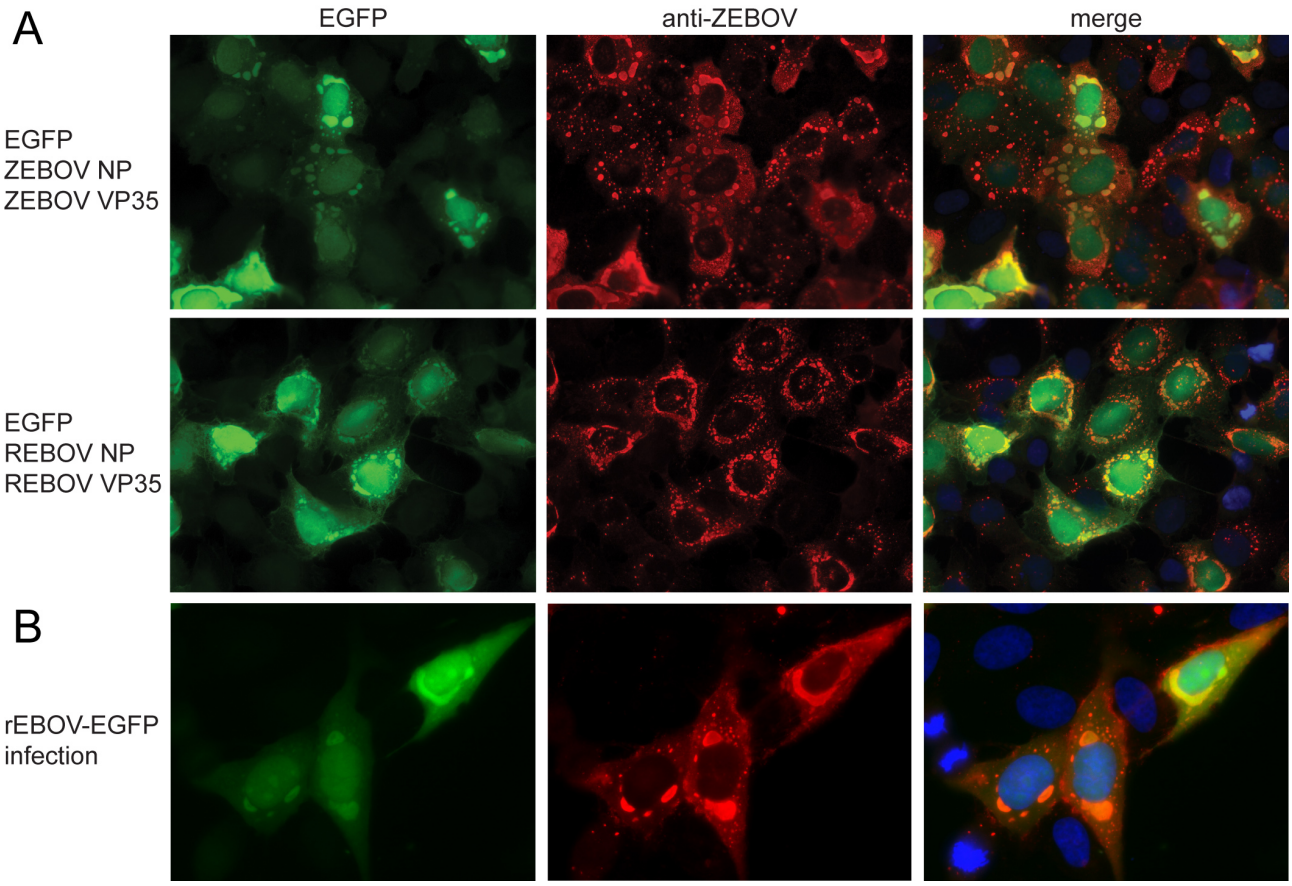


*Fig. 24: EGFP colocalization with EBOV. (A) Fluorescence microscopy analysis of EGFP coexpressed along with EBOV (upper panel) or RESTV (lower panel) NP and VP35 proteins in HT-1080 cells. Cells were subjected to immunofluorescence analysis at 1 day post transfection (dpt) using a goat anti-EBOV antiserum (1:500) that cross-reacts with RESTV NP. Experiments in A were performed by Dr. M. Schümann. (2) U2OS cells were infected with rEBOV-EGFP at an MOI of 1. At 1 dpi cells were fixed and subjected to immunofluorescence analysis using a goat antiserum directed against EBOV (1:500) and an anti-goat Alexa Fluor 594-labeled secondary antibody for detection.*

### Different fluorescent proteins relocated into the viral inclusions

To analyze if the association with filovirus inclusions is restricted to EGFP or can also be observed with other fluorescent proteins, we expressed MARV NP and VP35 proteins along with various fluorescent proteins from a range of different taxa and exhibiting different physico-chemical features. As genealogically different proteins, we selected TagRFP and DsRed, which share about 20% amino acid sequence identity with EGFP (Shaner et al., 2004; Chudakov et al., 2010). In addition, the monomeric mCherry derivative of the tetrameric DsRed was included (Shaner et al., 2004). Intriguingly, each of the fluorescent proteins colocalized with nucleocapsid-derived inclusions, when coexpressed with NP and VP35 (Fig. 25).

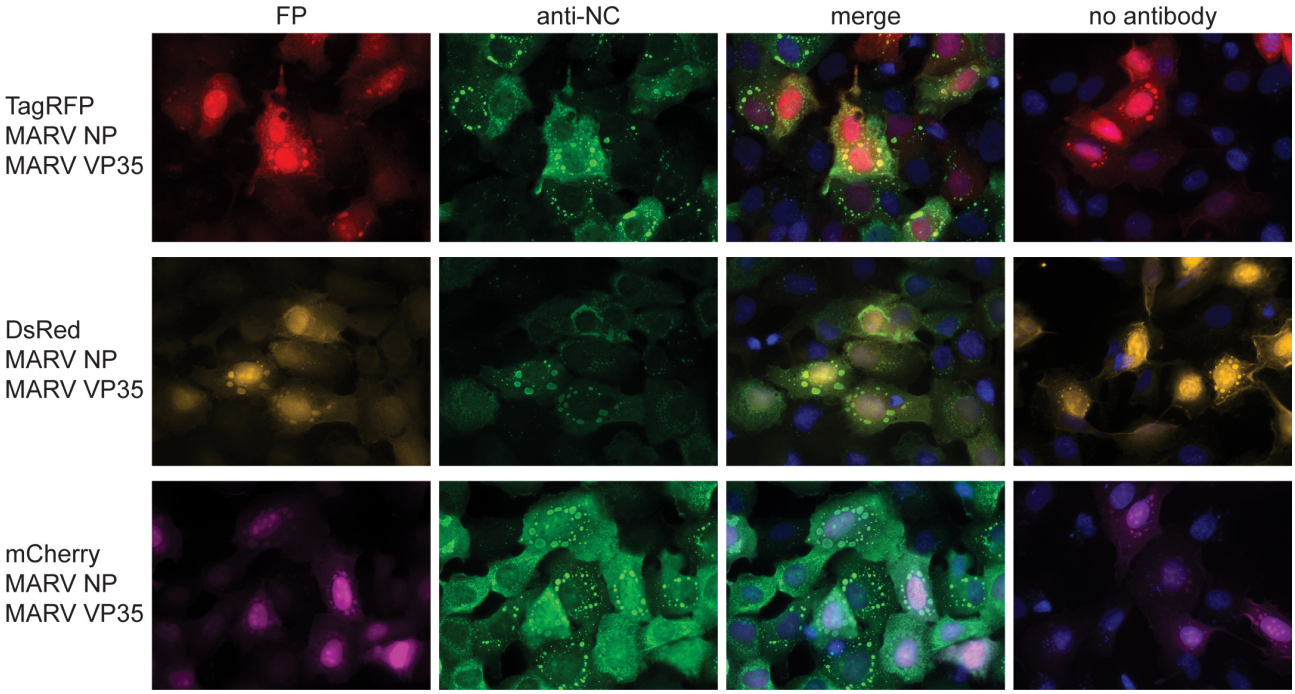


*Fig. 25: Accumulation of various coexpressed fluorescence proteins in inclusions induced by MARV NP and VP35. HT-1080 cells were transfected with 50 ng expression plasmid for TagRFP (red), DsRed (orange), or mCherry (pink) along with 500 ng of each MARV NP and VP35. For fluorescence microscopy analysis, samples were stained with either anti-NC antiserum (green) and DAPI (blue), or DAPI alone (right panels). FP: fluorescent protein. Experiments were performed by Dr. M. Schümann.*

Similar to EGFP, fluorescent inclusions were also observed when antibody staining was omitted (Fig. 25, right panels). As a control, the examined fluorescent proteins were expressed in the absence of NP and VP35 and were found to be homogeneously distributed in the cells (data not shown). These data demonstrate furthermore that accumulation of ectopically expressed proteins in NP-induced inclusions is not restricted to EGFP but a general feature of fluorescence proteins.

### GFP-tagged fusion proteins with altered localization do not colocalize with viral inclusions

To further analyze the relocation of ectopic fluorescent proteins, it was examined whether fluorescence-tagged proteins relocalized to NP-induced inclusions. Therefore, two host proteins

fused to GFP were tested for their ability to colocalize with inclusions formed by MARV NP and VP35 (Fig. 26).

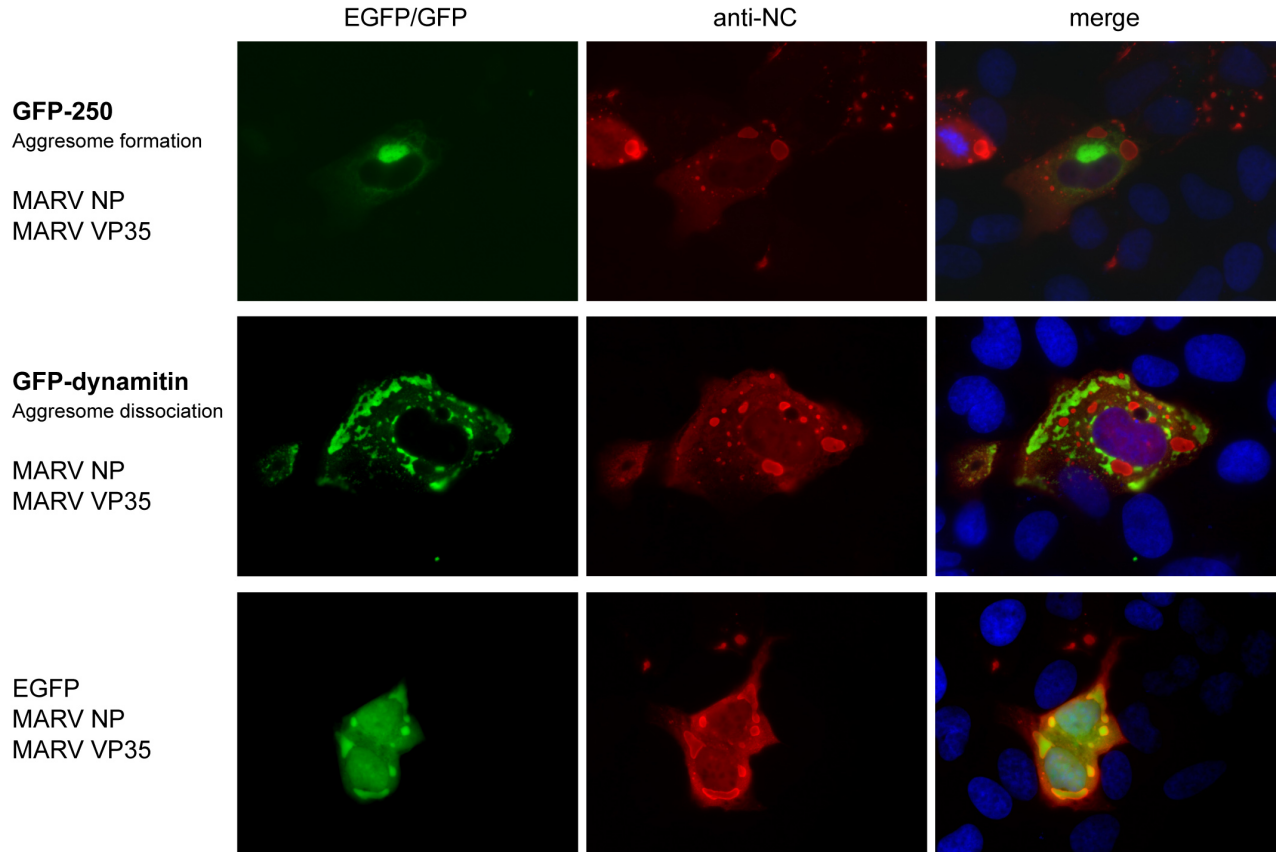


*Fig. 26: Ectopic GFP fusion proteins do not colocalize with viral inclusions. U2OS cells were transfected with plasmids encoding MARV NP and VP35$_{HA}$ along with GFP-250, GFP-dynamitin, or EGFP plasmid DNA. MARV inclusions were visualized using a rabbit serum directed against the MARV nucleocapsid (1:100) and an anti-rabbit Dylight 594-labled secondary antibody (1:100). Nuclei were stained with DAPI (1:2000).*

GFP-250 is a truncated version of the cellular protein p115 (containing the first 252 AS; kindly provided by E. Sztul, published in (García-Mata et al., 1999)). It has been shown that GFP-250 is a misfolded GFP fusion protein, which accumulates in aggresomes (García-Mata et al., 1999). Cells were transfected with GFP-250 plasmid DNA along with MARV NP and VP35. In the transfected cells, GFP-250 accumulated in juxtanuclear aggresomes as described in (García-Mata et al., 1999) and did not colocalize with NP-derived inclusions (Fig. 26).

The other fusion protein tested was GFP-dynamitin, which has been shown to block retrograde transport along the microtubules (kindly provided by R. B. Vallee). Since aggresome formation is dependent on dynein-mediated movement along the microtubules, inhibition of this microtubule function leads also to the inhibition of aggresome formation (García-Mata et al., 1999). GFP-dynamitin was coexpressed with MARV NP and VP35 (Fig. 26). NP-induced inclusion formation was observed in the cytoplasm of transfected cells. GFP-dynamitin was found in large aggregates in the cytoplasm of the cell, which did not colocalize with MARV inclusions.

These data show that GFP-tagged proteins, when targeted to specific cellular compartments/sites, are not redirected to MARV inclusions, indicating a weak interaction between EGFP and the NP-induced inclusions that can easily be overcome by specific localization signals.

### EGFP antibodies did not penetrate NP-induced inclusions

It is shown above that ectopically expressed fluorescent proteins relocalized into viral inclusions. Thus, it is imaginable that other ubiquitously expressed proteins also relocate but are not detected in the NP-derived inclusions via antibody staining. Accordingly, only autofluorescence proteins would be detectable inside the inclusions. Therefore, it was analyzed if antibody detection of EGFP proteins relocated to the inclusions formed by EBOV NP and VP35 is possible (Fig. 27).

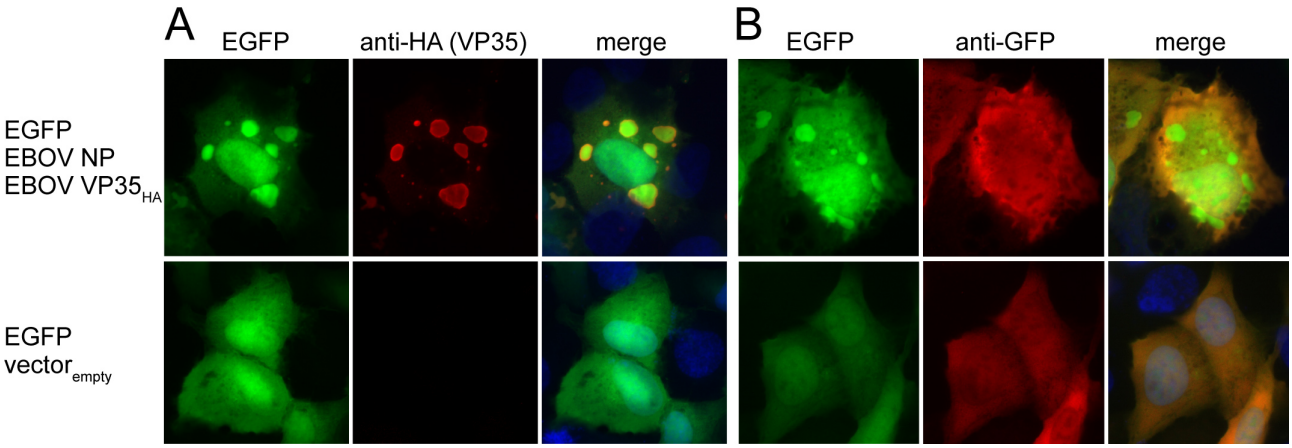


*Fig. 27: Antibodies directed against EGFP did not penetrate viral inclusions. U2OS cells were transfected with of 0.5 ug EGFP plasmid along with 0.75 ug of each plasmid encoding EBOV NP and $VP35_{HA}$. A. In immunofluorescence analysis $VP35_{HA}$ was detected by a mouse anti-HA antibody (1:500) and an anti-mouse Alexa Fluor 594-labed secondary antibody (1:100). B. For immunofluorescence detection of EGFP a mouse anti-GFP antibody (dilution 1:50) was used and incubated over night at 4°C. The secondary anti-mouse Alexa Fluor 594-labeled antibody (1:100) was incubated for 1h at room temperature.*

U2OS cells were transfected with EGFP along with EBOV NP and VP35, which led to the EGFP colocalization of EGFP with the viral inclusions as shown in Fig. 27A and described above. Antibody staining of the viral inclusions (shown in red) revealed bright rings surrounding the inclusions, whereas the inner part was less bright. EGFP autofluorescence did not appear as ring-like structure. Rather, inclusion-associated EGFP was evenly distributed.

In parallel, the transfected samples were used for immunofluorescence analysis using an antibody directed against EGFP. EGFP autofluorescence is shown in green and antibody staining of EGFP in red (Fig. 27B). While EGFP autofluorescence was concentrated in aggregates, antibody-stained EGFP was mostly evenly distributed in the cell and did not colocalize with inclusions.

This indicates that inclusion formation excludes antibody penetration.

## 5.2. Host cell stress response to Ebola virus infection

An important host antiviral defense mechanism is the stress-induced translational arrest, which is often accompanied by the formation of stress granules (SGs) and an increase in the number of processing bodies (PBs) present in the cytoplasm of the cell. The eIF2α subunit of the GTP-eIF2-$tRNA^{Met}$ ternary complex plays a central role in the control of translation. Phosphorylation of eIF2α by a small range of kinases leads to an arrest of the translation machinery and to the formation of SGs and PBs, containing stalled mRNP bodies. Many viruses including filoviruses depend on the cellular translation apparatus for viral protein synthesis and an increased yield of viral proteins. Therefore, phosphorylation of eIF2α is an effective antiviral defense mechanism to which viruses have evolved a certain level of tolerance.

The oxidative stressor sodium arsenite (As) externally induces eIF2α phosphorylation by the activation of the kinases PKR and HRI, resulting in SG formation.

This work focuses on the question of whether *Zaire ebolavirus* (EBOV) infection has an influence on the host cell stress response mediated by the formation of SGs and PBs.

### 5.2.1 Modulation of eIF3-containing SG formation in EBOV infection

SG formation in EBOV infection was examined using Vero E6 cells, which are commonly used to investigate the cellular response to filovirus infection.

Vero E6 cells were infected with EBOV and subjected to immunofluorescence analysis (Fig. 28A). Cells were examined for SG formation using an antibody against endogenous eukaryotic initiation factor 3 (eIF3), a SG marker protein in the cytoplasm. In EBOV-infected cells eIF3-containing SGs were not observed (Fig. 28A). This raised the question if the formation of eIF3-containing SGs were inhibited during EBOV infection. Therefore, SG formation was induced in EBOV-infected cells using As-mediated stress (Fig. 28B). In non-infected Vero cells, formation of eIF3-containing SGs was observed in almost all cells after As treatment (Fig. 28B). In EBOV-infected cells, SGs induced by As seemed to be reduced in number compared to the non-infected cells.

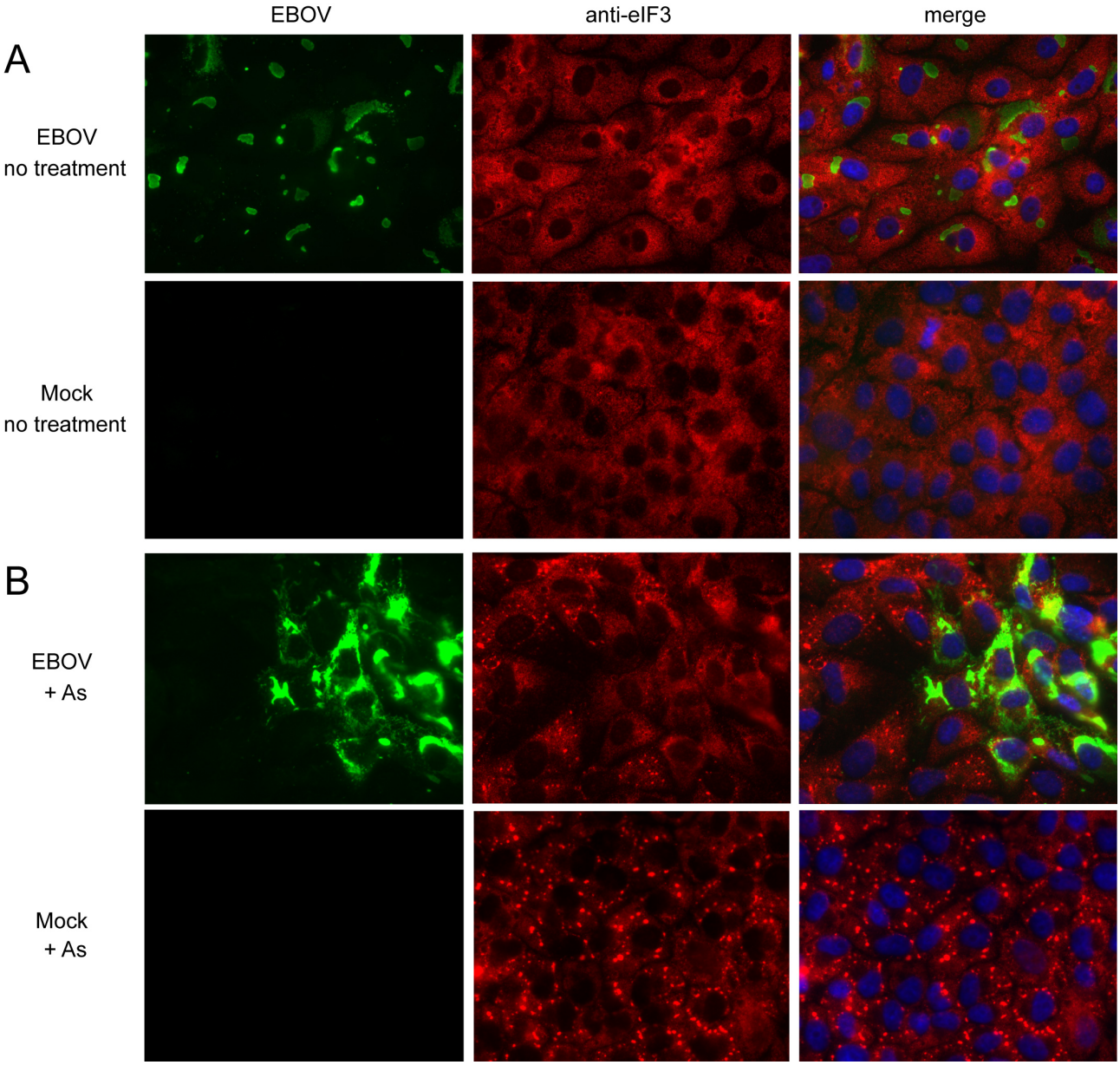


*Fig. 28: SG formation in EBOV-infected Vero E6 cells. Vero E6 cells were infected with EBOV at a high MOI. At 18 hpi Vero E6 cells were left untreated (A) or treated with As (2.5 mM) (B) and subjected to immunofluorescence analysis. (EBOV infection was detected using a monoclonal antibody directed against NP (dilution 1:15) and an anti-mouse FITC (dilution 1:100) antibody. SG formation was visualized using a goat antibody staining against endogenous eIF3 (dilution 1:50) and an anti-goat Alexa Fluor 594-labled secondary antibody (dilution 1:100). Nuclei were stained using DAPI (1:200).*

In order to quantify SG formation, the number of EBOV-infected and non-infected cells containing As-induced SGs was determined (Fig. 29).

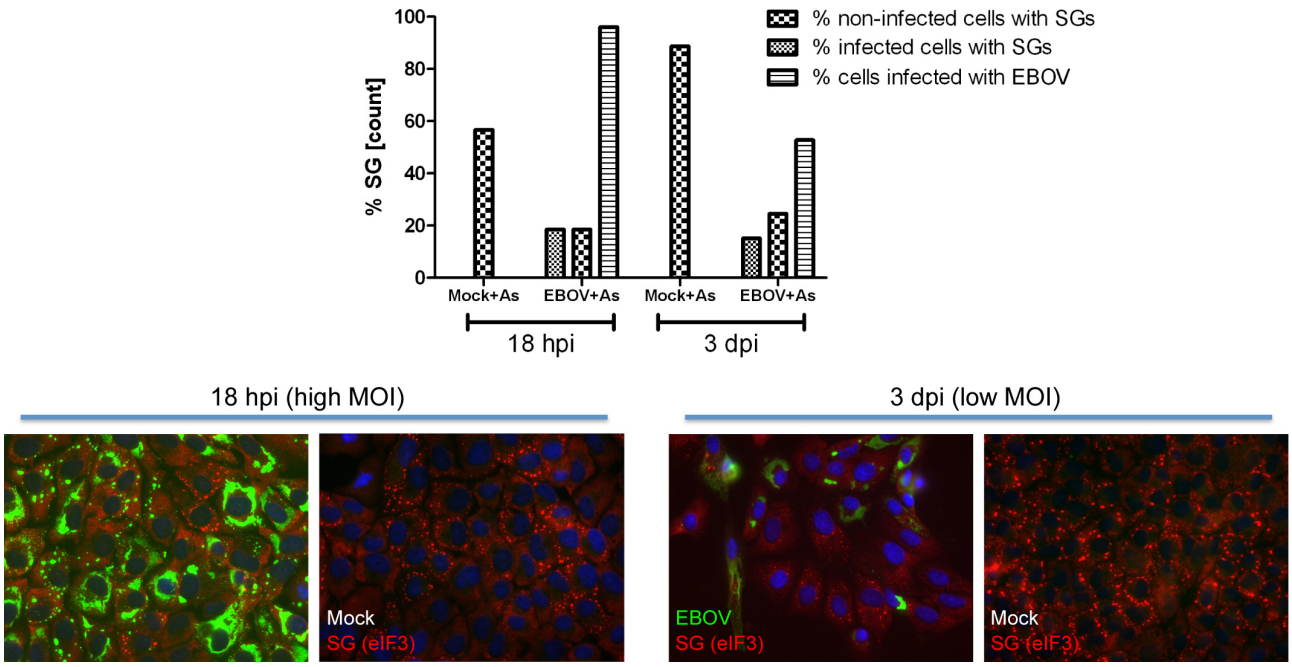


*Fig. 29: Reduced number of cells forming eIF3-positive SGs in EBOV infection in the presence of As. Vero E6 cells were infected with EBOV at a low MOI or a high MOI and harvested at 18 hpi (high MOI) or 3 dpi (low MOI). Two different virus preparations were used for the infection with supernatant harvested from EBOV-infected Vero E6 cells. Cells were treated with As (2.5 mM) and harvested for immunofluorescence analysis (for antibody staining see Fig. 28). SG formation was analyzed for a total number of 400 of either the infected or the non-infected.*

The cells infected with a low MOI were fixed at 3 dpi. The infection rate was 53%. Immunofluorescence analysis revealed formation of eIF3-containing SGs in 89% of the examined non-infected, treated cells. Compared to the non-infected cells, the ability to form eIF3-positive SGs was substantially reduced in EBOV-infected cells. In EBOV infection, SG formation was reduced in both the infected and non-infected cells; only 15% of the EBOV-infected cells and 25% of the non-infected cells showed formation of eIF3-positive SGs (Fig. 29).

When the infection was performed at a high MOI, EBOV-infected and non-infected cells were harvested at 18 hpi and analyzed by immunofluorescence. The infection rate was 96%. 57% of the non-infected, treated cells formed SGs compared to 19% of the EBOV-infected, treated cells (Fig. 29).

Using the eIF3 antibody for detection, formation of endogenous SGs was not observed in EBOV-infected Vero E6 cells. After treatment with As, SGs were detected in EBOV-infected cells albeit in a reduced number of cells compared to the non-infected cells. This indicates that EBOV is able to partially inhibit As-induced SG formation.

### 5.2.2 U2OS cell line expressing the SG marker protein G3BP was used to analyze the role of SGs in EBOV infection

The dynamic structure of SGs makes it impossible to isolate them. Therefore microscopy analysis was used to examine if cellular stress responses play a role during EBOV infection. This analysis required cells that were both suitable for immunofluorescence analysis and for studying the host stress response to EBOV. The Vero E6 cell line was not well suited for the experiments since it is a

non-human cell line and difficulties using the eIF3 antibody were experienced as it exhibited an unreliable staining. This might be due to the nature of the eIF3 complex which is composed of at least 11 protein subunits, some of which are present in distinct eIF3 subcomplexes (Zhou et al., 2005). A human epithelial osteosarcoma (U2OS) cell line was used after testing the cells for their suitability by establishing protocols for EBOV infection and transfection. The U2OS cell line is used extensively for studies of SG formation because the cells exhibit a large and flat morphology, which is crucial for immunofluorescence observation and quality imaging of the cytoplasm of single cells. In addition, it expresses wildtype p53 and has the ability to undergo cell cycle arrest on serum withdrawal. U2OS cell line expressing the SG marker proteins G3BP were kindly provided by N. Kedersha (detailed protocol for cell line generation in (Kedersha et al., 2008).

To analyze SG formation, U2OS cells stably expressing an EGFP-tagged SG marker protein, ras-GAP SH3 domain binding protein 1 (G3BP), were used (U2OS G3BP-EGFP cells; Fig. 30). Similar to the endogenous G3BP, the tagged version of the protein is located in G3BP-positive SGs after treatment with As or other stress inducers (Kedersha et al., 2008).

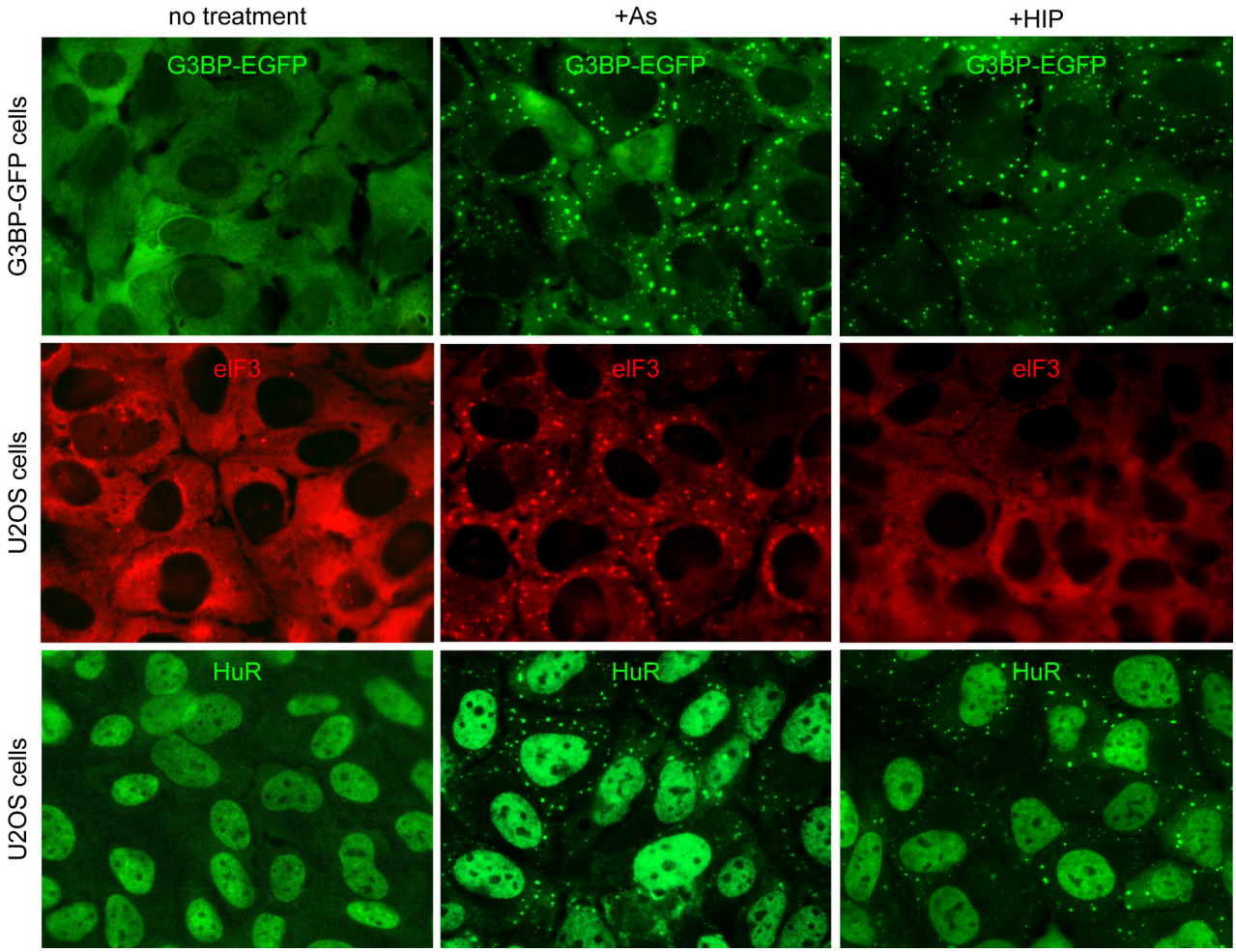


*Fig. 30: U2OS cell line expressing an SG marker protein. The different U2OS cell lines were treated with 2mM As or 1µM Hip for 30 minutes. In the parental U2OS cell line SG formation was detected using a goat anti-eIF3 antibody (dilution 1:50) or a mouse anti-HuR (dilution 1:10) antibody, incubated over night at 4°C. The stably expressed EGFP-tagged G3BP was detected by autofluorescence.*

The U2OS parental cell line was used to analyze endogenous SG marker proteins by immunofluorescence antibody staining (Fig 30). To confirm formation of SGs in the two cell lines, cells were treated with either As or hippuristanol (Hip). In contrast to As, Hip leads to SG formation by inhibiting eIF4A-dependent translation initiation, a process, which does not involve phosphorylation of eIF2α. While G3BP-EGFP was homogeneously distributed in the cytoplasm of untreated cells, treatment with As or Hip resulted in formation of G3BP-positive SGs in the cytoplasm of G3BP-EGFP-expressing cells (Fig 30). Both eIF3 and human antigen R (HuR) were redistributed in SGs in the parental U2OS cells after As treatment. Hip-induced SGs that formed in U2OS cells were not detectable using the eIF3 antibody, suggesting that these SGs did not contain eIF3 or the eIF3 subcomplex (Fig. 30). However, SGs were detected by using an antibody directed against HuR, confirming that Hip-induced SGs were formed.

### 5.2.3 Stress response in EBOV-infected U2OS G3BP-EGFP cells

The U2OS G3BP-EGFP cell line was used to further analyze SG formation during EBOV infection. Since As-treatment induces SG formation in a phospho-eIF2α-dependent manner, the question arose of whether the observed inhibition of SGs by EBOV is due to the ability of EBOV to block PKR-mediated phosphorylation of eIF2α. Therefore, EBOV-infected cells were either treated with As or Hip.

An overview of U2OS G3BP-EGFP cells infected with EBOV and either treated with As or Hip is shown in Figure 31. Most intriguingly, G3BP-EGFP-positive granules accumulated in viral inclusions, which are shown in red. The accumulation of G3BP granules in the viral inclusions was observed in treated and in non-treated cells. In non-treated cells infected with EBOV, these G3BP granules were completely restricted to the viral inclusions and not found in the cytoplasm of the cell (Fig. 31, 1$^{st}$ panel).

Cytoplasmic G3BP-EGFP-containing SGs were observed in EBOV-infected and non-infected cells after treatment with As or Hip. SG formation seemed to be impaired in some of the As-treated infected cells as reflected by the diffuse distribution of G3BP-EGFP in the cytoplasm (Fig. 31, 2$^{nd}$ panel, arrow). Nevertheless, G3BP granules accumulated in the viral inclusions in these cells, indicating that the absence of SGs in the cytoplasm was not due to a lack of G3BP-EGFP expression. In many infected cells treated with As, SGs were observed in the cytoplasm. In Hip-treated cells, impaired SG formation was not observed in the infected cells (Fig. 31, 3$^{rd}$ panel).

In general, a larger number of EBOV-infected cells formed G3BP-EGFP-containing SGs compared to EBOV-infected Vero cells stained for endogenous eIF3 (see discussion).

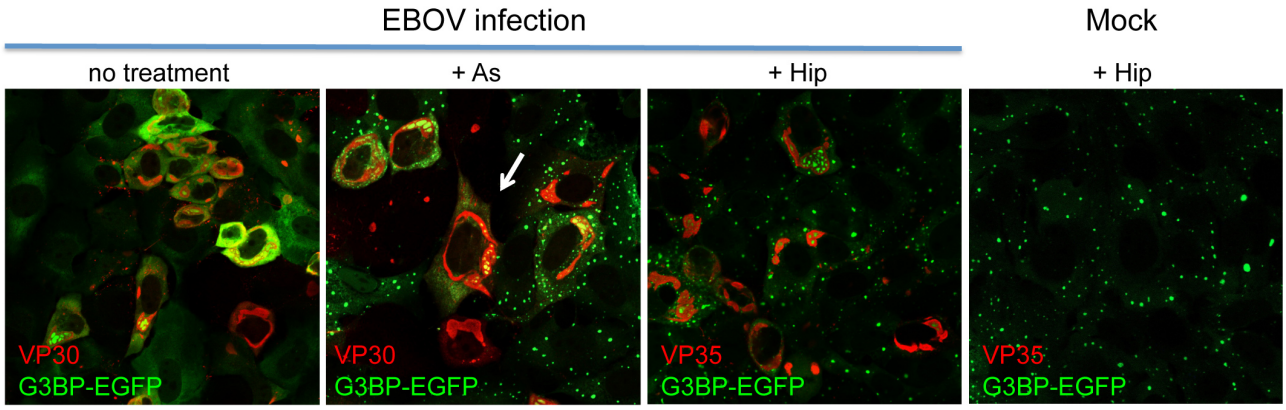


*Fig. 31: 2x10$^5$ G3BP-EGFP cells seeded on glass cover slips were infected with EBOV (Kikwit isolate) at an MOI of 1. At 2 dpi, cells were treated with As (2 mM) or Hip (1 µM). Cells were subjected to immunofluorescence analysis using a rabbit anti-VP30 antibody (1:100) or the mouse anti-VP35 antibody (1:400). As secondary antibodies mouse or rabbit Alexa Fluor 594-labeled (1:500) antibodies were used. Images were taken using a confocal microscope (Zeiss LSM710).*

A wide range of interactions between EBOV inclusions and G3BP-EGFP aggregates were observed in treated as well as in non-treated cells indicating a highly dynamic interaction process. Therefore a representative spectrum of EBOV-infected cells is depicted in Figure 32. Images from left to right show early stages of virus inclusion formation on the left and later stage inclusions on the right (Fig. 32).

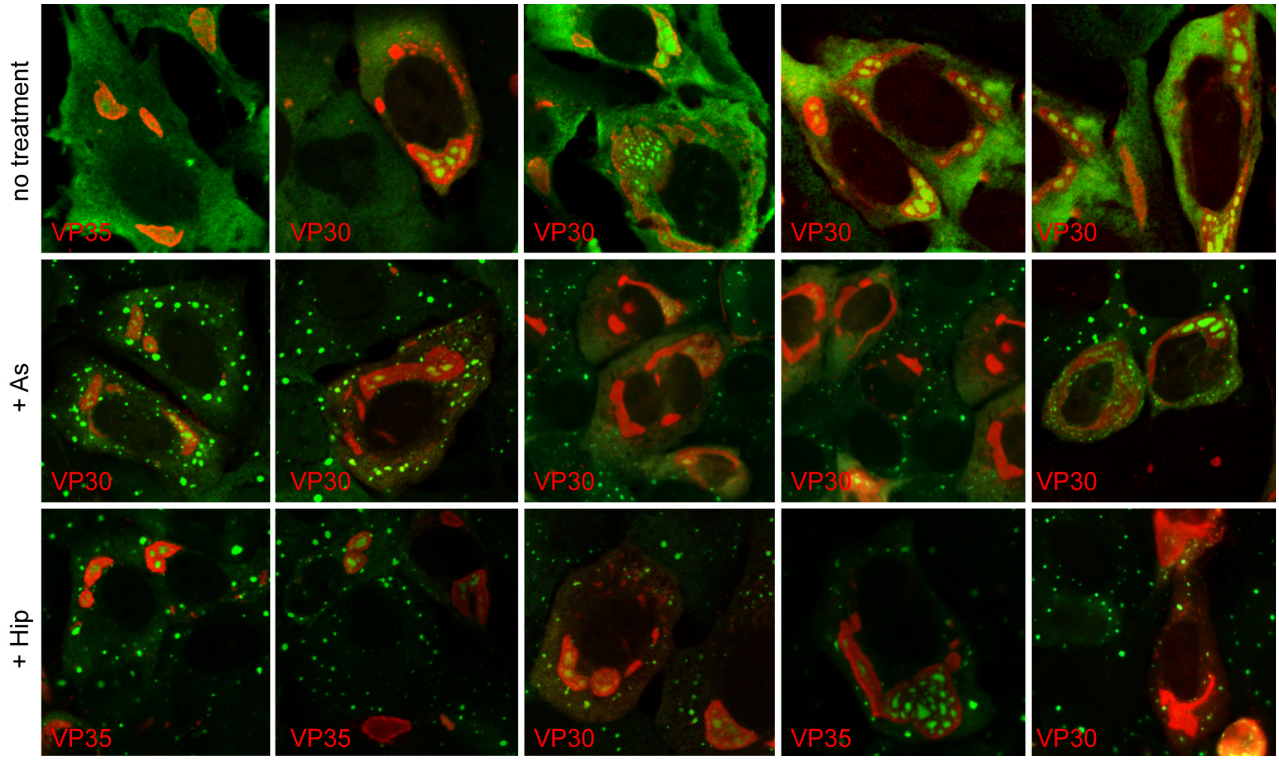


*Fig. 32: Spectrum of interactions of EBOV viral inclusions with G3BP-EGFP aggregates in EBOV-infected cells. For immunofluorescence labeling see Fig. 31.*

SG formation in the cytoplasm of the infected cells was negatively correlated with the size of the viral inclusions. Thus, in cells containing large viral inclusions, SG formation was reduced compared to cells containing smaller inclusions.

In contrast, G3BP-containg SG-like aggregates within the viral inclusion were observed at all stages of viral inclusion formation. Remarkably, G3BP-EGFP aggregates observed within the viral inclusions looked different from the cytoplasmic SGs, since they were aggregated but not as round-shaped compared to the cytoplasmic stress-induced SGs.

To determine if viral inclusion formation itself is sufficient for the aggregation of G3BP-granules within the inclusions, inclusion formation was induced by the expression of EBOV proteins. NP, which is the driving force for inclusion formation, was expressed in cells along with different combinations of EBOV nucleocapsid proteins. Since VP24 has been shown to be part of the nucleocapsid complex and crucial for viral inclusion formation (Huang et al., 2002), it was included in this study. The transfected cells were either left untreated or treated with either As or Hip (as indicated). G3BP-granule formation in transfected and infected cells was compared using confocal microscopy (Fig. 33).

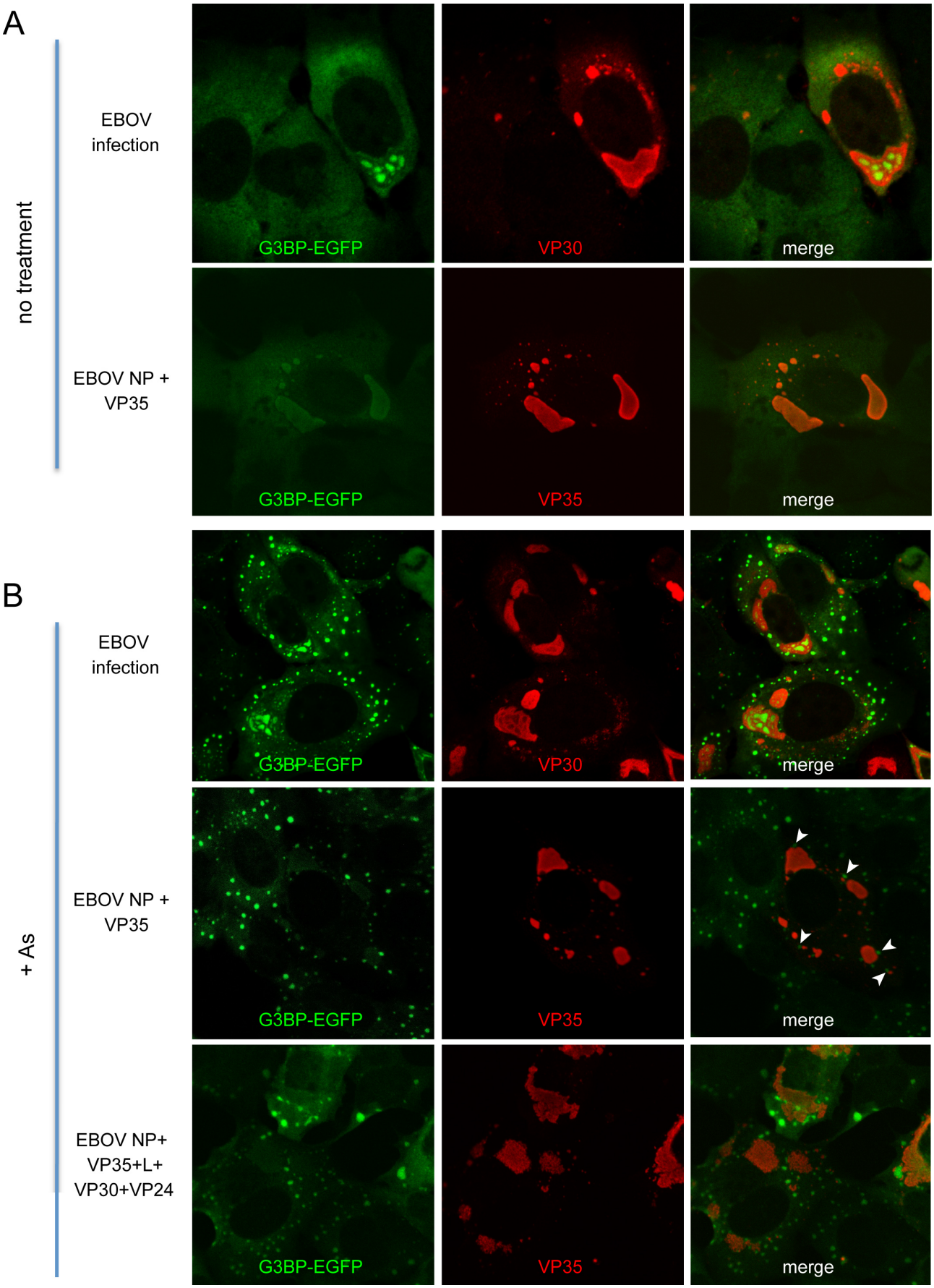
A
no treatment
EBOV infection
EBOV NP + VP35
G3BP-EGFP
VP30
merge
G3BP-EGFP
VP35
merge
B
+ As
EBOV infection
EBOV NP + VP35
EBOV NP+ VP35+L+ VP30+VP24
G3BP-EGFP
VP30
merge
G3BP-EGFP
VP35
merge
G3BP-EGFP
VP35
merge

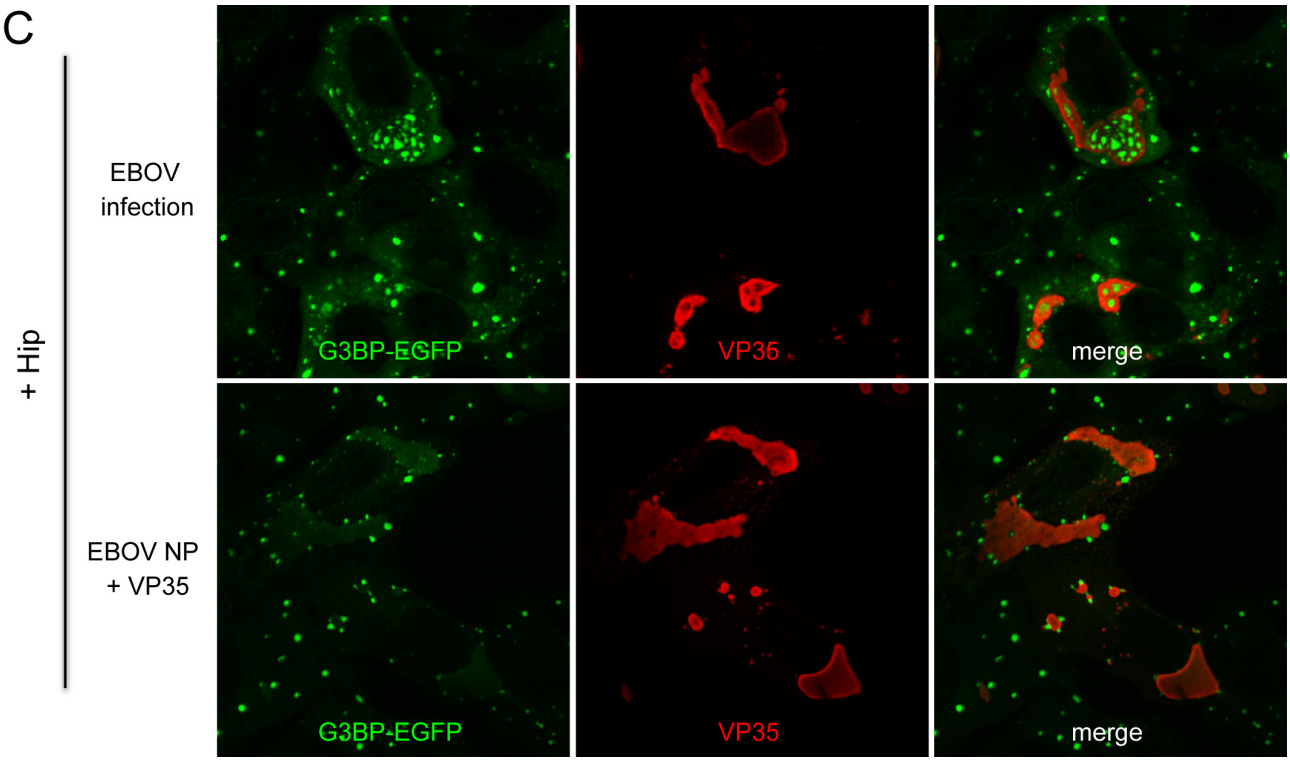


*Fig. 33: Comparison of EBOV-infected G3BP-EGFP cells with cells expressing EBOV-derived proteins involved in inclusion formation. The images of EBOV-infected cells are derived from the same samples shown in Fig. 31. G3BP-EGFP cells were transfected with 0.75 µg of each plasmid DNA encoding the EBOV nucleocapsid proteins (as indicated). At 2 dpt cells were (A) left untreated, (B) treated with As (2mM), or (C) treated with Hip (1 µM). The samples were stained using the same antibodies and concentrations as described in Fig. 31 (EBOV-infected samples). Images of the transfected cells were taken using a confocal microscope (Zeiss LSM5 Pascal).*

In non-treated transfected cells expressing NP and VP35, G3BP-EGFP was homogeneously distributed, but the EGFP autofluorescence diffusely colocalized with NP-induced inclusions (Fig. 33A). This interaction might be unspecific, since it has been observed that ectopic fluorescence proteins relocated to NP-derived inclusions (see part I). Nevertheless, formation of G3BP-EGFP aggregates was not observed in transfected cells, whereas almost all of the EBOV-infected cells contained G3BP granules inside the viral inclusions. This indicates that the EGFP portion of G3BP-EGFP did not mediate formation of G3BP-EGFP granules in the viral inclusions (see discussion).

As treatment led to the formation of SGs in the cytoplasm of transfected cells and partially in EBOV-infected cells (Fig. 33B). Transfection of NP and VP35 resulted in inclusion formation in the cytoplasm of the cell. In contrast to EBOV-infected cells, G3BP-containing SG-like granules were not observed inside of the inclusions. G3BP-EGFP-positive SGs were frequently observed in close proximity to the NP-induced inclusions but did not intermingle (Fig. 33B, arrowheads). This indicates a recruitment of SGs to the inclusions. In cells transfected with NP, VP35, VP30, and VP24, viral inclusions appeared more diffuse and were occasionally surrounded by SGs but never colocalized with them. In addition, As-induced SG formation was never impaired in the transfected cells, which is different to the observation made for the As-treated EBOV-infected cells. Transfected cells treated with Hip did not show a significant difference to As-treated transfected cells (Fig. 33C/B).

The diffuse colocalization of G3BP-EGFP with NP-derived inclusions observed in transfected cells (described for Fig. 33A) was most apparent in non-treated cells. After treatment with As or Hip, G3BP-EGFP was mostly observed inside of SGs.

In conclusion, accumulation of G3BP granules within viral inclusions of treated and non-treated cells suggests a mechanism of EBOV to interfere with SG components by protein sequestration. In addition, the size of the viral inclusion did not seem to influence the aggregation of G3BP. To date, it is not known if cellular components play a role in EBOV inclusion formation or if inclusions are utilized to sequester potentially antiviral cellular components.

The impaired G3BP-containing SG formation in some As-treated but not in Hip-treated cells suggests a reduced ability to form SGs in response to phospho-eIF2α-mediated stress in EBOV-infected cells. This inhibition seemed to be dependent on the size of the viral inclusions, suggesting that a certain level of viral protein expression is important for the inhibition.

Nevertheless, inclusion formation induced by the expression of nucleocapsid proteins was not sufficient for the accumulation of G3BP granules inside the inclusions or for the inhibition of SG formation observed in infected cells.

These results suggest that EBOV exhibits control strategies at the level of SG formation.

### 5.2.4 Impact of EBOV proteins on SG formation

To further analyze how EBOV interacts with SGs, EBOV proteins were examined for their ability to interfere with SG formation. The three NC proteins, NP, VP35 and VP30 represent promising candidates since all of them play a role in viral replication, are involved in NC formation, and furthermore are RNA-binding proteins. The viral glycoprotein, GP, was used as a control. As a surface protein, GP is not located in the cytoplasm but at the cell membrane, in the ER, and in the Golgi apparatus. SG formation was initiated by treatment with the external stressor As that leads to phosphorylation of eIF2α.

Expression of NP in the absence of other viral proteins results in the formation of inclusions, similar to those found in infected cells but less structured. In addition, NP forms loose coil-like helices that are distinct from the condensed ones in the viral NCs (Huang et al., 2002; Noda et al., 2006; Watanabe et al., 2007; Noda et al., 2010; Bharat et al., 2012).

In the absence of external stressors, G3BP-EGFP was mostly homogenously distributed throughout the cytoplasm (Fig. 34A). G3BP-EGFP was also observed at the sites of NP-derived inclusion formation. As discussed above, this colocalization might be unspecific and not due to a direct interaction between NP and G3BP. After treatment with As, G3BP-EGFP mostly relocated into SGs, but a small moiety also colocalized with the NP-derived inclusions (Fig. 34A). SGs were observed in close proximity, and often surrounding, NP-derived inclusions, which was similar to observations made for cells expressing NP and VP35 (see Fig. 33). However, NP never colocalized with SGs and SG formation was not impaired by the expression of NP.

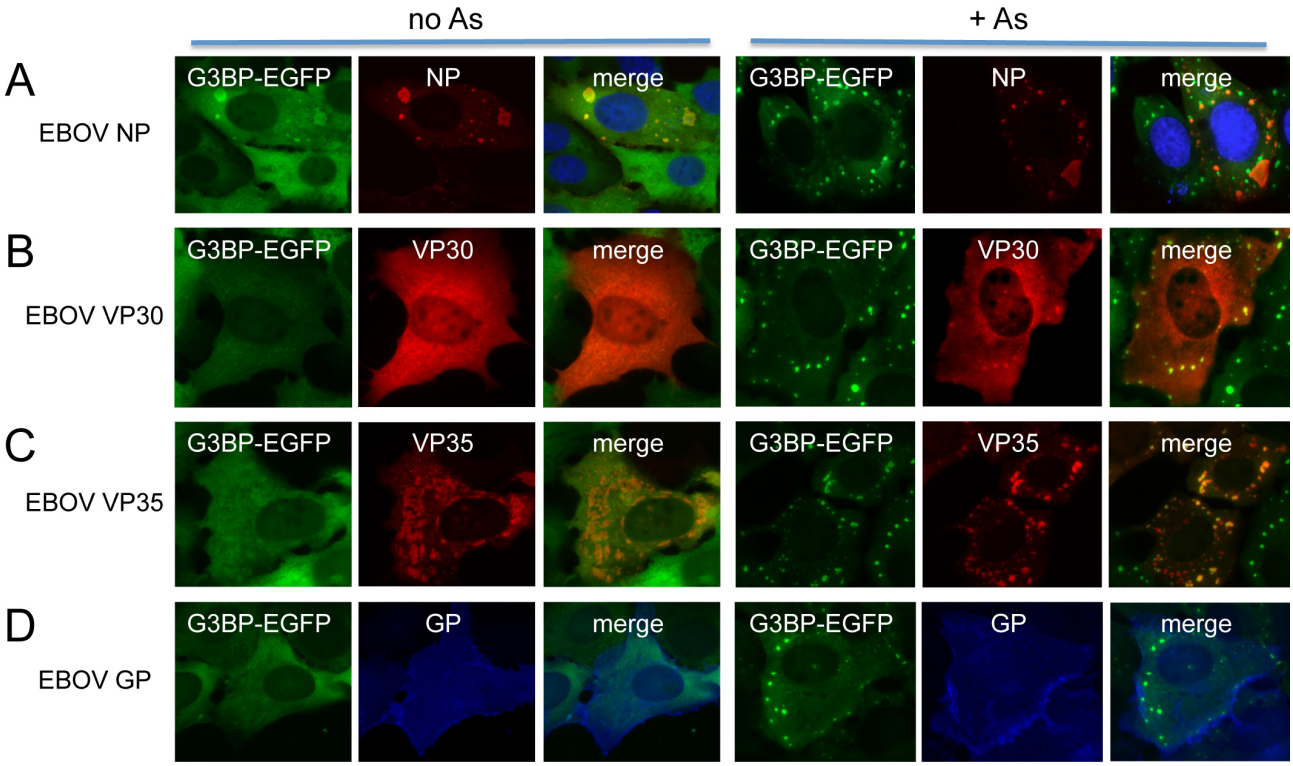


*Fig. 34: Impact of EBOV proteins on SG formation in the U2OS G3BP-EGFP cell line. G3BP-EGFP cells were transfected with expression plasmids encoding different EBOV proteins. (A) Cells were transfected with 0.75 µg NP expression plasmid (plus 0.75 µg pC-empty vector), treated with As (2mM) at 24 hpt and subjected to immunofluorescence using a monoclonal mouse NP antibody (B6C5 97, dilution 1:10). Antibody binding was visualized by using an Alexa Fluor 647-conjungated goat anti-mouse antibody (dilution 1:100). (B) Cells were transfected with 1 µg VP30 expression plasmid and treated with As (2 mM) at 48 hpt. VP30 expression was detected using a rabbit anti-VP30 antibody (dilution 1:100) and for visualization an anti-rabbit Cy3 (dilution 1:100). (C) 0.75 µg EBOV $VP35_{HA}$ plasmid DNA (plus 0.75 µg pC-empty vector) was transfected and cells were treated with As (2mM) at 24 hpt. $VP35_{HA}$ expression was detected using a mouse anti-HA antibody (dilution 1:500) and an anti-mouse Alexa Fluor 647-conjungated secondary antibody (dilution 1:100). (D) 1 µg of the GP expression plasmid was transfected along with 1 µg VP30 (not depicted) and cells were treated with As (2 mM) at 24 hpt. GP was visualized using a goat anti-EBOV antiserum (dilution 1:750) and an ultraviolet-excitable anti-goat Alexa Fluor 350 secondary antibody (dilution 1:100).*

The next protein analyzed was VP30 (Fig. 34B). VP30 has previously been shown to bind ssRNA, (John et al., 2007). VP30 contains an unconventional CCCH Zn-finger motif that is required for efficient viral transcription ((Weik et al., 2002; Modrof et al., 2003). Many cellular RNA-binding proteins that accumulate in SGs also contain this unconventional domain, which allows them to interact and regulate mRNA stability.

VP30 and G3BP-EGFP were both homogenously distributed in the cytoplasm of non-treated cells (Fig. 34B). When As-stress was applied, G3BP-EGFP relocated into SGs. VP30 was partially homogenously distributed but also relocated and colocalized with the SGs (Fig. 34B). SG formation did not seem to be impaired in VP30-transfected cells.

The effect of VP35 expression on SG formation was examined next. The multifunctional VP35 protein is a crucial virulence factor that blocks the host innate immune response and RNA silencing pathways, which are important in context of SG formation (reviewed in (Ramanan et al., 2011)). VP35 formed patch-like structures in the cytoplasm of non-treated cells, whereas G3BP-EGFP was homogenously distributed (Fig. 34C). As treatment led to SG formation and a distinct redistribution

of VP35, which colocalized with SGs (Fig. 34C). Interestingly, SG formation seemed to be influenced by the expression of VP35 in the G3BP-EGFP cell line, which will be analyzed in more detail (see below).

The non-cytoplasmic GP was predicted to not colocalize with SGs. GP was found to locate mostly to the cell membrane and around the nucleus rather than in close proximity to SGs (Fig. 34D). This distribution did not change after As treatment.

Since GP did not interact with SGs, it was not further examined. The observed interaction between SGs and the EBOV RNA-binding NC proteins NP, VP30, and VP35 was analyzed in more detail.

### Interaction of NP-derived viral inclusions with SGs

It was analyzed if Hip-induced and As-induced SGs show a different pattern of interaction with NP in the G3BP-EGFP cell line. After Hip treatment, SG formation was observed and formation of NP-derived inclusions was not impaired by the treatment (Fig. 35). SGs were located in close proximity to NP-derived inclusions, similar to the observation made for As-treated cells. This suggests that NP-derived inclusions relocate SGs to the sites of inclusion formation.

NP was never observed in colocalization with As- or Hip-derived SGs. This indicates that NP does not relocate into SGs induced by As or Hip. As shown above, the colocalization of diffusely distributed G3BP-EGFP with NP-derived inclusions was more abundant in non-treated cells (Fig. 35, insert) but also visible in As and Hip-treated cells (Fig. 35, inserts).

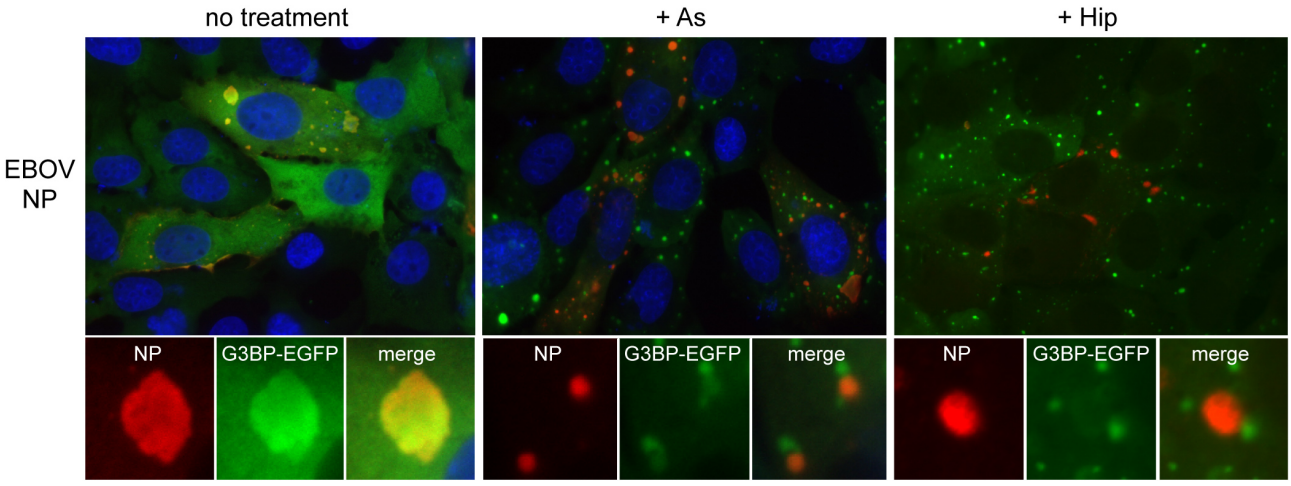


*Fig. 35: Interaction of NP-derived inclusions with G3BP-containing SGs. G3BP-EGFP cells were transfected with 0.75 µg NP expression plasmid (plus 0.75 µg pC-empty vector). At 24 hpt, cells were treated with As (2mM) or Hip (1 µM) and stained using a monoclonal mouse NP antibody (B6C5 97, 1:10) and a secondary anti-mouse Alexa Fluor 647-labeled antibody (1:100).*

### Interaction of VP30 and SGs

To further analyze the effects of VP30 on SG formation, VP30 was expressed in G3BP-EGFP-containing cells and subsequently treated with either As or Hip. In the absence of external stressors, G3BP-EGFP was homogenously distributed in the cytoplasm. It aggregated into SGs when either As or Hip was applied (Fig. 36). In As and Hip-treated cells, a fraction of the otherwise

homogeneously distributed VP30 accumulated in aggregates colocalizing with G3BP-EGFP SGs (Fig. 36). However, the interaction with VP30 did not seem to influence the formation or distribution of the G3BP-containing SGs.

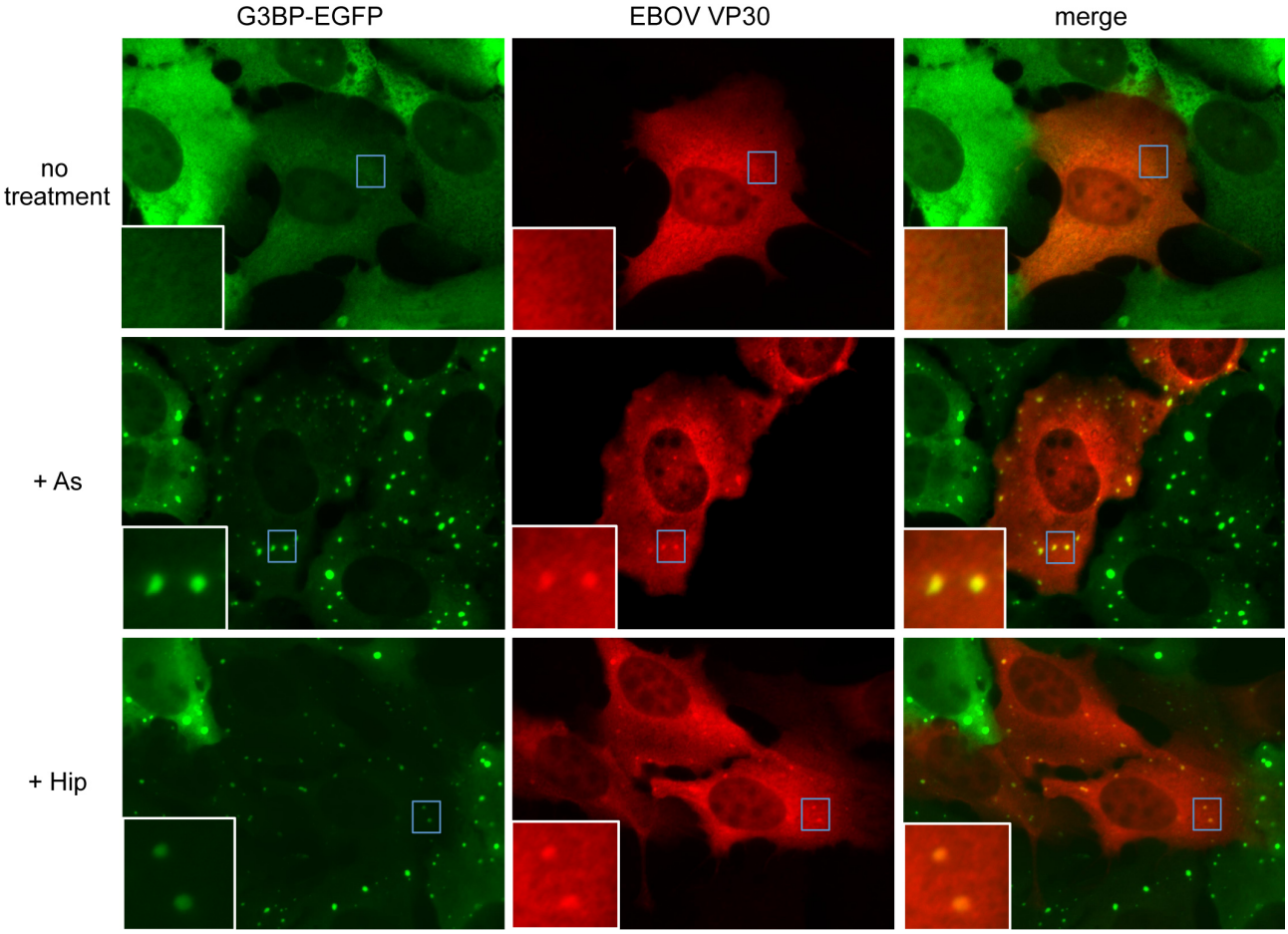


*Fig. 36: Colocalization of EBOV VP30 with G3BP-EGFP-containing SGs. U2OS G3BP-EGFP cells were transfected with 1 µg VP30 plasmid DNA. At 48 hpt, cells were treated with As (2 mM) or Hip (1 µM) and subjected to immunofluorescence analysis using an antibody directed against EBOV VP30 (rabbit anti-VP30, dilution 1:100) and for visualization an anti-rabbit Cy3 (dilution 1:100). Experiment was performed n=5 and representative images were chosen.*

To confirm the colocalization of VP30 and G3BP-EGFP, VP30-expressing cells treated with Hip were examined by confocal microscopy (Fig. 37). A set of images was captured axial throughout the sample (z-stack) in order to ensure that SGs residing outside of the focal plane were accounted for. The single image of confocal z-stack depicted in Figure 37A was then used for intensity measurements of the different wavelengths within the G3BP-EGFP-containing SGs of VP30-expressing cells and cells in which VP30 was not expressed (Fig. 37B).

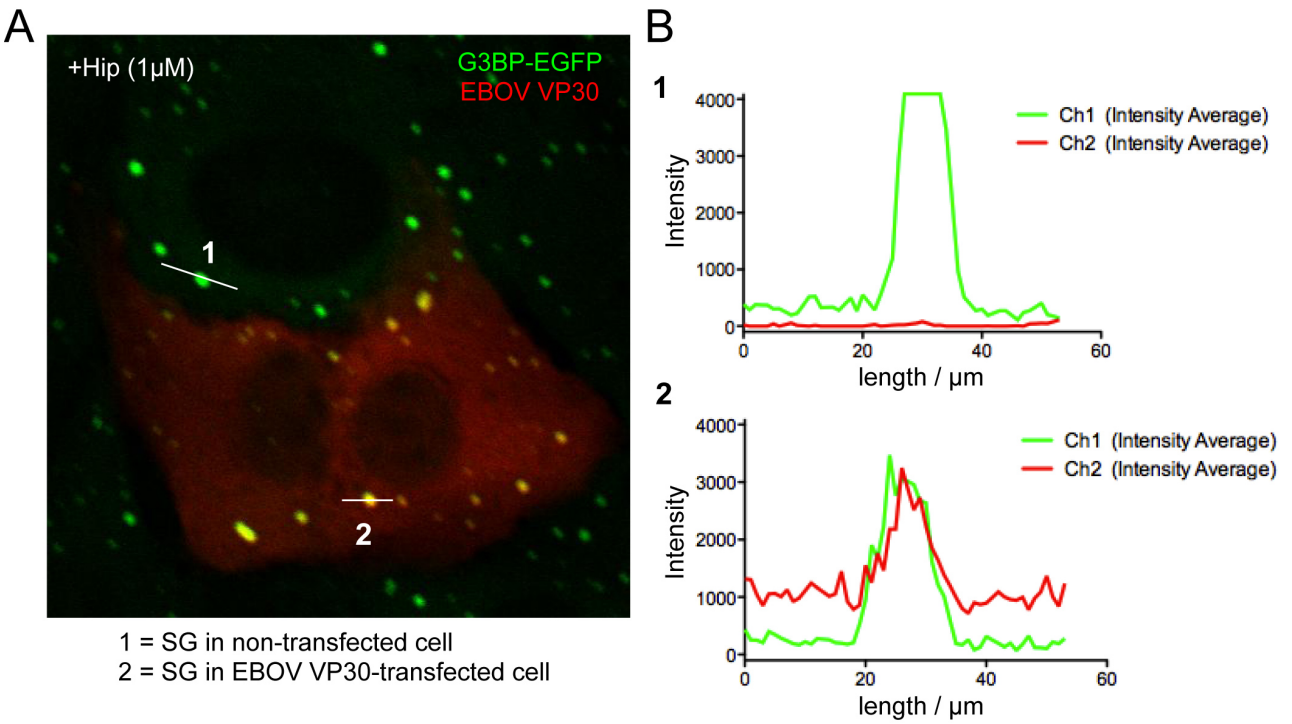


*Fig. 37: Confirmation of the colocalization of VP30 and G3BP-EGFP-containing SGs by confocal microscopy. U2OS G3BP-EGFP cells were transfected with a plasmid expressing VP30 and analyzed by immunofluorescence staining (see Fig. 36). (A) Single image of captured z-stack by confocal microscopy (Olympus FV1000) used for colocalization analysis. (B) VP30 localization to G3BP-EGFP-positive SGs was detected by line scans within the image. Fluorescence intensities were plotted measuring G3BP-EGFP in SGs of untransfected cells (line 1) and in VP30-transfected cells (line 2).*

In VP30-expressing cells, two distinct but overlapping peaks were measured (Fig. 37B, line 2), whereas in the absence of VP30 only the EGFP emission peak was detected (Fig. 37B, line 1). This confirmed the close proximity of VP30 and the G3BP-EGFP-containing SGs.

### Interaction of VP30 and SGs when coexpressed with NP

NP interacts with VP30, leading to the relocalization of VP30 into NP-derived inclusion. To analyze if NP has an influence on the observed colocalization of VP30 with SGs, VP30 was coexpressed with NP in G3BP-EGFP-expressing cells (Fig. 38).

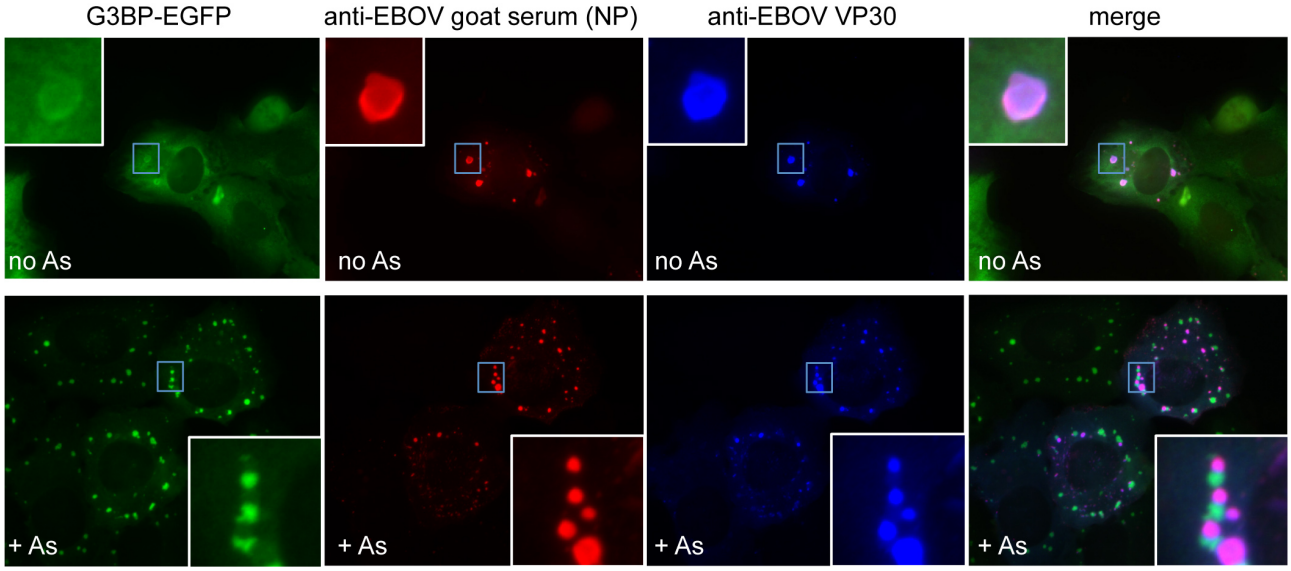


*Fig. 38: Relocation of VP30 in the presence of NP. The U2OS G3BP-EGFP cell line was transfected with 1 µg VP30 expression plasmid along with 1 µg of the EBOV NP plasmid. At 24 hpt, cells were treated with As (2 mM) and subjected to immunofluorescence staining. NP was detected using an anti-EBOV antiserum (goat anti-EBOV serum, dilution 1:750) and a donkey anti-goat Alexa Fluor 594-labeled antibody (dilution 1:100). VP30 was detected using a rabbit-VP30 antibody (dilution 1:100) and, as secondary antibodies, an ultraviolet-excitable anti-rabbit Alexa Fluor 350-labeled antibody (1:100) was used.*

Expression of VP30 along with NP led to the relocalization of VP30 into viral inclusions formed by NP. NP and VP30 colocalized in untreated and As-treated cells (Fig. 38). As described above for NP-VP35 inclusions (Fig. 33), G3BP-EGFP colocalized with NP-VP30 inclusions in untreated cells, although most of the protein was homogenously distributed in the cytoplasm (Fig. 38). In As-stressed cells, SGs were shown to be in close contact with the NP-VP30 inclusions (Fig. 38). Neither NP nor VP30 were observed at the site of SG formation.

Figure 39 shows a cell, which formed large NP-VP30 inclusions. Formation of large inclusions is most likely due to large quantities of expressed viral proteins. Interestingly, a different viral protein distribution was observed in cells containing large viral inclusions. A small moiety of VP30 that was not relocalized in NP inclusions colocalized with the SGs (Fig. 39, detail view, arrows).

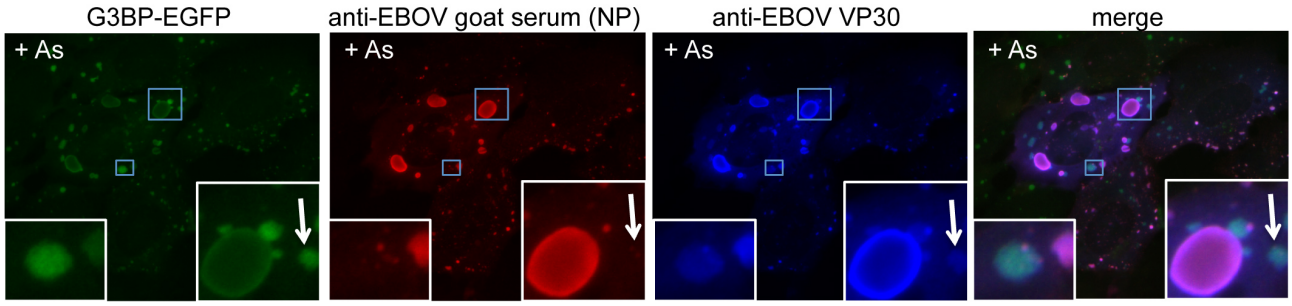


*Fig. 39: Interaction of VP30 with SGs in the presence of NP. For transfection and immunofluorescence staining procedure see Fig. 38.*

Antibody staining of VP30 and NP revealed a ring-like pattern around the inclusions, which furthermore colocalized with the G3BP-EGFP autofluorescence (Fig. 39). This was often observed

for large inclusions, suggesting that the antibodies were not able to penetrate the inclusions efficiently and predominately bound to the surface of the inclusions. Also, colocalization of G3BP-EGFP with viral inclusions was more frequently observed for large inclusions, suggesting that larger inclusions are more prone to recruit ectopic proteins non-specifically.

These results indicate that in the presence of NP VP30 was primarily localized in viral inclusions but also colocalized with G3BP-positive SGs in a protein expression-dependent manner.

**Interaction of VP35 with G3BP-EGFP-containing SGs**

As shown above VP35 colocalized with SGs in As-treated cells (Fig. 34). However the VP35 distribution was different than the distribution of VP30. To analyze this colocalization in more detail, VP35 was expressed in the U2OS G3BP-EGFP cell line and treated with As. VP35 and G3BP-EGFP did not colocalize in unstressed cells. While G3BP-EGFP was homogenously distributed in the cytoplasm of VP35-expressing cells, VP35 was found to accumulate in patches without an obvious pattern (Fig. 40). No interaction was observed between VP35 and G3BP-EGFP in untreated cells. The uneven distribution of VP35 did not change when different amounts of plasmid DNA encoding VP35 were transfected. Even low amounts of VP35 DNA (0.3 µg) led to a non-homogenous distribution of VP35 in the transfected cells (data not shown). In As-stressed cells, the VP35 aggregates relocalized and colocalized with the G3BP-positive SGs (Fig. 40). Three immunofluorescence images were selected that show an increasing accumulation of VP35 from top to bottom (Fig. 40, panels i to iii). Interestingly, these images revealed that increased expression of VP35 corresponded to altered SG formation. VP35 colocalized with SGs but also aggregated in small globular structures surrounding the SGs (Fig. 40, panels i and ii). SGs colocalizing with VP35 were frequently different from typical SGs. Instead of being round and globular they exhibited a more diffuse, polymorphic shape (Fig. 40, panels i) In cells expressing large amounts of VP35, G3BP-EGFP colocalized with VP35 patches and SG formation was not observed (Fig. 40, panels iii). These results suggest that As-induced G3BP-containing SG formation was inhibited in cells expressing VP35, in a manner that appeared to be dependent on VP35 protein expression level.

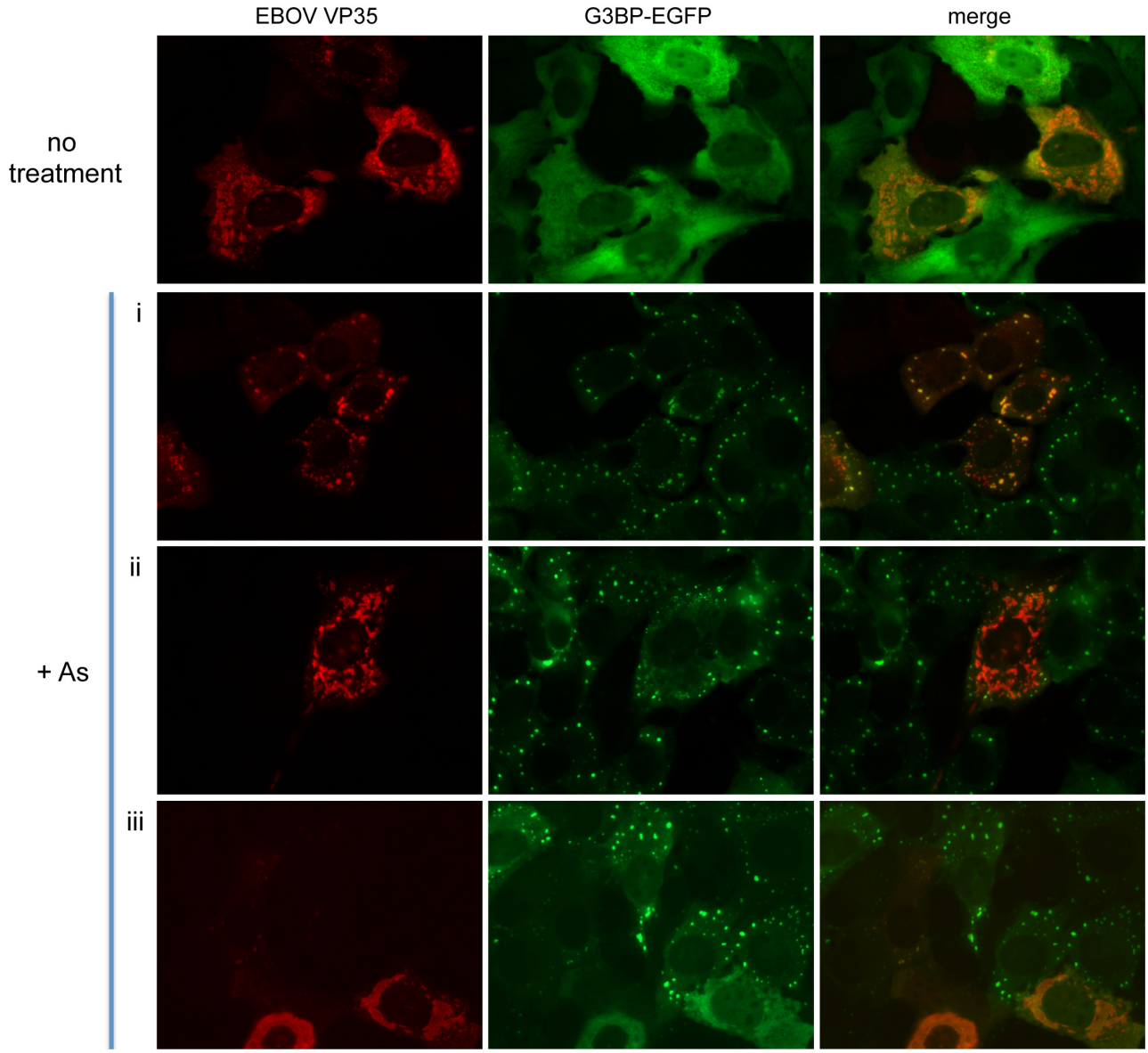


*Fig. 40: VP35 expression alters G3BP-EGFP-containing SG formation in As-treated cells. G3BP-EGFP cells were transfected with 0.75 µg EBOV VP35$_{HA}$ plasmid DNA (plus 0.75 µg pC-empty vector). At 24 hpt, cells were treated with As (2mM) where indicated (rows 2-4). VP35$_{HA}$ expression was detected using a mouse anti-HA antibody (dilution 1:500) and an anti-mouse Alexa Fluor 647-labeled secondary antibody (dilution 1:100). The experiment was performed 5 times. Representative images are depicted.*

It was further investigated if the ability of VP35 to block SG formation was restricted to phospho-eIF2α-mediated stress. Therefore, in addition to the As treatment, VP35-transfected G3BP-EGFP cells were stressed using Hip, an eIF2α-independent inducer of SG formation (Fig. 41). The distribution of VP35 was compared in the differently treated cells.

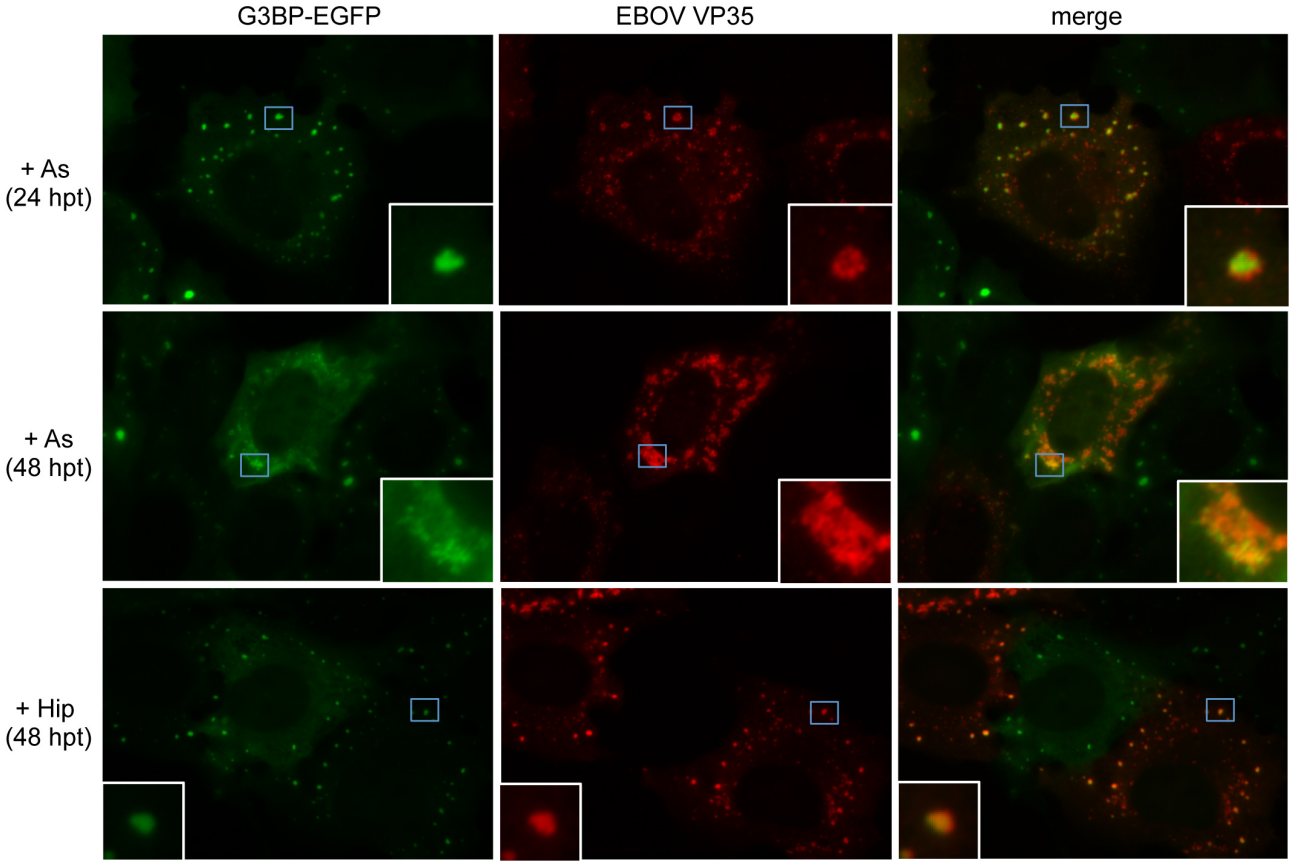


*Fig. 41: VP35 shows different localization patterns in As or Hip-treated G3BP-EGFP cells. As-treated cells were harvested after 24 hpt (upper panel) and 48 hpt (middle panel). Hip (1 µM) treated samples were transfected in parallel with As-treated samples and were harvested 48 hpt (bottom panel). Transfection and immunofluorescence staining are described in Fig. 40.*

As-treated cells were harvested after 24 h and 48 hpt (Fig. 41). At 24 hpt, VP35 was found to accumulate in small, round aggregates that surrounded the SGs in As-treated cells (Fig 41, 24 hpt). At 48 hpt, the amount of VP35 increased (Fig. 41, 48 hpt) which correlated with the inhibition of G3BP-EGFP containing SG formation.

Hip-treated cells expressing VP35 were transfected in parallel with As-treated cells (see Fig. 40). It is shown in the insert of Figure 41 that VP35 accumulated in small, round aggregates, which colocalized with the SG. VP35 showed a punctate localization pattern different from that in As-treated cells (Fig. 41).

In conclusion, expressed VP35 seemed to exhibit an inhibitory effect on G3BP-containing SG formation at high VP35 expression levels. A different distribution pattern of VP35 was observed in As and Hip-treated samples, suggesting an interaction with differently distributed components.

### Interaction of VP35 with endogenous eIF3-containing SGs

Based on the observed effects of VP35 on SG formation in G3BP-EGFP-expressing cells it was of interest to determine if similar results could be seen with endogenous SGs in cells, which do not overexpress SG proteins. Therefore, the intracellular distribution of VP35 and endogenous eIF3,

an SG marker protein, was examined in the parental U2OS cell line. The results were compared to those obtained from the G3BP-EGFP-expressing cell line.

The distribution of VP35 was similar in both the parental U2OS and U2OS G3BP-EGFP cell lines (compare Fig. 40 and 42). In non-treated cells, VP35 was not homogenously distributed but was found to be aggregated (Fig. 42). These aggregates did not correspond to the distribution pattern observed for endogenous eIF3.

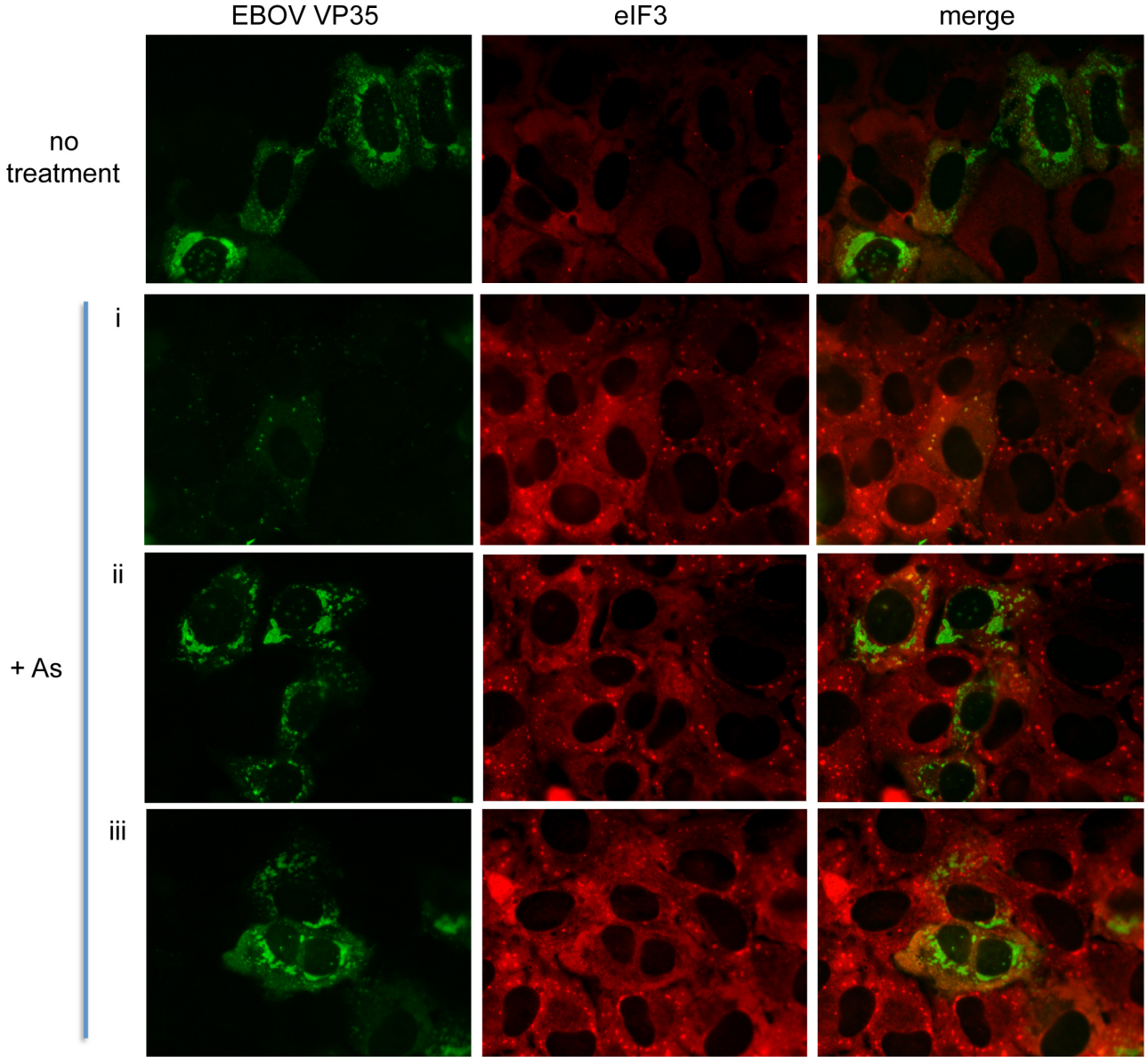


*Fig. 42: Increased expression of VP35 alters eIF3-containing SG formation in U2OS cells treated with As. U2OS cells were transfected with 0.75 µg EBOV VP35$_{HA}$ plasmid DNA (plus 0.75 µg pC-empty vector). At 2 dpt cells were treated with As (2mM) and subjected to immunofluorescence analysis. VP35$_{HA}$ expression was detected using a mouse anti-HA (1:500) and a chicken anti-mouse Alexa Fluor 488-labled secondary antibody (1:100). Endogenous eIF3 was detected using a goat anti-eIF3 antibody (1:50) and a donkey anti-goat Alexa Flour 594-labeled secondary antibody (1:100). Increasing protein expression of VP35 is indicated by i to iii (from low to high). The experiment was performed 5 times. Representative images are depicted.*

When different levels of VP35 expression (Fig. 42, panels i to iii, low to high expression) were compared in As-treated cells, the VP35 distribution was similar to that observed in G3BP-EGFP cells. VP35 was distributed in small globular aggregates in cells expressing low amounts of VP35. These aggregates accumulated when the expression level increased. High expression levels of VP35 correlated with decreased or the complete absence of eIF3-containg SG formation.

Next, the interaction of VP35 with eIF3-positive SGs was examined in more detail (Fig. 43).

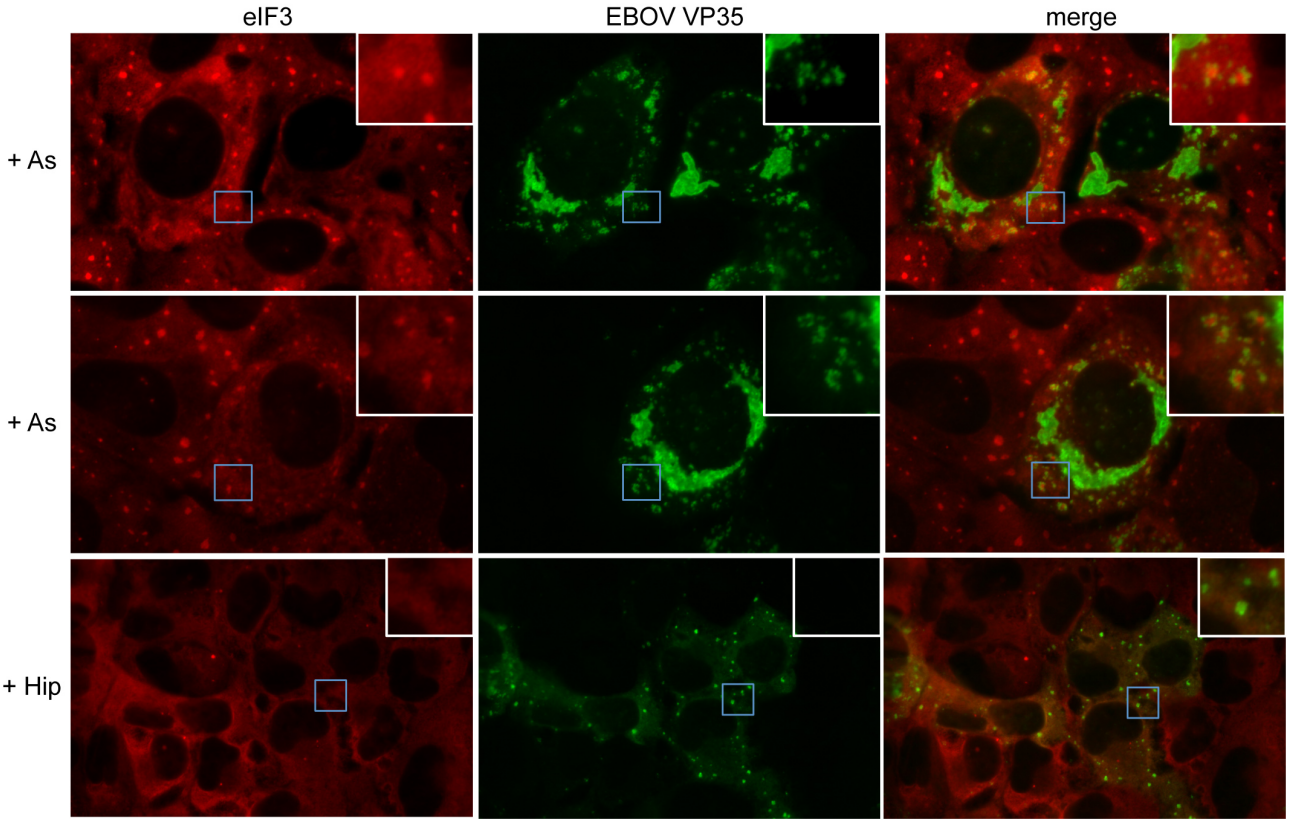


*Fig. 43: VP35 surrounds eIF3-containing SGs in cells treated with As. U2OS cells expressing $VP35_{HA}$ were transfected in parallel (see Fig. 42) and treated with As (2 mM) or Hip (1 µM). For antibody staining details see Fig. 42.*

In As-treated cells, small VP35 aggregates surrounded the eIF3-positive SGs. Although Hip-treatment did not lead to eIF3-positive SG formation (see Fig. 30) the cytoplasmic distribution of VP35 differed from that in As-treated cells (Fig. 43). The punctate appearance of VP35 in Hip-treated cells was similar to that observed in Hip-treated G3BP-EGFP cells (see Fig. 41) but differed from the As-treated cells (Fig. 43). In G3BP-EGFP cells, VP35 completely colocalized with the G3BP-positive SGs upon Hip-treatment. Taken together, this supports the observation that VP35 interacts differently with SGs formed independently of eIF2α phosphorylation. The eIF3 antibody staining in the Hip-treated cells also indicated that VP35 does not bind to eIF3 since no colocalization was observed between eIF3 and VP35.

Finally, the impact of VP35 on SG formation in the presence of NP was analyzed using U2OS cells. SG formation in As-treated cells was visualized using an anti-eIF3 antibody. The data obtained from G3BP-EGFP cells expressing NP and VP35 are described above (Fig. 33). As a control, NP was expressed in U2OS cells in the absence of VP35. Similar to the NP-transfected

G3BP-EGFP cells (Fig. 35), NP expression led to inclusion formation in both non-treated and As-or Hip-treated cells (Fig. 44A).

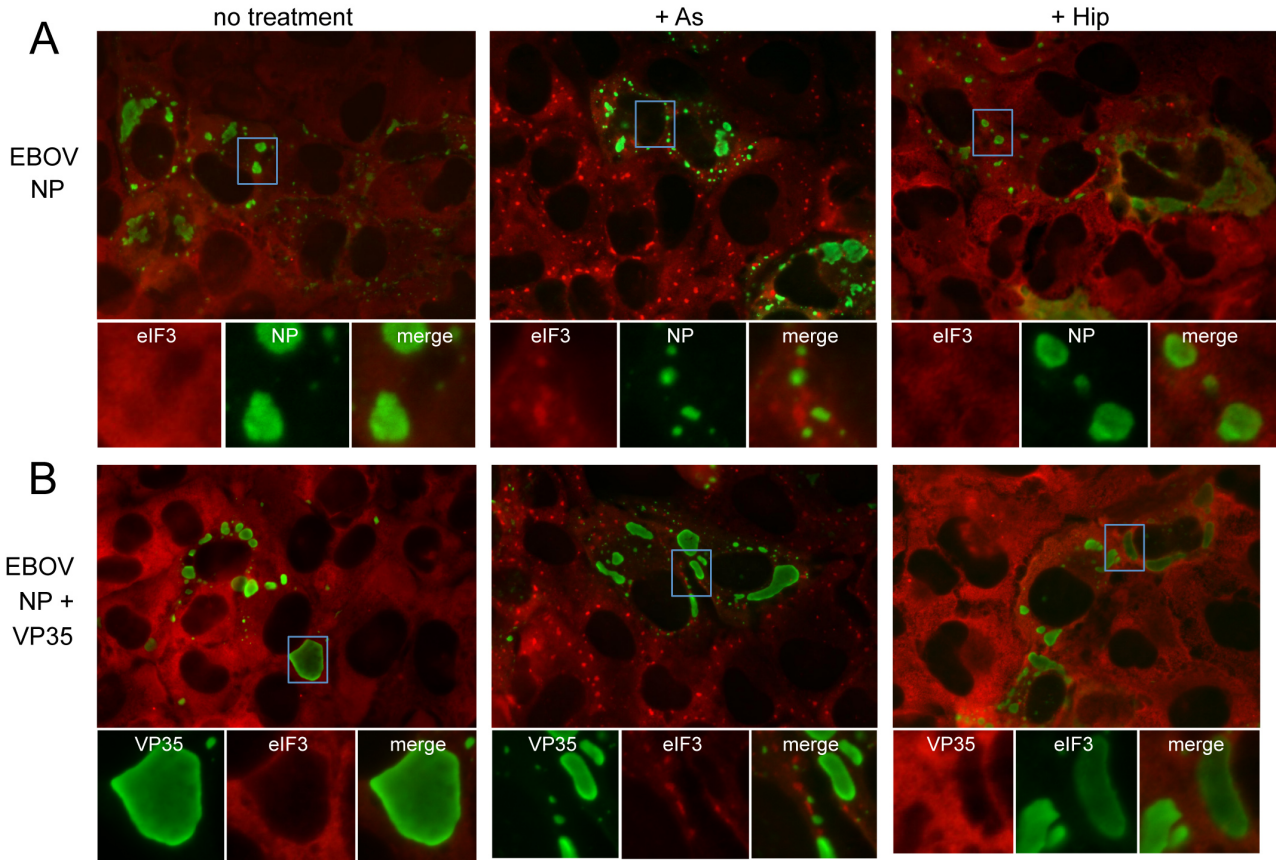


*Fig. 44: NP-derived inclusions are frequently located adjacent to eIF3-positive SGs. U2OS cells were transfected with 0.75 µg NP alone or along with 0.75 µg $VP35_{HA}$ as indicated. At 2 dpt cells were treated with As (2mM) or Hip (1 µM). Immunofluorescence staining of (A) NP was performed using a monoclonal mouse-anti NP (B6C5) antibody (1:10) and (B) $VP35_{HA}$ was performed using a mouse anti-HA antibody (1:500). A chicken anti-mouse Alexa Fluor 488-labeled secondary antibody (1:100) was used for (A) and (B). eIF3-positive SGs were detected as described in Fig. 42. The experiment was performed 5 times. Representative images shown.*

In cells cotransfected with VP35 and NP, VP35 colocalized in the NP-mediated inclusions (Fig. 44B). The viral inclusions were found in close proximity to the eIF3-positive SGs in As-treated cells, however the colocalization of VP35 with eIF3-containg SGs was no longer detected. eIF3 was homogeneously distributed in the cytoplasm of the untreated cells. eIF3 staining was not observed at the sites where the inclusions were localized (Fig. 44B). This was observed in untreated and treated (As and Hip) cells. These data further support the previous observation that antibodies are not able to efficiently penetrate the NP-derived inclusions (see part I). Another possible explanation for the observed lack of eIF3 staining in the inclusions could be that eIF3 is physically displaced by the inclusions.

In summary, in VP35-expressing cells treated with As, leading to phospho-eIF2α-mediated stress, VP35 and SGs were found in close proximity. High magnification immunofluorescence analysis revealed that SGs were surrounded by VP35. This was observed in both G3BP and eIF3-

containing SGs. In contrast, after Hip-induced stress VP35 exhibited a punctate distribution pattern that colocalized with G3BP-positive SGs.

Inhibition of phospho-eIF2α-mediated SG formation was shown when VP35 was expressed at high levels and in the absence of other viral proteins. It was not observed when VP35 was located in NP-derived inclusions, which further suggests that the inhibition of SG formation by VP35 depends on the VP35 protein expression level. This is in line with the observation that the reduction in G3BP-containing SGs in EBOV-infected cells seemed to be dependent on the level of viral protein expressed.

It is important to emphasize that the observed colocalization of VP30 and VP35 with SGs was strongly reduced or absent in cells coexpressing NP and in EBOV-infected G3BP-EGFP cells. This indicates that only free VP35 and VP30 are able to colocalize with SG proteins and that both proteins are preferentially relocated to viral inclusions. It is conceivable that the amount of free VP35 and VP30 in infected cells is too low to be detected by immunofluorescence analysis. Of note, SGs were not detected in NP-VP35 or NP-VP30 inclusions, suggesting that this environment does not allow for SG formation.

### Interaction of VP35-3A with G3BP- or eIF3-containing SGs

In EBOV-infected cells, G3BP-EGFP-containing granules are often formed in viral inclusions even in the absence of cytoplasmic SGs. The results of the VP35 transfection experiments suggest an inhibition of SG formation in an eIF2α phosphorylation-dependent manner by VP35. To further investigate the role of VP35 in the host stress response, a VP35 mutant (VP35-3A) containing three mutations in the C-terminal dsRNA-binding domain (R305A, K309A, and R312A; VP35-3A) was tested. VP35-3A has been previously reported to be defective in dsRNA binding-mediated IFN inhibition and PKR inhibition (Cardenas et al., 2006; Schumann et al., 2009).

For the first set of experiments, VP35-3A was analyzed for its ability to interact with SGs and/or inhibit their formation. VP35-3A was expressed in both the parental U2OS cells and the U2OS-G3BP-EGFP cell line. Overall the VP35-3A distribution was very similar in U2OS-G3BP-EGFP and U2OS-transfected cells (Fig. 45).

In non-treated G3BP-EGFP and U2OS cells, VP35-3A was mostly homogeneously distributed throughout the cell (Fig. 45A and B). In cells expressing high levels of VP35-3A, aggregated globular and a few small ring-like structures were visible. The ring-like structures had not been seen in VP35 wt-transfected cells (compare to Fig. 41 and 43 ).

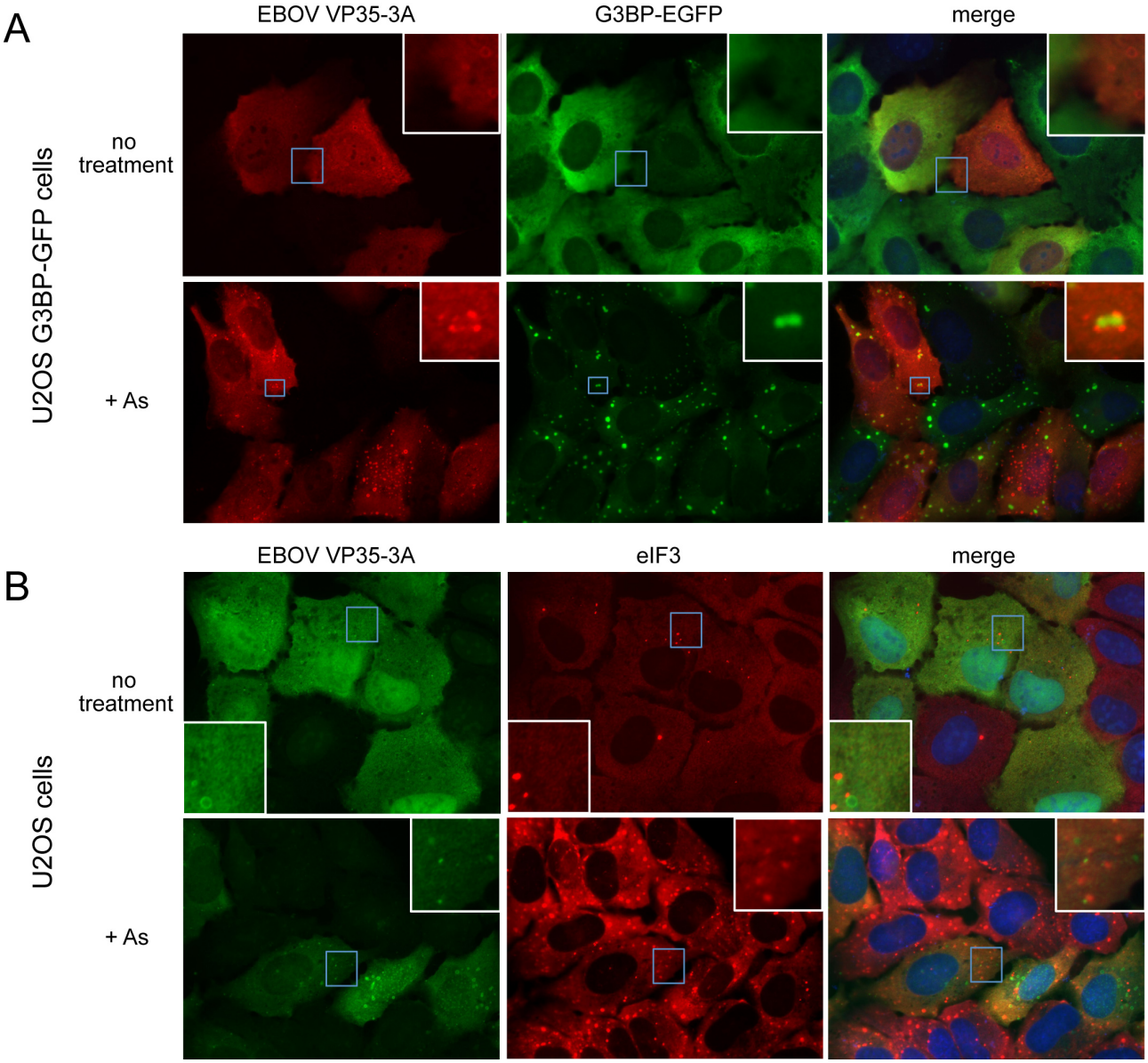


*Fig. 45: VP35-3A is not able to inhibit SG formation. U2OS G3BP-EGFP (A) and U2OS cells (B) were transfected with 0.75 µg of VP35-3A$_{HA}$ plasmid. At 2 dpt VP35-3A$_{HA}$-transfected cells were treated with As (2 mM). SG formation was detected by expression of G3BP-EGFP (A, green) or by eIF3-antibody staining (B, red). VP35-3A$_{HA}$ was detected using a mouse anti-HA antibody (1:500) and an anti-mouse Alexa Fluor 594-labeled secondary antibody (A, red, dilution 1:100) or a chicken anti-mouse Alexa Fluor 488-labled secondary antibody (B, green, dilution 1:100) were used for visualization. SGs (B) were detected by using a goat anti-eIF3 antibody (1:50) and an Alexa-Flour 594-labeled secondary antibody.*

During As stress, the number and size of the globular aggregates formed by VP35-3A increased (Fig. 45). These VP35-3A structures accumulated next to and around the SGs, which were either detected by G3BP-EGFP (Fig. 45A, green) or by eIF3-antibody staining (Fig. 45B, red). The interaction of VP35-3A with SGs is similar to the observations made for wt VP35 at low expression levels (see Fig. 40i and 42i). Depending on the expression level, VP35-3A appeared in ring-like structures, which were increased in size and number compared to the non-stressed cells. These ring-like structures were also localized next to SGs but not in all cases. Interestingly, VP35-3A did not accumulate in large aggregates shown for the wt VP35 and was not able to inhibit SG formation in either cell line (Fig. 45).

In conclusion, VP35-3A was not able to inhibit As-induced SG formation. In addition, large VP35 aggregates observed in wt VP35-expressing cells that correlated with SG inhibition were not detected. This further indicates that the accumulation might important for the inhibition of SGs. VP35-3A has also been described to exhibit lower expression levels than the wild-type (wt) VP35, which is likely due to its inability to inhibit PKR (Schumann et al., 2009).

To analyze if the VP35-3A mutant behaves differently than the wt VP35, inclusion formation was induced by cotransfection of NP. The VP35-3A mutant colocalized with the NP-derived inclusions since the NP binding domain is not affected by the mutation (REID et al., 2005) (Fig. 46).

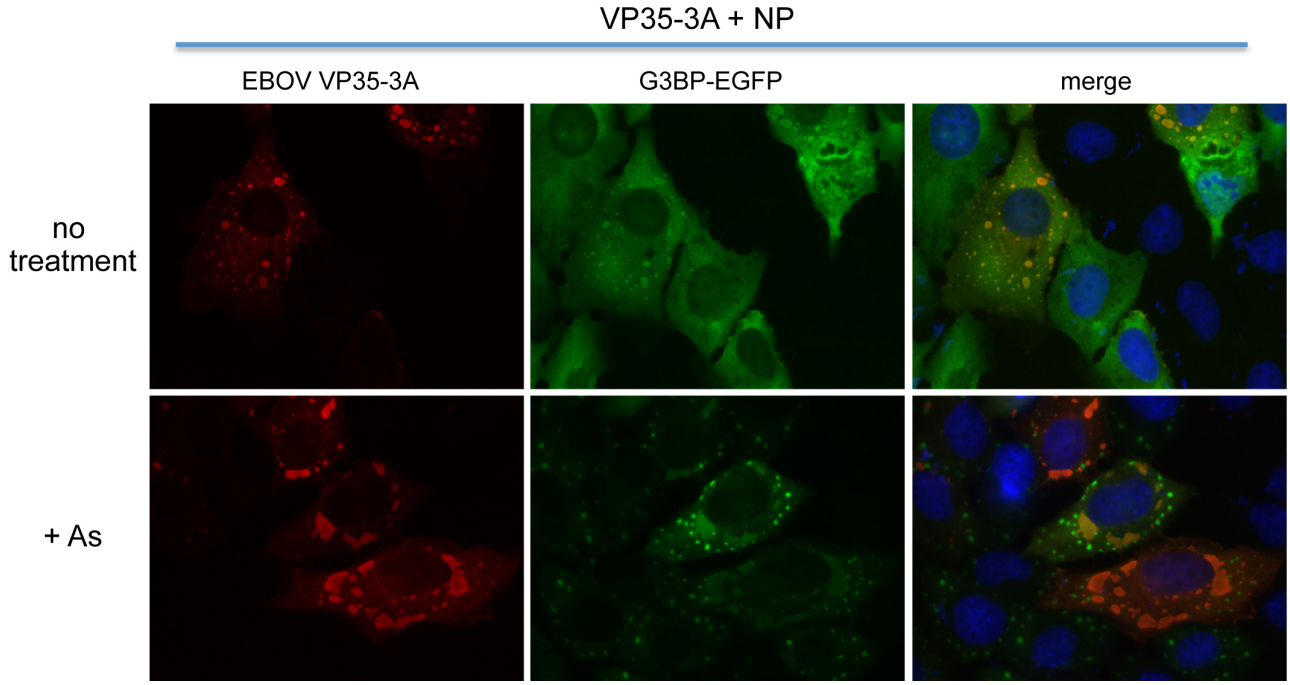


*Fig. 46: Interaction of viral inclusions formed by NP and VP35-3A with G3BP-containing SGs. G3BP-EGFP cells were transfected with 0.75 µg of NP and 0.75 µg $VP35_{HA}$-3A expression plasmids. At 2 dpt cells were treated with As (2mM). Immunofluorescence staining of NP was performed using a monoclonal mouse-anti NP (B6C5) antibody (1:10) and a chicken anti-mouse Alexa Fluor 488-labeled secondary antibody.*

Inclusions formed by NP and VP35-3A did not colocalize with SGs, and were similar to those formed by NP and VP35wt, described above (see Fig. 33). VP35-3A was relocated to the viral inclusions and did not colocalize with SGs. Therefore, only the G3BP-EGFP transfected cells are depicted, however these results were also verified in the U2OS cell line.

### 5.2.5 Phosphorylation of PKR and eIF2α in EBOV-infected cells treated with As

Oxidative As-induced stress has been shown to activate the kinase PKR. Different environmental stressors, such as heat, UV irradiation, and dsRNA also activate PKR (Williams, 2001). Activation leads to autophosphorylation of PKR and subsequently to eIF2α phosphorylation and translational arrest. It has been shown that wt VP35 is able to inhibit dsRNA-mediated activation of PKR (Feng et al., 2006; Schumann et al., 2009).

To examine the ability of EBOV to block the activation of PKR by oxidative stress, it was analyzed, whether PKR and eIF2α are phosphorylated in EBOV-infected cells after treatment with As.

HeLa cells have been extensively used to analyze PKR and eIF2α phosphorylation during EBOV infection. HeLa cells were used for Western blot analysis of PKR and eIF2α phosphorylation in EBOV-infected cells treated with As (Fig. 47). Immunofluorescence analysis was performed to evaluate the infection efficiency and revealed that approximately 90% of the cells were infected with EBOV (data not shown).

Western blot analysis of the EBOV-infected samples in the absence of As showed that neither PKR nor eIF2α were phosphorylated (Fig. 47). After As treatment, PKR and eIF2α were phosphorylated in both non-infected and EBOV-infected cells. This suggests that EBOV was not able to antagonize As-induced phosphorylation of PKR.

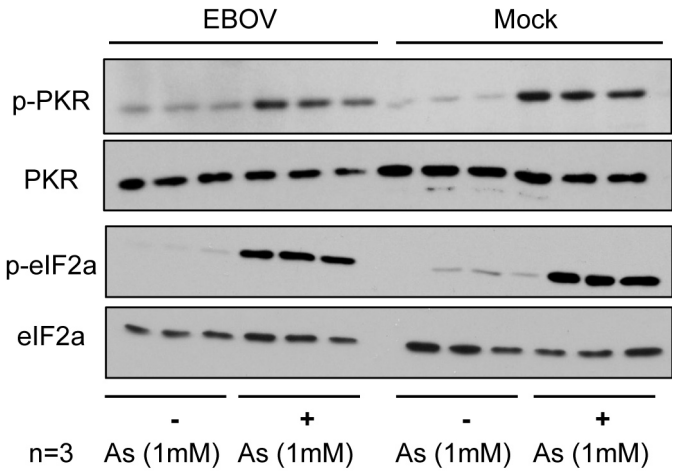


*Fig. 47: EBOV is not able to antagonize PKR and eIF2α phosphorylation induced by As. HeLa cells were seeded at $4x10^4$ (low confluence) in a 6-well plate and infected with EBOV at an MOI of 1. At 24 hpi cells were either treated with As (1 mM) or left untreated and subjected to Western blot analysis. EBOV- and non-infected cells were harvested in 50 µl cell lysis buffer (see material and methods) and subjected to Western blot analysis using antibodies directed against PKR (dilution 1:5000), phospho-PKR (dilution 1:500) incubated over night at 4°C and eIF2α (dilution 1:300) and phospho-eIF2α (dilution 1:1000) incubated for 1 h at room temperature. The corresponding horseradish peroxidase-conjugated secondary antibodies (dilution 1:40.000) were incubated for 1 h at room temperature. Western blot samples were obtained in triplicate.*

In conclusion, phosphorylation of PKR and eIF2α has been shown to be inhibited in EBOV-infected cells, even when induced by Sendai virus infection or poly(I:C) (unpublished data Olejnik et al.). However, EBOV was not able to inhibit As-induced phosphorylation of PKR and eIF2α. This indicates an additional mechanism leading to PKR phosphorylation, which is not antagonized by EBOV.

### 5.2.6 Binding of VP35 and PACT is disrupted during As-stress

During environmental stress, such as As treatment, the cellular protein PACT is able to bind and activate PKR (Patel and Sen, 1998). Since VP35 has been shown to bind to PACT in unstressed cells (Fabozzi et al., 2011), the interaction of PACT and VP35 was analyzed during As-induced cellular stress. The observed phosphorylation of PKR in EBOV-infected cells treated with As could potentially be a result of a disrupted binding of VP35 and PACT.

VP35 was coexpressed with PACT in HEK293T cells. The cells were treated with As or left untreated and subjected to immunoprecipitation. In non-stressed cells expressing VP35 and PACT,

PACT coimmunoprecipitated with VP35, indicating that the proteins interact (Fig. 48A, lanes 2 and 6). This result is in line with previously published data (Fabozzi et al., 2011).

Interestingly, in As-treated cells expressing VP35 and PACT, PACT did not coimmunoprecipitate with VP35, indicating that PACT did not bind to VP35 (Fig. 48A, lanes 3 and 7). As a control, PACT and VP35 were individually expressed along with EGFP and immunoprecipitated (Fig. 48A, lanes 4, 5, 8, 9 and Fig. 48B lanes 1, 2, 5, 6).

To verify these results, the experiment was repeated using an antibody immunoprecipitating PACT (Fig. 48B). While PACT was bound to VP35 in the absence of As (Fig. 48B, lane 3), it was not possible pull-down VP35 in As-treated cells (Fig. 48B, lane 4). This confirmed an interaction between coexpressed VP35 and PACT, which is disrupted during As-treatment.

Interestingly, previous studies have reported that PACT can enhance expression of cotransfected reporter genes, which has also been shown for VP35 (Li and Sen, 2003; Yang, 2004; Schumann et al., 2009). This could be related to the observed high expression levels of VP35 and PACT (Fig. 48B). The Western blot films depicted were exposed for 10 seconds. In addition, longer exposure times were performed to exclude that weaker bands remain undetected (data not shown).

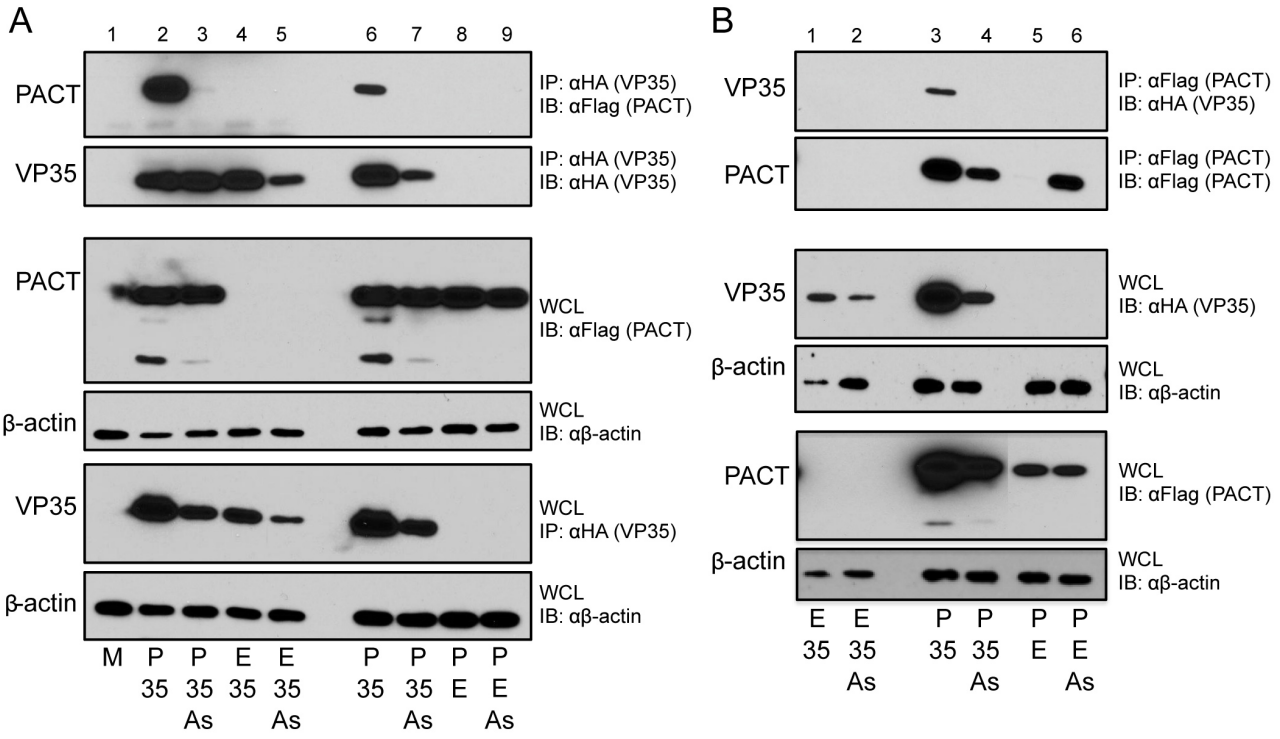


*Fig. 48: PACT does not bind to VP35 during As stress. HEK293T cells were transfected with 12 µg $PACT_{Flag}$ expression plasmid along with 12 µg EBOV $VP35_{HA}$ or 12 µg EGFP plasmid DNA. At 2 dpt, cells were treated with As (2 mM) or left untreated and subjected to immunoprecipitation (IP) using protein A/G agarose beads followed by immunoblotting (IB). For IP, mouse anti-HA antibodies (panel A, dilution 1:2000) or mouse anti-Flag antibodies (panel B, dilution 1:2000) were used. For Western blot analysis, mouse anti-Flag (dilution 1:2000) and mouse anti-HA (dilution 1:2000) antibodies were used. For β-actin, a mouse anti-β-actin antibody (dilution 1:5000) was used. For detection, horseradish peroxidase-conjugated secondary antibodies (dilution 1:40.000) were used. Abbreviations: P=PACT, 35=VP35, E=EGFP, WCL=Whole-cell lysate.*

An additional band of about 24 kDa was detected by the anti-Flag (PACT) antibody, which only appeared in the whole-cell lysates when PACT was expressed along with VP35. It is possible that

this band represents a cleaved version or a degradation product of PACT, however, further investigation is required to test this.

In conclusion, the loss of binding between VP35 and PACT in As-treated cells might lead to the inability of VP35 to sequester PACT from binding to PKR, such that PKR can be activated. This would further explain the presence of SGs in EBOV-infected cells treated with As. A similar mechanism has been described for TRBP. Dissociation of TRBP and PACT in As-stressed cells led to an increased binding and activation of PKR by PACT (Daher et al., 2009; Singh et al., 2011). The observed inhibition of SG formation in some As-treated EBOV-infected cells might happen at the level of protein interaction with SG components or by inhibiting other pathways leading to As-induced SG formation.

### 5.2.7 Formation of DCP1a-containing PBs is altered in EBOV infection

PBs, like SGs are multicomponent mRNP bodies, which regulate translational silencing. In distinction from SGs, PBs store and degrade mRNAs coopting RNAi components. PBs and SGs are frequently seen adjacent to one another, raising the possibility that mRNPs traffic from one structure to the other (Kedersha et al., 2005; Wilczynska, 2005).

The dsRNA-binding domain of VP35 has been shown to be important for suppressing the host RNAi pathway (Haasnoot et al., 2007; Zhu et al., 2012). A recent study showed that both EBOV proteins, VP30 and VP35, interact with various components of active RNA-induced silencing complex (RISC) including Dicer, TRBP, and PACT (Fabozzi et al., 2011).

Since PBs are formed as a result of RNA-mediated gene silencing, the question of whether EBOV-infection has an influence on PB formation was addressed. The U2OS cell line expressing the PB marker protein mRNA-decapping enzyme 1A (DCP1a) fused to mRFP (U2OS DCP1a-mRFP cells; Fig. 49) was used for these studies. DCP1a is part of the mRNA degradation complex.

In the U2OS cell line, DCP1a-mRFP protein expression levels varied and DCP1a-mRFP protein aggregates were observed quite frequently, especially in cells of a higher passage number. This might be due to non-specific protein aggregation. For consistency all experiments were performed in early passages of the cell lines.

#### Reduced number of PBs in EBOV-infected cells treated with As

In order to observe PB formation during EBOV infection, U2OS DCP1a-mRFP cells were infected with EBOV. In non-infected cells, only a few DCP1a-containing PBs were visible in the absence of As which increased in number during As-treatment (Fig. 49A).

In Fig. 49B different stages of EBOV infection are depicted. In untreated cells, limited PB formation was observed and the number of PBs did not substantially differ in infected and non-infected cells. Similarly to G3BP-EGFP, DCP1a-mRFP autofluorescence was observed to colocalize with the viral inclusions as described previously (see Fig. 33)**.** In As-treated cells, PB formation was observed during early stages of inclusion formation (Fig. 49B, right panels). At later stages, cells containing larger inclusions exhibited signs of cell death, including shrinkage of the cell, and PBs were not detected anymore. However, DCP1a-mRFP still colocalized with the viral inclusions.

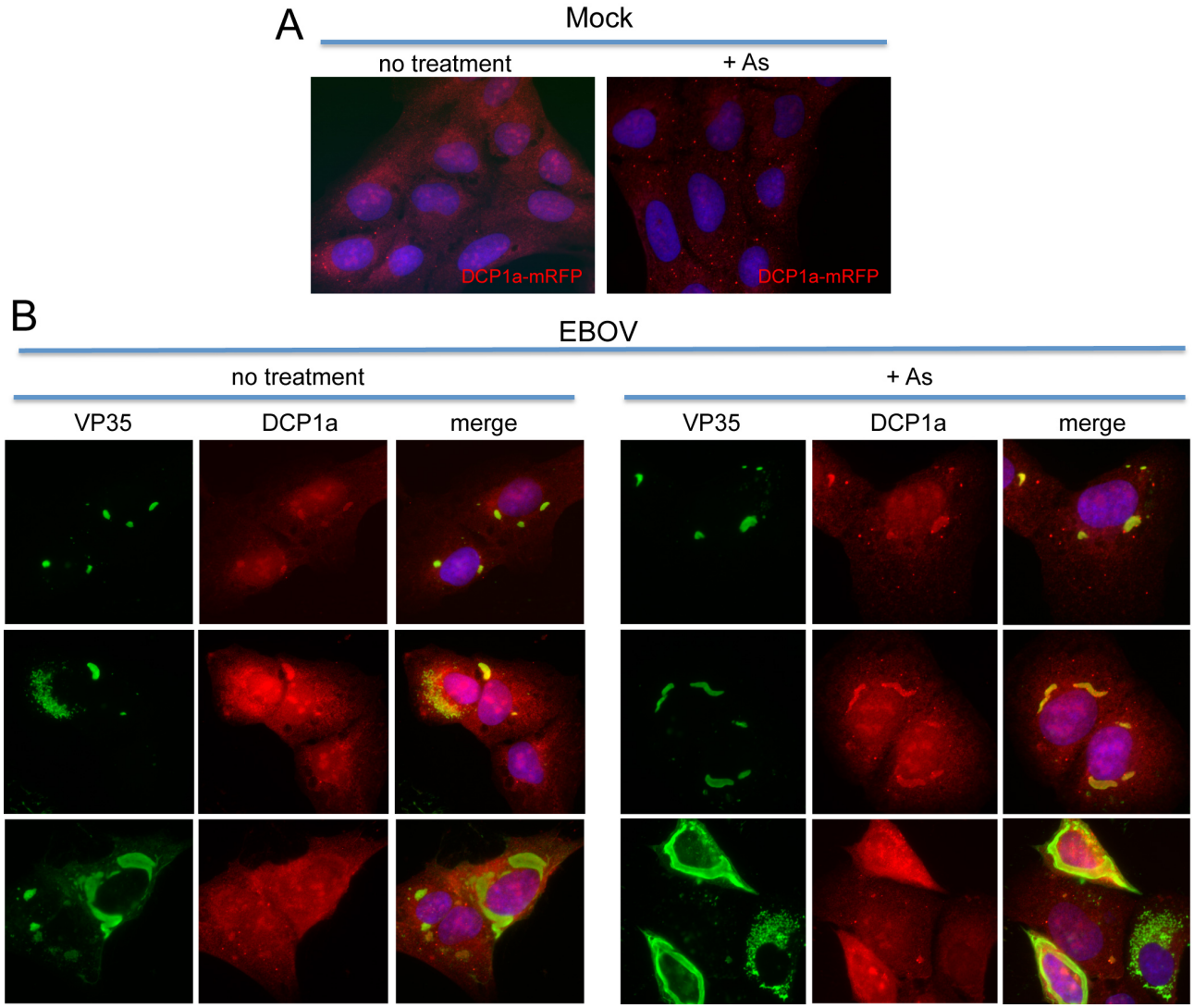


*Fig. 49: Reduced PB formation in EBOV-infected cells following As treatment. U2OS DCP1a-mRFP cells were left uninfected (A) or infected with EBOV (B) using a 1:2 dilution of supernatant fluid obtained from EBOV-infected Vero E6 cells. At 2 dpi, cells were left untreated (left panels) or treated with As (2 mM) (right panels). Cells were subjected to immunofluorescence analysis using a mouse anti-VP35 antibody (1:400) and a secondary chicken anti-mouse Alexa Fluor 488-labeled antibody. DCP1a-mRFP-containing PBs are red in fluorescence.*

As-induced PBs were observed to be localized next to viral inclusions. This suggests that PBs are recruited to viral inclusions (see discussion).

### Impact of EBOV proteins on PB formation

It was further analyzed if the EBOV RNA-binding proteins VP30, VP35, or NP expressed in U2OS DCP1a-mRFP cells have an influence on PB formation.

First, it was examined if NP-derived inclusion formation has an influence on PBs. In U2OS DCP1a-mRFP cells transfected with NP, inclusion formation was visible (Fig. 50). Formation of PBs was not influenced by the expression of NP in the absence of other viral proteins. The inclusions were often in close contact to the As-induced DCP1a-mRFP-containing PBs but did not colocalize with the PBs. This is similar to the observed interaction between SGs and NP-mediated inclusions.

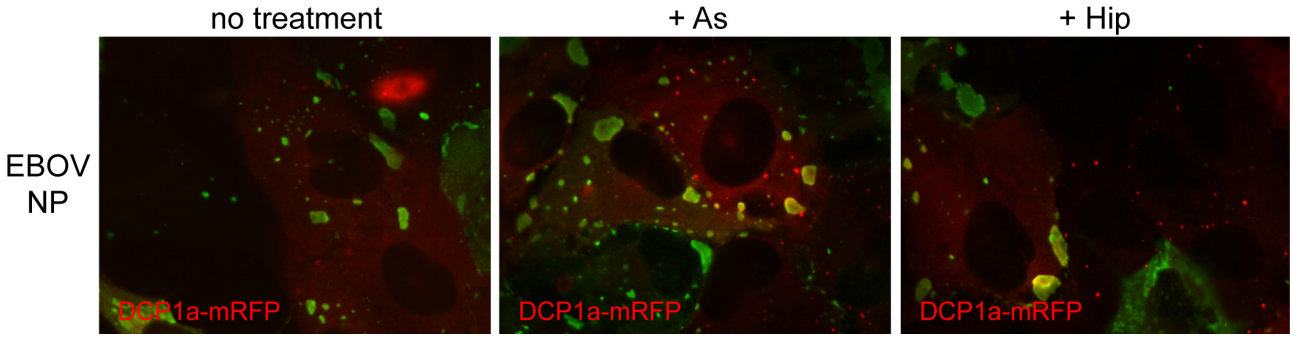


*Fig. 50: DCP1a-mRFP-containing PBs interact but do not colocalize with NP-derived inclusions. DCP1a-mRFP cells were transfected with 0.75 µg of NP expression plasmid. Cells were treated with As (2 mM) and Hip (1 µM) at 2 dpt. NP (green) was detected using a mouse anti-NP antibody (1:15) and a chicken anti-mouse Alexa Fluor 488-labeled secondary antibody (1:100).*

Next, the impact of VP30 on PBs was investigated. Therefore, VP30 was expressed in U2OS DCP1a-mRFP cells. In some cells, constitutively expressed DCP1a-mRFP accumulated in aggregates even in the absence of external stress. These protein aggregations were bigger than those seen in cells treated with As to induce PB formation. In VP30-transfected cells, the DCP1a-mRFP aggregates did not colocalize with VP30 (Fig. 51, no treatment). In the presence of As, PB formation was observed. VP30 was seen to form aggregates, which were in close contact to the PBs but did not colocalize. Since VP30 was shown to colocalize with SGs (see above), the VP30 aggregates are considered to be SGs (Fig. 51).

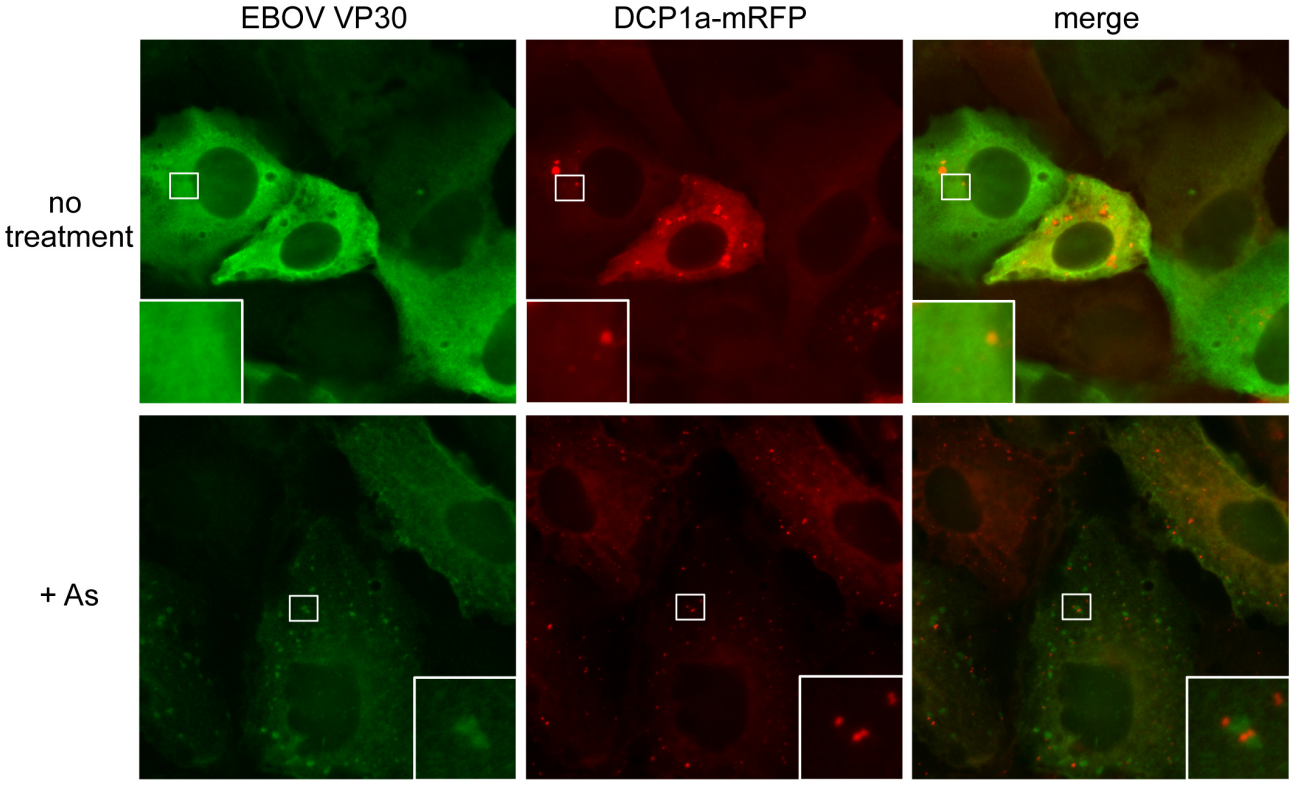


*Fig. 51: PBs containing DCP1a-mRFP interacted but did not colocalize with VP30. U2OS DCP1a-mRFP cells were transfected with 0.75 µg of VP30 expression plasmid. Cells were treated with As (2 mM) at 2 dpt. For detection of VP30, a rabbit anti-VP30 antibody (1:100) and an Alexa Fluor 488-labeled secondary antibody (1:100) were used.*

In conclusion, VP30 did not colocalize with PBs in As-treated cells. The close proximity to PBs might be explained by its shown interaction with SGs. In addition, PB formation did not seem to be influenced by VP30 expression.

Since VP35 was observed to have an effect on As-induced SG formation, it was interesting to examine its impact on PBs. U2OS DCP1a-mRFP cells were transfected with VP35 (Fig. 52 A). The distribution of VP35 in untreated and As-treated U2OS DCP1a-mRFP was similar to that observed in the other used cell lines (see Fig. 41 and 43). In As-treated cells, small VP35 aggregates colocalized with the DCP1a-mRFP-positive PBs (Fig. 52, insert).

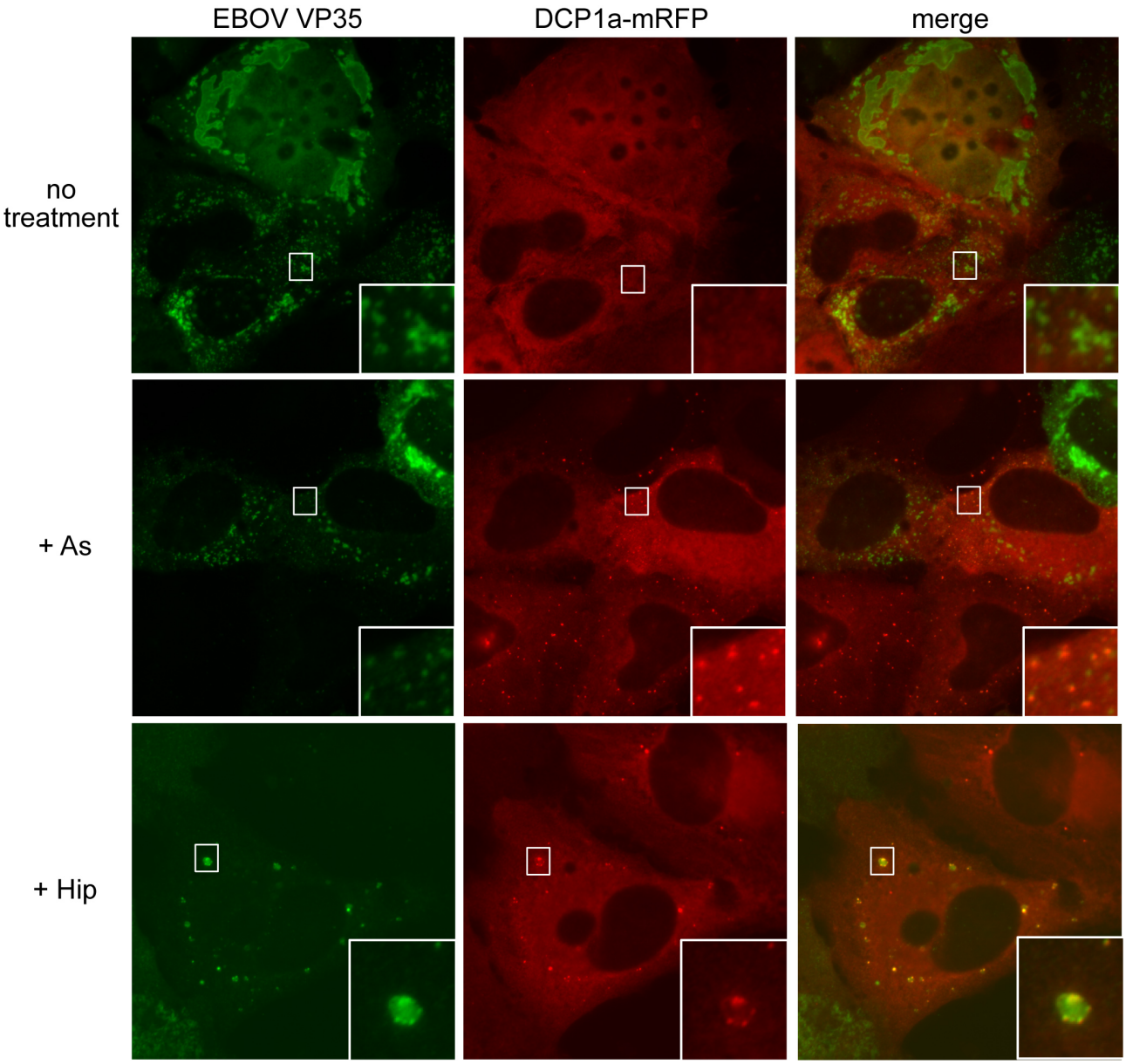


*Fig. 52: PBs containing DCP1a-mRFP colocalize with VP35. DCP1a-mRFP cells were transfected with 0.75 µg of plasmid expressing $VP35_{HA}$. For the detection of $VP35_{HA}$ a mouse anti-HA (1:500) and an anti-mouse Alexa Fluor 488-labled secondary antibody (1:100) were used. Cells were treated with As (2 mM) and Hip (1 µM) at 2 dpt.*

In Hip-treated cells, the VP35 aggregates showed a punctate, dot-like pattern similar to the VP35 distribution observed in other Hip-treated U2OS cells (compare Fig. 52 with Fig. xy above). Detailed observation revealed that the VP35 aggregates were surrounded by smaller globular aggregates of VP35 (Fig. 52 + Hip, insert). Colocalization of these small globular VP35 aggregates with the DCP1a-mRFP-positive PBs was observed. It is possible that the punctate pattern represents an interaction of VP35 with Hip-induced SGs, which were not detected in these samples.

This suggests that VP35 interacts with PB components during As and Hip-induced stress. PBs have been shown to contain components involved in miRNA-mediated gene silencing, such as Ago2, and RCK/p54. These constitute potential interaction partners, since VP35 has been shown to bind other RISC components (see discussion). In contrast to SG formation, PB formation was not influenced by the expression of VP35, neither in As nor in Hip-treated cells.

VP35 has been shown to interact with both PBs and SGs. However, the interaction was different, since SG but not PB formation was observed to be impaired in As-treated cells. To further analyze this, U2OS cells constitutively expressing both DCP1a-mRFP and G3BP-EGFP (described in Ohn et al., 2008) were transfected with VP35 and treated with As (Fig. 53).

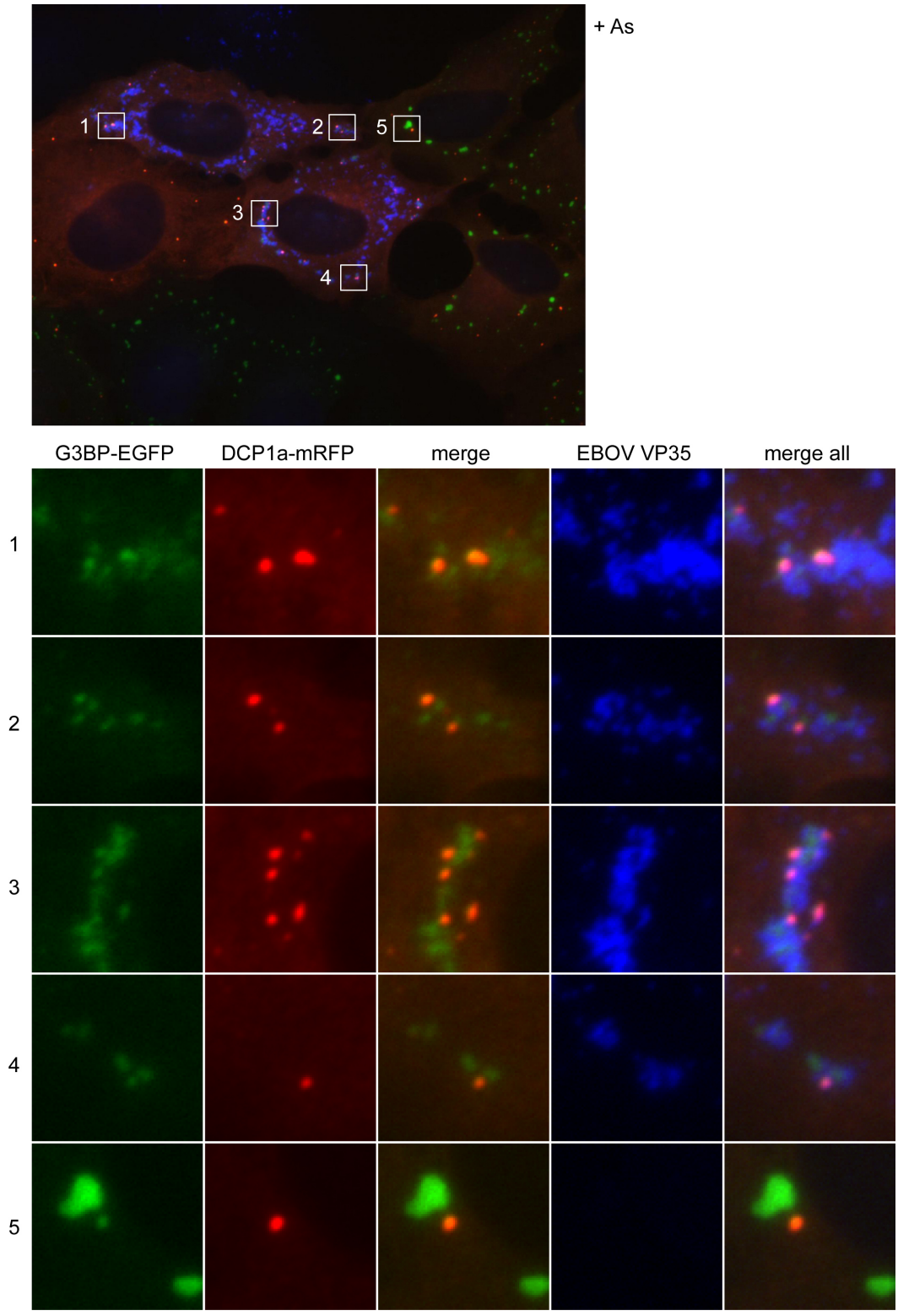


*Fig. 53: VP35 interaction with DCP1a-mRFP and G3BP-EGFP. U2OS cells constitutively expressing DCP1a-mRFP and G3BP-EGFP were transfected with 1 µg of $VP35_{HA}$ expression plasmid. At 2 dpt cells were treated with As (1 mM). $VP35_{HA}$ was detected by using a mouse anti-HA (1:1000) antibody and an anti-mouse Alexa Fluor 405-labeled secondary antibody.*

Overall VP35 aggregates colocalized with SGs and PBs. G3BP-containing SG formation was inhibited in VP35-positive cells (Fig. 53, detail images 1-4), whereas SG formation was observed in VP35-negative cells (Fig. 53, detail 5). These observations are in line with the results obtained from the G3BP-expressing cells (Fig. 53). Although SG formation did not occur, G3BP-EGFP formed diffuse aggregates, which colocalized with VP35. In contrast, DCP1a-mRFP-containing PB formation was not affected by VP35 expression and the PBs also colocalized with VP35. Intriguingly, the aggregated G3BP-EGFP, the DCP1a-mRFP-positive PBs, and VP35 colocalized and intermingled in VP35-expressing cells. This suggests that VP35 interacts and links constituents of PBs and SGs, which might be otherwise separated.

In order to analyze if VP35-3A might exhibit a different interaction pattern with PBs than the wt VP35, DCP1a-mRFP cells were transfected with the VP35-3A mutant (Fig. 54). The VP35-3A distribution in non-treated cells was consistent with results described above (see Fig. 45). DCP1a-mRFP formed aggregates in non-treated cells that were similar to those observed in VP35 wt-transfected DCP1a-mRFP cells. These DCP1a aggregates were surrounded by ring-like structures formed by VP35-3A (described above, Fig. 45). As mentioned above, these ring-like structures were only observed in cells expressing VP35-3A but not in cells expressing wt VP35, which needs to be further investigated. In As-treated cells, a different distribution was observed, as DCP1a-mRFP relocalized to form PBs, which colocalized with globular VP35-3A aggregates. This suggests that the ability of VP35 to bind dsRNA is not a requirement for the interaction with PBs, since VP35-3A was observed to colocalize with PBs.

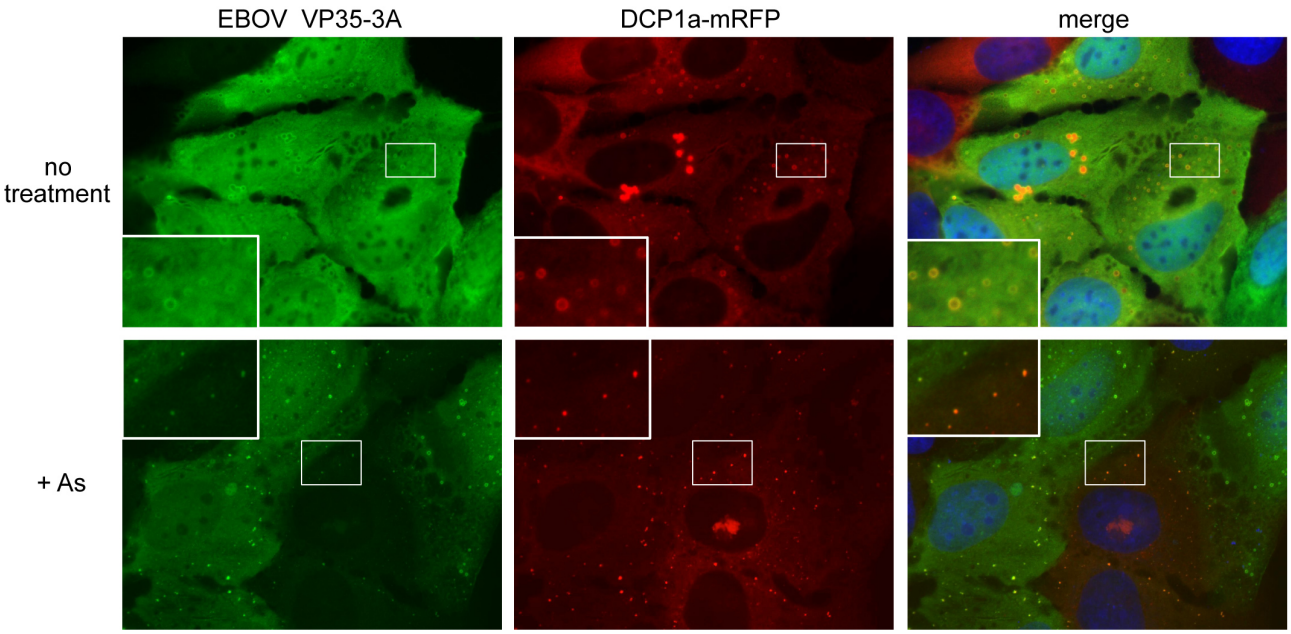


*Fig. 54: PBs containing DCP1a-mRFP colocalize with VP35-3A$_{HA}$. U2OS DCP1a-mRFP cells were transfected with 0.75 µg of plasmids expressing VP35-3A$_{HA}$. For As treatment and immunofluorescence staining see Fig. 52.*

# 6. Discussion

## 6.1. Generation of a recombinant MARV clone expressing EGFP

The generation of recombinant EGFP-expressing viruses has significantly improved the study of their life cycle and opened up the possibility for the rapid screening of antiviral drugs. Rescue systems to recover infectious virus from full-length cDNA clones have been established for both MARV and EBOV (Enterlein et al., 2006; Ebihara et al., 2007; Halfmann et al., 2008). These techniques were used to generate a recombinant EBOV containing the EGFP gene within an ATU (Ebihara et al., 2007). Other viruses of the order *Mononegavirales* containing fluorescence proteins have been generated including a recombinant measles virus (Duprex et al., 1999; Duprex and Rima, 2011).

This work describes the successful rescue of an rMARV containing the EGFP ORF inserted in an ATU between the VP35 and VP40 genes. The rationale for the positioning of the EGFP ORF near the 3' end of the viral genome was to maximize the number of EGFP transcripts and thereby increase the sensitivity of virus detection. At the same time it was essential to avoid alterations in the balance between expression of NP (first gene product) and VP35 (second gene product), since previous results using a MARV minigenome system suggested that the ratio of NP to VP35 is critical for efficient transcription and replication (Muhlberger et al., 1998). EGFP has been expressed from the closely related EBOV from multiple positions within the genome. Insertion of the ATU between the NP and VP35 genes did not lead to significant growth defects in cell culture but showed attenuation in a STAT1 knockout mouse model (Towner et al., 2005; Ebihara et al., 2007). Similar effects were observed with an rEBOV containing EGFP in an ATU between the VP30 and VP24 genes (fifth and sixth genes). This virus showed no or mild growth defects in cell culture depending on the cell line used for propagation, was moderately attenuated in the mouse model, and was severely attenuated in a non-human primate model (Ebihara et al., 2007). Another rEBOV in which the ATU was added between the VP35 and VP40 genes (second and third genes) was rescued and propagated in cell culture (Martinez et al., 2008). Taken together, these data show that EBOV tolerates the addition of a foreign gene at many different positions, although the insertion of extra non-viral genetic material may lead to reduced virulence in animal models.

In contrast to rEBOV, the rescue of wt MARV from cDNA clones under the control of the T7 RNA polymerase promoter was very inefficient and succeeded only after several transfections. Interestingly, it has been shown that virus rescue of the recombinant clone of Saffold virus type 3 (SAFV-3) was impossible due a premature termination of transcription by the T7 RNA polymerase (Himeda et al., 2011). SAFV-3 was found to contain a sequence, which is homologous to a conserved pausing/termination sequence (A/C/TATCTGTT followed by a T rich sequence) of the T7 RNA polymerase (Lyakhov et al., 1998). It is shown that after substitution mutations of the sequence, rescue of the recombinant SAFV-3 with virus titers comparable to the wt SAFV-3 were observed (Himeda et al., 2011). The same sequence is present in the rMARV-EGFP genome (AATCTGTT; nt 9438-9447) but not in the EBOV genome. This sequence therefore might lead to a decrease of full-length infectious RNA and subsequently to significantly decreased virus production and decreased viral rescue. This will be further addressed in collaboration with Dr. H. Ebihara from the Rocky Mountain Laboratories, USA.

A growth restriction of rMARV-EGFP has been observed compared to the growth kinetics of wt rMARV. This was determined by quantification of the protein expression of NP and VP40. The results indicate that the presence of the ATU affects the recombinant MARV-EGFP protein expression rate, since genes downstream of the insertion were expressed less efficiently.

However, viral spread of rMARV-EGFP was successfully monitored in living cells. Our data suggest that virus spread occurs predominantly through cell-to-cell-contact. Release of viral particles from MARV-infected cells has been shown to take place at filamentous protrusions, the filopodia (Kolesnikova et al., 2007). Since filopodia act as sensory organelles to explore the extracellular environment and contact neighboring cells (Mellor, 2010), it has been suggested that MARV particles may bud into adjacent cells via filopodia-mediated cell-to-cell contact (Kolesnikova et al., 2007). Our data received from live cell imaging shows that also virus replication in actively dividing cells seems to be an important mechanism of MARV spread in cell culture. Cell division is not inhibited by MARV infection, indicating that MARV does not interfere with cell cycle progression. Towards the end of the observation period of 9 days cell rounding, blebbing, and finally detachment of EGFP-expressing infected cells was observed, which correlates with impeding cell death.

The collected data clearly illustrate the usefulness of live-cell imaging, which allows for the investigation of intracellular dynamic processes during the course of infection. Live-cell analysis of infected cells also facilitates the fast and quantitative readout of antiviral drug screening assays and virus spread studies.

Surprisingly, EGFP was found to accumulate in filoviral inclusions. A similar observation was reported for some members of the nucleorhabdoviruses, where GFP colocalized with viral nucleocapsid protein in loci within and around the nuclei (Goodin et al., 2005). In contrast, EGFP was found to be homogenously distributed in the nuclei and cytoplasm of cells infected with EGFP-expressing measles virus, which also produces intracytoplasmic inclusions (Duprex et al., 1999). The intracellular distribution of EGFP was examined by live-cell imaging and immunofluorescence analysis using infected and transfected cells. The fluorescence intensity of homogenously distributed EGFP surrounding the intracytoplasmic EGFP aggregates was higher in living cells, making it difficult to distinguish between EGFP aggregates and non-specific distributed EGFP. Moreover, when large amounts of EGFP plasmid were used for transfection (500 ng), the punctate pattern of EGFP was not observed in cells coexpressing MARV NP and VP35, suggesting that the EGFP aggregates were masked when overall EGFP expression was high, illustrating the importance of making observations in cells which do not extensively overexpress the protein of interest. In fixed and permeabilized cells, punctate EGFP was clearly visible in both infected cells and transfected cells coexpressing NP and VP35, suggesting that the intensity of EGFP autofluorescence was reduced by the treatment of the cells. EGFP aggregation was induced by expression of NP in the absence of other viral proteins but was more pronounced when coexpressed with VP35. Expression of VP35 alone does not lead to inclusion formation and EGFP was accordingly homogenously distributed in these cells.

Intriguingly, EGFP not only colocalized with MARV inclusions but also with EBOV and RESTV inclusions formed by NP and VP35. EGFP expressed from an ATU between NP and VP35 in rEBOV-infected cells was also tested and confirmed the EGFP aggregation.

In addition to EGFP, other fluorescent proteins were found to colocalize with MARV inclusions. These data indicate that the accumulation of ectopic proteins in filoviral inclusions is most likely not

mediated by direct, specific protein-protein interaction. The observed colocalization of ectopically expressed fluorescent proteins with filovirus inclusions may be useful in the investigation of nucleocapsid maturation and transport in infected cells.

The relocalization of fluorescence proteins into MARV inclusions was further examined using GFP-tagged proteins. Various versions of GFP fusion proteins involved in cytoplasmic aggresome formation were analyzed to determine if MARV NP and VP35 inclusion formation alters their localization. GFP-250 is a misfolded chimeric protein that leads to aggresome formation in the cytoplasm when overexpressed (García-Mata et al., 1999). Aggresome formation is accompanied by the redistribution of the intermediate filament protein vimentin, proteasomes, heat shock protein (Hsp) 70, and the chaperonin system of chaperones. Aggresome formation involves retrograde transport along the microtubules from the periphery towards the microtubule organization center (MTOC) region. Here, GFP-250-induced aggresomes remain as distinct but closely apposed particulate structures. In addition, the GFP-tagged dynein motor protein, p50 dynamitin (GFP-dynamitin), which causes the dissociation of the dynactin complex was tested (Burkhardt et al., 1997). Taken together, neither of the two GFP-fusion proteins relocated into inclusions formed by MARV NP and VP35. This indicates that homogeneously distributed fluorescent proteins are more likely to relocate into viral inclusions than GFP fusion proteins that are actively targeted to specific cellular compartments. This further suggests that the observed colocalization of fluorescent proteins with the MARV NP-derived inclusions is not due to a strong, specific interaction, since the intracellular distribution of GFP-fusion proteins was not altered. Aggresome formation itself was also not altered by the expression of MARV NP and VP35.

Interestingly, although aggregation of untagged EGFP in coexpression with MARV NP and VP35 was visible by EGFP autofluorescence, EGFP aggregation was not detected by immunofluorescence analysis using an antibody directed against GFP. This indicates that inclusion formation excludes antibody penetration. This has also been shown for the overexpressed cellular protein CREB-binding protein (CBP), which forms intranuclear inclusions that could not be penetrated by antibodies (McCampbell et al., 2000). These findings suggest that other proteins that might be located within the NP-derived inclusions are undetected by antibody-based immunofluorescence.

## 6.2. Host cell stress response to EBOV infection

An important host antiviral defense mechanism is stress-induced translational arrest, which is often accompanied by the formation of SGs and an increase in the number of PBs present in the cytoplasm of the cell. The eIF2α subunit within the GTP-eIF2-tRNA$^{Met}$ ternary complex plays a central role in the control of translation. Phosphorylation of eIF2α by a small range of kinases leads to an arrest of the translational machinery and to SG formation. Like many viruses, filoviruses depend on the cellular translation apparatus for viral protein synthesis. Therefore, phosphorylation of eIF2α is an effective antiviral defense mechanism to which many viruses have evolved a certain level of tolerance either by the inhibition of eIF2α phosphorylation or by eIF2α-independent translation. The external oxidative stressor As induces eIF2α phosphorylation and SG formation by activation of the kinases PKR and HRI (McEwen, 2005; Daher et al., 2009; Singh et al., 2011).

In this work, the impact of EBOV infection on the SG- and PB-mediated host cell stress response was analyzed.

### SG formation in EBOV-infected cells

To analyze the role that the cellular stress response plays in EBOV infection, SG formation was determined in EBOV-infected Vero E6 cells. Using an eIF3 antibody to look at SG formation, EBOV-infected cells were not found to induce SGs. After treatment with As, SGs were detected in EBOV-infected cells albeit in fewer cells compared to the non-infected cells This indicates that EBOV is able to partially inhibit As-induced SG formation.

An inhibition of SG formation, even in response to As treatment, was seen in rotaviruses (*Reoviridae*) and Human immunodeficiency virus 1 (HIV-1) (*Retroviridae*) infected cells (Montero et al., 2008; Abrahamyan et al., 2010). Interestingly, for both infections, high levels of eIF2α phosphorylation were shown in response to As treatment, indicating the inhibition of SG formation by a mechanism downstream of eIF2α. Junin virus, a member of the arenavirus family, inhibited SG formation in response to As treatment by an undefined mechanism, that was dependent on the expression of the nucleoprotein (N) or the glycoprotein precursor (GPC) (Linero et al., 2011). However, the inhibition of SGs correlated with low levels of eIF2α phosphorylation.

Since As treatment induces SG formation in a phospho-eIF2α-dependent manner, the question arose of whether the observed inhibition of SGs by EBOV is due to the ability of EBOV to block PKR-mediated phosphorylation of eIF2α (Hartman et al., 2004; Feng et al., 2006; Schumann et al., 2009).

### G3BP-containing granules in EBOV-infected cells

For better visualization of SGs, a U2OS cell line expressing the SG maker protein G3BP fused to EGFP was used. The most intriguing observation made in the EBOV-infected G3BP-EGFP cells was that G3BP-EGFP-containing granules formed within the viral inclusions. In contrast to SGs, which were observed in the cytoplasm after treatment with stress inducers during the considerably short time window of 30 minutes, these SG-like G3BP-EGFP aggregates were present even in non-treated cells. Accumulation of G3BP granules in non-treated cells was restricted completely to viral inclusions of all sizes. This indicates that these granules formed concurrently with viral

inclusions during the infection period of 2 days. These G3BP granules are distinct from the round, globular structure of SGs and are more diffusely aggregated and not round-shaped.

As treatment induces dephosphorylation of G3BP, which allows self-oligomerization. Only the non-phosphorylated form of G3BP is able to self-aggregate and thereby initiate SG assembly (Tourrière, 2003). G3BP requires phosphorylation for its catalytic endoribonuclease activity (Gallouzi et al., 1998). G3BP contains a C-terminal RNA-binding domain that has an especially important role in SG formation and participates in mRNA metabolism (Parker et al., 1996; Tourrière et al., 2001; Tourrière, 2003; Atlas et al., 2004).

To date, it is not known if G3BP is phosphorylated in EBOV-infected cells, which would be most interesting to analyze. The G3BP of the SG-like aggregates within the viral inclusions could be dephosphorylated or partially dephosphorylated, since G3BP is able to aggregate but the aggregates appeared to be not as round-shaped as in cytoplasmic SGs. In a dephosphorylated state, G3BP would not be able to exhibit its RNase activity, leading to the protection of viral RNA in the inclusions

Several positive-sense RNA viruses, including flaviviruses such as HCV, West Nile virus (WNV), and dengue virus (DV) as well as rubella virus (*Togaviridae*) and poliovirus (*Picornaviridae*), have been shown to induce the redistribution of G3BP. During HCV infection G3BP and other SG components are recruited to the viral replication factories, and several SG markers, including G3BP, colocalize with the HCV core protein even in the presence of stress (Ariumi et al., 2011). G3BP interacts with the HCV RNA-dependent RNA polymerase, NS5B, and the 5' terminus of the negative-strand RNA replication intermediate during HCV infection to mediate efficient replication of the viral genomic RNA (Yi et al., 2011). It also has been shown that G3BP binds with the genomic 3' UTR and 5' UTR of DV (Ward et al., 2011). The function of this interaction is not known. Furthermore, both DV and WNV inhibit SG formation in response to exogenous stress by sequestering TIA-1 and TIAR through specific binding to the minus strand 3' terminal stem loop structure, an interaction that is required for viral replication (Li et al., 2002; Emara and Brinton, 2007).

Since viruses are master manipulators of cellular processes, it is not surprising that SG factors such as G3BP or TIA-1 interact with positive-strand RNA virus components. Still, the question remains if such sequestration is a result of a selective pressure to inhibit SGs or an active requirement to facilitate viral replication. For filoviruses, it is assumed that viral inclusions are sites of active viral replication, but this has not been experimentally confirmed. It is also not currently known if cellular components are localized at the sites of inclusion formation. This further raises the possibility that viral inclusion formation is connected to the cellular stress response and their components.

The location of G3BP granules within the EBOV inclusions as well as their different shape raises the question as to whether they are functional SGs. As established by several reports, SGs are defined as highly dynamic poly $(A)^+$ RNA-containing cytoplasmic foci that transiently accumulate in response to stress, and SGs are in equilibrium with polysomes (Nover et al., 1989; Kedersha et al., 1999; 2002). Hence, it remains to be further investigated whether the observed G3BP granules exhibit SG characteristics. The question could be analyzed using drugs that either stabilize polysomes while disintegrating SG formation (e.g. emetine and cycloheximide) or destabilize polysomes and consequently enhance assembly of SGs (e.g. puromycin). It is also important to analyze the possible presence of other SG maker proteins within filoviral inclusions. The G3BP

granules observed in colocalization with viral ssRNA in perinuclear clusters at late stages in rubella-infected cells were found to differ from As-induced SGs in composition and response to cyclohexamide treatment (Matthews and Frey, 2011).

However, the observation of G3BP granules within the viral inclusions was only made for EBOV-infected G3BP-EGFP containing cells and not for eIF3-stained SGs in EBOV-infected Vero E6 cells. As mentioned above, antibodies might not be able to penetrate the viral inclusions. Therefore, it is possible that only fluorescence-tagged proteins can be visualized within viral inclusions.

To further investigate which EBOV component is responsible for the relocation of G3BP-EGFP into viral inclusions, cells were transfected with different combinations of viral proteins involved in NC formation. Interestingly, Inclusion formation induced by expression of viral nucleocapsid proteins was not sufficient for the accumulation of G3BP granules inside the inclusions. Considering the known RNA-binding capacity of G3BP and its interaction with viral ssRNA genomes, it is conceivable that active replication complexes or viral genomic or antigenomic RNA are key factors for the relocalization of G3BP. However, relocalization due to the EGFP portion of G3BP observed earlier for ectopic EGFP is not likely to play a role, since aggregation of G3BP-EGFP was not observed in transient expression of EBOV NC proteins, which were sufficient for the relocalization of EGFP.

Together this data suggest a mechanism of EBOV to interfere with SGs by sequestering SG components in the viral inclusions.

### G3BP-containing SG formation in EBOV-infected cells

In EBOV-infected G3BP-EGFP-expressing cells, SG formation was induced by As and hippuristanol (Hip). Cellular stress induced by Hip leads to SG formation by inhibiting eIF4A-dependent translation initiation, a process, which does not involve phosphorylation of eIF2α (Bordeleau et al., 2006). To date it is not known if SGs induced by these two different chemical compounds contain a different composition of constituents.

Cytoplasmic G3BP-EGFP-containing SG formation was observed in EBOV-infected and non-infected G3BP-EGFP cells upon treatment with As. Although G3BP-positive SG formation was reduced in EBOV-infected cells, it occurred in higher numbers than previously detected in EBOV-infected Vero cells stained for endogenous eIF3. Transient overexpression of G3BP-EGFP has been shown to induce spontaneous SG formation in the absence of extracellular stress (Kedersha et al., 2005). Unlike transient transfections, G3BP-EGFP constitutively expressed in U2OS cells does not exhibit spontaneous SGs but instead displays a homogeneous distribution (Kedersha et al., 2008). G3BP-EGFP in the U2OS cell line (characterized by Kedersha and coworkers) exhibits a behavior similar to endogenous G3BP albeit G3BP-EGFP is expressed at about 10-fold higher levels relative to the endogenous proteins (Kedersha et al., 2008). Therefore it is possible that these cells are more sensitive to stress signals and more prone to form G3BP-EGFP-containing SGs. This might explain why an increased number of cells were observed to form G3BP-EGFP-containing SGs in As-treated cells infected with EBOV. However, in a number of EBOV-infected cells cytoplasmic SG formation was not observed, even though G3BP-EGFP SG-like granules were detected within the viral inclusions. This indicates that these cells were potentially able to form SGs, since G3BP-EGFP was expressed, but they were inhibited by the infection with EBOV.

As treatment was compared to Hip treatment in EBOV-infected cells. In some cells treated with As, G3BP-EGFP was diffusely distributed and SG formation was impaired. This was not seen in Hip-treated cells, suggesting that EBOV inhibits SG formation in response to phospho-eIF2α-mediated stress. This inhibition seemed to be dependent on the size of the viral inclusions, suggesting that a certain level of viral protein expression is required.

In contrast to SG inhibition, accumulation of G3BP-positive SG-like granules within viral inclusions (discussed above) was very similar in As/Hip-treated cells as well as in non-treated cells and was seen in viral inclusions of all sizes during EBOV infection.

Interestingly, Junin virus infection led to the inhibition of As-induced SG formation, but did not inhibit SG formation induced by Hip (Linero et al., 2011). The mechanism of this inhibition is unknown.

### Interplay of EBOV proteins with SGs

Since our results revealed that SG formation induced by exogenous stressors is reduced in EBOV-infected cells, we sought to identify the viral protein(s) involved in antagonizing SG formation. Since many of the proteins located in SGs have the ability to bind RNA, the EBOV RNA-binding proteins NP, VP30, and VP35 were examined. SGs interacted with the nucleocapsid proteins VP30 and VP35, whereas NP-derived inclusions did not colocalize with SGs.

### VP30 and SG

VP30 showed striking colocalization with G3BP-EGFP-containing SGs induced by either As or Hip. VP30 has previously been shown to bind ssRNA, and RNA binding activity was dependent on the presence of $Zn^{2+}$ ions (John et al., 2007). VP30 contains an unconventional CCCH Zn-finger motif, similar to motifs found in some cellular RNA-binding proteins (Weik et al., 2002; Modrof et al., 2003). It is not yet clear if the VP30 CCCH motif is directly involved in RNA binding. N-terminal VP30 deletion mutants containing the CCCH motif did not bind to RNA, suggesting that the CCCH motif alone is not sufficient for RNA binding (John et al., 2007). Proteins containing a CCCH Zn-finger motif often bind and regulate the stability of mRNAs containing AREs. The CCCH Zn-finger proteins TTP and BRF1 have a major regulatory role in controlling ARE-containing cytokine mRNAs such as TNFα and Interleukin-6. TTP and BRF1 also accumulate in SGs and PBs during environmental stress, where they deliver mRNAs to PBs and promote their deadenylation and degradation thereby exerting anti-inflammatory effects (Kedersha et al., 2005; Franks and Lykke-Andersen, 2008). The observed colocalization of VP30 with SGs suggests that VP30 interacts with SG components and likely ARE-containing mRNAs. This raises the possibility that VP30 might play a similar regulatory role by binding ARE-containing mRNAs of antiviral cytokines important during filovirus infections. SG formation itself was not visibly altered by the expression of VP30. Overexpression of TTP and BRF1 also stabilizes the association between SGs and PBs. NP- and VP30-derived inclusions were found in close proximity to SGs, seemingly strung together like pearls in some cells.

### VP35 and SG

A different interaction pattern has been observed between SGs and VP35. EBOV VP35 is a component of the nucleocapsid and plays an important role in viral replication. This multifunctional dsRNA-binding protein is also a crucial virulence factor that blocks the IFN-mediated antiviral host immune response and RNA silencing pathways (Basler et al., 2003; Hartman et al., 2004; Haasnoot et al., 2007; Zhu et al., 2012). During As-induced stress, VP35 colocalized with but also surrounded SGs, seemingly sequestering them from the cytoplasm. This was observed for both G3BP-EGFP-containing and eIF3-containing SGs. In contrast, in the presence of Hip, VP35 exhibited a punctate pattern that was observed to completely colocalize with the G3BP-positive SGs. In treated and untreated cells expressing high levels of VP35, VP35 accumulated in large aggregates. Interestingly, As-induced SG formation was reduced or completely inhibited in these cells, and the distribution pattern of SG proteins was diffuse. . This was determined by analyzing both G3BP-EGFP-positive and eIF3-positive SGs. These results differed from those in Hip-treated cells where VP35 did not form large aggregates but showed in a punctate distribution without modulating the formation of SGs.

To investigate if VP35's ability to bind dsRNA, antagonize interferon-induced pathways, and block PKR activation is involved in its ability to interact with SGs, a VP35 mutant (VP35-3A) that is inhibited in all three functions was tested (Leung et al., 2009; Schumann et al., 2009; Zhu et al., 2012). In immunofluorescence analysis VP35-3A colocalized with SGs in a manner similar to wildtype (wt) VP35 at low protein expression levels. In contrast to wt VP35, VP35-3A did not inhibit As-induced SG formation. Also, VP35-3A did not form large aggregates, which correlated with SG inhibition in cells expressing wt VP35. A reduced expression of VP35-3A compared to wt VP35 has been reported (Schumann et al., 2009), which might correlate with the inability to inhibit SG formation. This was observed in both SGs containing G3BP-EGFP and SGs containing endogenous eIF3. These results indicate that EBOV exhibits control strategies at the level of SG formation and that the ability to antagonize SG formation depends on the protein expression level of VP35.

Inhibition of SG formation induced by phospho-eIF2α-mediated stress was shown when VP35 was expressed at high levels in the absence of other viral proteins, suggesting that this inhibition process functions in a dose-dependent manner. Inhibition was not observed when VP35 was located in NP-derived inclusions. This indicates that only free VP35 is able to colocalize with SGs and that VP35 is preferentially relocated to viral inclusions. Binding of VP35 to NP is facilitated by the N-terminus, whereas the C-terminus contains the dsRNA-binding and IFN inhibitory domain (IID) (REID et al., 2005). It is conceivable that the N-terminus contains a motif, which interacts with components of SGs when VP35 is not bound to NP but is not accessible after binding of VP35 to NP. Since the majority of VP35 is relocated into the viral inclusions, it is also possible that the amount of free VP35 was not sufficient for the inhibition of SG in cells coexpressing NP.

Similarly, in the presence of NP, VP30 mainly relocated into NP-derived inclusions. However, some colocalization was observed between VP30 and SGs, which also seemed to be dependent on the VP30 expression level. In EBOV infection colocalization of VP30 or VP35 with the G3BP-positive SGs was not detected. It is conceivable that the amount of free VP35 and VP30 in infected cells was too low to be detected. Although SG formation was reduced to a certain level in EBOV-infected cells with As the amount of VP35 expressed in EBOV infection might not be sufficient to completely inhibit phopho-eIF2α-induced SGs. Consequently, G3BP-positive SG formation was

only inhibited in some infected cells, particularly those in which large viral inclusions were observed.

The diffuse appearance of SGs in VP35-expressing cells indicates that key components for SG formation were inhibited. A possible mechanism for the inhibition of SG formation could take place at the level of SG assembly by protein aggregation. As mentioned previously, G3BP is a key component in SG formation due to its self-aggregation and RNA-binding capacity. For poliovirus (PV) it was found that inhibition of SG formation correlated closely to the cleavage of G3BP, which is mediated by the viral proteinase 3C. Cleavage of G3BP separates the G3BP RNA-binding motif from the protein-interaction domains (White et al., 2007). Thus, it is possible that overexpression of VP35 leads to the inhibition of G3BP and accordingly to SG disassembly. If this were the case, a decrease in the number of cells containing SGs would also be detected in the eIF3 antibody staining. The sequestration of G3BP granules within viral inclusions in EBOV-infected cells, which also appeared diffuse in shape, could be a mechanism of EBOV evasion of host antiviral defense (also discussed above).

**Mechanism of VP35 action**

The type I IFN response is crucial for establishing an antiviral state in the host cell and subsequently for activating the adaptive immune response. EBOV encodes several components that inhibit the type I IFN response. VP35 has been shown to antagonize the phosphorylation of PKR, and consequently, the PKR substrate eIF2α was not phosphorylated in cells expressing VP35 (Schumann et al., 2009). The classical activator of PKR is dsRNA, which is produced during viral infections. Activation of PKR mediates the arrest of the host translational machinery and subsequently leads to SG formation.

For influenza A it has been shown that SG formation is actively inhibited by the NS1 protein by blocking PKR activation (Khaperskyy et al., 2011). VP35 and NS1 both play a role in the inhibition of the IFN response and contain similar non-canonical dsRNA-binding domains (Chien et al., 1997; Liu et al., 1997; Leung et al., 2009). VP35 is able to functionally substitute for NS1 in growth complementation assays using an influenza virus mutant lacking NS1 (Basler et al., 2000). The similarities between VP35 and NS1 indicate that VP35 has a similar role in the inhibition of SGs, which has to be further investigated.

*VP35 does not bind to PACT in cells exposed to exogenous stress*

As-induced SG formation was observed in EBOV-infected cells, albeit in fewer cells, indicating that eIF2α may be phosphorylated in these cells. Therefore the phosphorylation status of PKR and its substrate eIF2α was determined during As-induced stress in EBOV-infected cells. Interestingly, phosphorylation of PKR and eIF2α was detected in these cells, suggesting that EBOV is not able to antagonize PKR phosphorylation in cells exposed to As stress. In As-treated cells, phosphorylation of PKR by the cellular protein PACT has been described (Patel and Sen, 1998); (Daher et al., 2009). PACT only binds and activates PKR during cellular stress. Since it has been shown that VP35 is able to bind to PACT in non-stressed cells (Fabozzi et al., 2011), it was hypothesized that VP35 bound to PACT inhibits the binding of PACT to PKR and thereby prevents activation of PKR in EBOV-infected cells and consequently, formation of SGs. In this thesis, the interaction of VP35 and PACT in non-stressed cells was confirmed. In addition, it was shown that

VP35 is not able to bind PACT during As stress. This suggests that binding of VP35 to PACT sequesters PACT from binding to PKR and thereby inhibits PKR activation. However, during phospho-eIF2α-mediated stress induced by As, VP35 loses the ability to bind PACT, leading to the phosphorylation of PKR and its substrate eIF2α, as observed in EBOV-infected cells treated with As. This would further explain the formation of SGs in these cells. Possible mechanisms for the reduced SG formation have been discussed above. As mentioned above, in HIV-1 and rotavirus infection, high levels of phosphorylated eIF2α were detected in response to As treatment despite an inhibition of SGs (Montero et al., 2008; Abrahamyan et al., 2010).

The Us11 protein of herpes simplex virus type 1 is an example of a viral protein that can inhibit the action of PACT on PKR (Peters et al., 2002). Us11 blocks PKR activation by PACT both *in vitro* and *in vivo*. Although Us11 can bind to both PKR and PACT, mutational analyses revealed that the binding of Us11 to PKR, and not to PACT, was essential for its inhibitory action. The binding of Us11 to PKR did not block the binding of PKR to PACT but prevented PKR activation.

PACT contains two domains implicated in dsRNA binding and responsible for the interaction with PKR. The mechanism of how VP35 interacts with PACT, either directly or via a linker protein or RNA, remains to be determined.

Since PACT only activates PKR in certain stress environments (and not through dsRNA), one could assume that infection with EBOV induces cellular stress. Moreover, it is possible that this represents a redundant mechanism of VP35 to ensure PKR inhibition.

**P bodies**

Another important part of the antiviral host stress response is the sequestration and possible degradation of RNAs in PBs, which also form as a result of cellular stress. PBs are closely associated with the RNA interference system and have been suggested to be involved in long-term storage of miRNA-regulated mRNAs (Shih et al., 2011). In non-infected cells, an increased number of DCP1a-mRFP-containing PBs were observed during As-induced stress. In EBOV-infected cells, DCP1a-containing PBs were observed during early stages of infection, but not at later stages. These PBs were localized next to the viral inclusions. Furthermore, DCP1a-positve PBs colocalized with VP35 and the VP35-3A mutant, but not with VP30.

It has been reported that VP35 suppresses the RNAi pathway. This activity depends on an intact dsRNA-binding domain, which is destroyed in the VP35-3A mutant (Haasnoot et al., 2007). In addition, VP35 has been shown to bind siRNA, whereas the VP35-3A mutant was unable to do so (Zhu et al., 2012). Since both, wt VP35 and VP35-3A colocalize with PBs, a miRNA-mediated recruitment of VP35 to PBs does not seem likely. However, it is possible that miRNA-dependent linker proteins are involved in a relocalization of VP35, leading to the observed colocalization of VP35 and PBs. Interestingly, VP35 has been shown to interact with various components of RISC including Dicer, TRBP, and PACT but not Ago2 (Fabozzi et al., 2011) A dynamic movement of Ago2 from SGs to PBs in a micro-RNA-dependent manner was detected by establishing a stably expressing EGFP-Ago2 cell line (Leung et al., 2006). As yet, it is not known if VP35 interacts with Ago2. Another potential interaction partner for VP35 is the PB marker protein RCK/p54, which is involved in miRNA-mediated gene silencing (Chu and Rana, 2006). This protein has been shown to bind to viral RNAs including the genomic 3'UTR and 5'UTR of DV as well as the 5' terminus of

the negative-strand antigenomic RNA of HCV (Ariumi et al., 2011; Ward et al., 2011), Knockdown experiments indicate a role in viral replication for both viruses.

To summarize, the results presented here indicate that EBOV exhibits control strategies at the level of SG formation by sequestering components essential for SG formation, such as G3BP, to evade the antiviral stress response. The virus further inhibits SG formation via expression of VP35, which seems to be a key player in the inhibition of SG formation. VP35 was shown to alter induced SG formation and interact with cellular stress components of SGs and PBs. Furthermore, it was shown to interact with PACT, a cellular activator of PKR.VP35's ability to bind dsRNA is most likely not important for the interaction with SGs and PBs, since VP35-3A, a VP35 mutant which lost the dsRNA binding activity, was observed to colocalize with both.

# 7. References

Abrahamyan, L.G., Chatel-Chaix, L., Ajamian, L., Milev, M.P., Monette, A., Clément, J.-F., Song, R., Lehmann, M., DesGroseillers, L., Laughrea, M., Boccaccio, G., Mouland, A.J., 2010. Novel Staufen1 ribonucleoproteins prevent formation of stress granules but favour encapsidation of HIV-1 genomic RNA. J. Cell. Sci. 123, 369–383.

Andrei, M.A., 2005. A role for eIF4E and eIF4E-transporter in targeting mRNPs to mammalian processing bodies. RNA 11, 717–727.

Ariumi, Y., Kuroki, M., Kushima, Y., Osugi, K., Hijikata, M., Maki, M., Ikeda, M., Kato, N., 2011. Hepatitis C Virus Hijacks P-Body and Stress Granule Components around Lipid Droplets. J Virol 85, 6882–6892.

Atlas, R., Behar, L., Elliott, E., Ginzburg, I., 2004. The insulin-like growth factor mRNA binding-protein IMP-1 and the Ras-regulatory protein G3BP associate with tau mRNA and HuD protein in differentiated P19 neuronal cells. J Neurochem 89, 613–626.

Baize, S., Leroy, E.M., Georges-Courbot, M.C., Capron, M., Lansoud-Soukate, J., Debre, P., Fisher-Hoch, S.P., McCormick, J.B., Georges, A.J., 1999. Defective humoral responses and extensive intravascular apoptosis are associated with fatal outcome in Ebola virus-infected patients. Nat Med 5, 423–426.

Basler, C.F., Mikulasova, A., Martinez-Sobrido, L., Paragas, J., Mühlberger, E., Bray, M., Klenk, H.-D., Palese, P., García-Sastre, A., 2003. The Ebola virus VP35 protein inhibits activation of interferon regulatory factor 3. J Virol 77, 7945–7956.

Basler, C.F., Wang, X., Muhlberger, E., Volchkov, V., Paragas, J., Klenk, H.D., Garcia-Sastre, A., Palese, P., 2000. The Ebola virus VP35 protein functions as a type I IFN antagonist. Proc Natl Acad Sci USA 97, 12289–12294.

Becker, S., Rinne, C., Hofsäss, U., Klenk, H.D., Muhlberger, E., 1998. Interactions of Marburg virus nucleocapsid proteins. Virology 249, 406–417.

Bedard, K.M., Walter, B.L., Semler, B.L., 2004. Multimerization of poly(rC) binding protein 2 is required for translation initiation mediated by a viral IRES. RNA 10, 1266–1276.

Benkirane, M., Neuveut, C., Chun, R.F., Smith, S.M., Samuel, C.E., Gatignol, A., Jeang, K.T., 1997. Oncogenic potential of TAR RNA binding protein TRBP and its regulatory interaction with RNA-dependent protein kinase PKR. EMBO J. 16, 611–624.

Berlanga, J.J., Santoyo, J., De Haro, C., 1999. Characterization of a mammalian homolog of the GCN2 eukaryotic initiation factor 2alpha kinase. Eur J Biochem 265, 754–762.

Berlanga, J.J., Ventoso, I., Harding, H.P., Deng, J., Ron, D., Sonenberg, N., Carrasco, L., de Haro, C., 2006. Antiviral effect of the mammalian translation initiation factor 2alpha kinase GCN2 against RNA viruses. EMBO J. 25, 1730–1740.

Bharat, T.A.M., Noda, T., Riches, J.D., Kraehling, V., Kolesnikova, L., Becker, S., Kawaoka, Y., Briggs, J.A.G., 2012. Structural dissection of Ebola virus and its assembly determinants using cryo-electron tomography. Proceedings of the National Academy of Sciences.

Bharat, T.A.M., Riches, J.D., Kolesnikova, L., Welsch, S., Krähling, V., Davey, N., Parsy, M.-L., Becker, S., Briggs, J.A.G., 2011. Cryo-Electron Tomography of Marburg Virus Particles and Their Morphogenesis within Infected Cells. PLoS Biol 9, e1001196.

Bordeleau, M.-E., Mori, A., Oberer, M., Lindqvist, L., Chard, L.S., Higa, T., Belsham, G.J., Wagner, G., Tanaka, J., Pelletier, J., 2006. Functional characterization of IRESes by an inhibitor of the RNA helicase eIF4A. Nat Chem Biol 2, 213–220.

Bradfute, S.B., Warfield, K.L., Bavari, S., 2008. Functional CD8+ T cell responses in lethal Ebola virus infection. J Immunol 180, 4058–4066.

Brengues, M., Teixeira, D., Parker, R., 2005. Movement of eukaryotic mRNAs between polysomes and cytoplasmic processing bodies. Science 310, 486–489.

Burkhardt, J.K., Echeverri, C.J., Nilsson, T., Vallee, R.B., 1997. Overexpression of the dynamitin (p50) subunit of the dynactin complex disrupts dynein-dependent maintenance of membrane organelle distribution. J Cell Biol 139, 469–484.

Bwaka, M.A., Bonnet, M.J., Calain, P., Colebunders, R., De Roo, A., Guimard, Y., Katwiki, K.R., Kibadi, K., Kipasa, M.A., Kuvula, K.J., Mapanda, B.B., Massamba, M., Mupapa, K.D., Muyembe-Tamfum, J.J., Ndaberey, E., Peters, C.J., Rollin, P.E., Van den Enden, E., Van den Enden, E., 1999. Ebola hemorrhagic fever in Kikwit, Democratic Republic of the Congo: clinical observations in 103 patients. J Infect Dis 179 Suppl 1, S1–7.

Cardenas, W.B., Loo, Y.M., Gale, M., Hartman, A.L., Kimberlin, C.R., Martinez-Sobrido, L., Saphire, E.O., Basler, C.F., 2006. Ebola Virus VP35 Protein Binds Double-Stranded RNA and Inhibits Alpha/Beta Interferon Production Induced by RIG-I Signaling. J Virol 80, 5168–5178.

CDC, DHHS, NIH, 2009. Biosafety in Microbiological and Biomedical Laboratories (BMBL), 5th ed. Washington, D.C.

Chang, T.-H., Kubota, T., Matsuoka, M., Jones, S., Bradfute, S.B., Bray, M., Ozato, K., 2009. Ebola Zaire Virus Blocks Type I Interferon Production by Exploiting the Host SUMO Modification Machinery. PLoS Pathog. 5, e1000493.

Chien, C.Y., Tejero, R., Huang, Y., Zimmerman, D.E., Rios, C.B., Krug, R.M., Montelione, G.T., 1997. A novel RNA-binding motif in influenza A virus non-structural protein 1. Nat Struct Biol 4, 891–895.

Chu, C.-Y., Rana, T.M., 2006. Translation repression in human cells by microRNA-induced gene silencing requires RCK/p54. PLoS Biol 4, e210.

Chudakov, D.M., Matz, M.V., Lukyanov, S., Lukyanov, K.A., 2010. Fluorescent proteins and their applications in imaging living cells and tissues. Physiol Rev 90, 1103–1163.

Cougot, N., van Dijk, E., Babajko, S., Séraphin, B., 2004. “Cap-tabolism.” Trends in Biochemical Sciences 29, 436–444.

Daher, A., Laraki, G., Singh, M., Melendez-Peña, C.E., Bannwarth, S., Peters, A.H.F.M., Meurs, E.F., Braun, R.E., Patel, R.C., Gatignol, A., 2009. TRBP control of PACT-induced phosphorylation of protein kinase R is reversed by stress. Molecular and Cellular Biology 29, 254–265.

Duprex, P., Rima, B., 2011. Using Green Fluorescent Protein to Monitor Measels Virus cell-to-cell spread by time-lapse confocal microscopy 1–11.

Duprex, W.P., McQuaid, S., Hangartner, L., Billeter, M.A., Rima, B.K., 1999. Observation of measles virus cell-to-cell spread in astrocytoma cells by using a green fluorescent protein-expressing recombinant virus. J Virol 73, 9568–9575.

Ebihara, H., Theriault, S., Neumann, G., Alimonti, J.B., Geisbert, J.B., Hensley, L.E., Groseth, A., Jones, S.M., Geisbert, T.W., Kawaoka, Y., Feldmann, H., 2007. In Vitro and In Vivo Characterization of Recombinant Ebola Viruses Expressing Enhanced Green Fluorescent Protein. J Infect Dis 196, S313–S322.

Emara, M.M., Brinton, M.A., 2007. Interaction of TIA-1/TIAR with West Nile and dengue virus products in infected cells interferes with stress granule formation and processing body assembly. Proc Natl Acad Sci USA 104, 9041–9046.

Enterlein, S., Schmidt, K.M., Schümann, M., Conrad, D., Krähling, V., Olejnik, J., Mühlberger, E., 2009. The marburg virus 3' noncoding region structurally and functionally differs from that of ebola virus. J Virol 83, 4508–4519.

Enterlein, S., Volchkov, V., Weik, M., Kolesnikova, L., Volchkova, V., Klenk, H.-D., Mühlberger, E., 2006. Rescue of recombinant Marburg virus from cDNA is dependent on nucleocapsid protein VP30. J Virol 80, 1038–1043.

Eulalio, A., Behm-Ansmant, I., Izaurralde, E., 2007. P bodies: at the crossroads of post-transcriptional pathways. Nature Publishing Group 8, 9–22.

Eystathioy, T., Chan, E.K.L., Tenenbaum, S.A., Keene, J.D., Griffith, K., Fritzler, M.J., 2002. A phosphorylated cytoplasmic autoantigen, GW182, associates with a unique population of human mRNAs within novel cytoplasmic speckles. Mol. Biol. Cell 13, 1338–1351.

Fabozzi, G., Nabel, C.S., Dolan, M.A., Sullivan, N.J., 2011. Ebolavirus Proteins Suppress the Effects of Small Interfering RNA by Direct Interaction with the Mammalian RNA Interference Pathway. J Virol 85, 2512–2523.

Feldmann, H., Geisbert, T.W., 2011. Ebola haemorrhagic fever. The Lancet 377, 849–862.

Feng, Z., Cerveny, M., Yan, Z., He, B., 2006. The VP35 Protein of Ebola Virus Inhibits the Antiviral Effect Mediated by Double-Stranded RNA-Dependent Protein Kinase PKR. J Virol 81, 182–192.

Franks, T.M., Lykke-Andersen, J., 2007. TTP and BRF proteins nucleate processing body formation to silence mRNAs with AU-rich elements. Genes & Development 21, 719–735.

Franks, T.M., Lykke-Andersen, J., 2008. The Control of mRNA Decapping and P-Body Formation. Mol. Cell 32, 605–615.

Fujimura, K., Kano, F., Murata, M., 2008. Identification of PCBP2, a facilitator of IRES-mediated translation, as a novel constituent of stress granules and processing bodies. RNA 14, 425–431.

Gallouzi, I.E., Parker, F., Chebli, K., Maurier, F., Labourier, E., Barlat, I., Capony, J.P., Tocque, B., Tazi, J., 1998. A novel phosphorylation-dependent RNase activity of GAP-SH3 binding protein: a potential link between signal transduction and RNA stability. Molecular and Cellular Biology 18, 3956–3965.

García-Mata, R., Bebök, Z., Sorscher, E.J., Sztul, E.S., 1999. Characterization and dynamics of aggresome formation by a cytosolic GFP-chimera. J Cell Biol 146, 1239–1254.

Geisbert, T.W., Young, H.A., Jahrling, P.B., Davis, K.J., Larsen, T., Kagan, E., Hensley, L.E., 2003. Pathogenesis of Ebola hemorrhagic fever in primate models: evidence that hemorrhage is not a direct effect of virus-induced cytolysis of endothelial cells. Am. J. Pathol. 163, 2371–2382.

Gil, J., Esteban, M., 2000. Induction of apoptosis by the dsRNA-dependent protein kinase (PKR): mechanism of action. Apoptosis 5, 107–114.

Gilks, N., Kedersha, N., Ayodele, M., Shen, L., Stoecklin, G., Dember, L.M., Anderson, P., 2004. Stress granule assembly is mediated by prion-like aggregation of TIA-1. Mol. Biol. Cell 15, 5383–5398.

Goodin, M., Yelton, S., Ghosh, D., Mathews, S., Lesnaw, J., 2005. Live-cell imaging of rhabdovirus-induced morphological changes in plant nuclear membranes. Mol. Plant Microbe Interact. 18, 703–709.

Gradi, A., Svitkin, Y.V., Imataka, H., Sonenberg, N., 1998. Proteolysis of human eukaryotic translation initiation factor eIF4GII, but not eIF4GI, coincides with the shutoff of host protein synthesis after poliovirus infection. Proc Natl Acad Sci USA 95, 11089–11094.

Gupta, V., 2003. The carboxy-terminal, M3 motifs of PACT and TRBP have opposite effects on PKR activity. Virology 315, 283–291.

Haasnoot, J., de Vries, W., Geutjes, E.-J., Prins, M., de Haan, P., Berkhout, B., 2007. The Ebola virus VP35 protein is a suppressor of RNA silencing. PLoS Pathog. 3, e86.

Habjan, M., Andersson, I., Klingström, J., Schümann, M., Martin, A., Zimmermann, P., Wagner, V., Pichlmair, A., Schneider, U., Mühlberger, E., Mirazimi, A., Weber, F., 2008. Processing of Genome 5′ Termini as a Strategy of Negative-Strand RNA Viruses to Avoid RIG-I-Dependent Interferon Induction. PLoS ONE 3, e2032.

Halfmann, P., Kim, J.H., Ebihara, H., Noda, T., Neumann, G., Feldmann, H., Kawaoka, Y., 2008. Generation of biologically contained Ebola viruses. Proceedings of the National Academy of Sciences 105, 1129–1133.

Han, A.P., Yu, C., Lu, L., Fujiwara, Y., Browne, C., Chin, G., Fleming, M., Leboulch, P., Orkin, S.H., Chen, J.J., 2001. Heme-regulated eIF2alpha kinase (HRI) is required for translational regulation and survival of erythroid precursors in iron deficiency. EMBO J. 20, 6909–6918.

Hanley, L.L., McGivern, D.R., Teng, M.N., Djang, R., Collins, P.L., Fearns, R., 2010. Roles of the respiratory syncytial virus trailer region: Effects of mutations on genome production and stress granule formation. Virology 406, 241–252.

Harding, H.P., Novoa, I., Zhang, Y., Zeng, H., Wek, R., Schapira, M., Ron, D., 2000. Regulated translation initiation controls stress-induced gene expression in mammalian cells. Mol. Cell 6, 1099–1108.

Harding, H.P., Zhang, Y., Bertolotti, A., Zeng, H., Ron, D., 2000. Perk is essential for translational regulation and cell survival during the unfolded protein response. Mol. Cell 5, 897–904.

Harding, H.P., Zhang, Y., Ron, D., 1999. Protein translation and folding are coupled by an endoplasmic-reticulum-resident kinase. Nature 397, 271–274.

Hartman, A.L., Towner, J.S., Nichol, S.T., 2004. A C-terminal basic amino acid motif of Zaire ebolavirus VP35 is essential for type I interferon antagonism and displays high identity with the RNA-binding domain of another interferon antagonist, the NS1 protein of influenza A virus. Virology 328, 177–184.

Hierholzer, J., Killington, R., 1996. Virus isolation and quantitation. Virology methods manual.

Himeda, T., Hosomi, T., Asif, N., Shimizu, H., Okuwa, T., Muraki, Y., Ohara, Y., 2011. The preparation of an infectious full-length cDNA clone of Saffold virus. Virology Journal 8, 110.

Hoenen, T., Jung, S., Herwig, A., Groseth, A., Becker, S., 2010. Both matrix proteins of Ebola virus contribute to the regulation of viral genome replication and transcription. Virology 403, 56–66.

Hovanessian, A.G., 1989. The double stranded RNA-activated protein kinase induced by interferon: dsRNA-PK. J Interferon Res 9, 641–647.

Huang, Y., Xu, L., Sun, Y., Nabel, G.J., 2002. The assembly of Ebola virus nucleocapsid requires virion-associated proteins 35 and 24 and posttranslational modification of nucleoprotein. Mol. Cell 10, 307–316.

Imataka, H., Gradi, A., Sonenberg, N., 1998. A newly identified N-terminal amino acid sequence of human eIF4G binds poly(A)-binding protein and functions in poly(A)-dependent translation. EMBO J. 17, 7480–7489.

Jakymiw, A., Lian, S., Eystathioy, T., Li, S., Satoh, M., Hamel, J.C., Fritzler, M.J., Chan, E.K.L., 2005. Disruption of GW bodies impairs mammalian RNA interference. Nat Cell Biol 7, 1167–1174.

John, S.P., Wang, T., Steffen, S., Longhi, S., Schmaljohn, C.S., Jonsson, C.B., 2007. Ebola Virus

VP30 Is an RNA Binding Protein. J Virol 81, 8967–8976.

Kahvejian, A., Svitkin, Y.V., Sukarieh, R., M'Boutchou, M.-N., Sonenberg, N., 2005. Mammalian poly(A)-binding protein is a eukaryotic translation initiation factor, which acts via multiple mechanisms. Genes & Development 19, 104–113.

Kedersha, N., Anderson, P., 2002. Stress granules: sites of mRNA triage that regulate mRNA stability and translatability. Biochem. Soc. Trans. 30, 963–969.

Kedersha, N., Chen, S., Gilks, N., Li, W., Miller, I.J., Stahl, J., Anderson, P., 2002. Evidence that ternary complex (eIF2-GTP-tRNA(i)(Met))-deficient preinitiation complexes are core constituents of mammalian stress granules. Mol. Biol. Cell 13, 195–210.

Kedersha, N., Stoecklin, G., Ayodele, M., Yacono, P., Lykke-Andersen, J., Fritzler, M.J., Scheuner, D., Kaufman, R.J., Golan, D.E., Anderson, P., 2005. Stress granules and processing bodies are dynamically linked sites of mRNP remodeling. J Cell Biol 871–884.

Kedersha, N., Tisdale, S., Hickman, T., Anderson, P., 2008. Chapter 26 - Real-Time and Quantitative Imaging of Mammalian Stress Granules and Processing Bodies. RNA Turnover in Eukaryotes: Nucleases, Pathways and Anaylsis of mRNA Decay 448, 521–552.

Kedersha, N.L., Gupta, M., Li, W., Miller, I., Anderson, P., 1999. RNA-binding proteins TIA-1 and TIAR link the phosphorylation of eIF-2 alpha to the assembly of mammalian stress granules. J Cell Biol 147, 1431–1442.

Khaperskyy, D.A., Hatchette, T.F., McCormick, C., 2011. Influenza A virus inhibits cytoplasmic stress granule formation. The FASEB Journal.

Kok, K.H., Ng, M.-H.J., Ching, Y.-P., Jin, D.-Y., 2007. Human TRBP and PACT directly interact with each other and associate with dicer to facilitate the production of small interfering RNA. J Biol Chem 282, 17649–17657.

Kolesnikova, L., Bohil, A.B., Cheney, R.E., Becker, S., 2007. Budding of Marburgvirus is associated with filopodia. Cell Microbiol 9, 939–951.

Kolesnikova, L., Muhlberger, E., Ryabchikova, E., Becker, S., 2000. Ultrastructural Organization of Recombinant Marburg Virus Nucleoprotein: Comparison with Marburg Virus Inclusions. J Virol 74, 3899–3904.

Kuhn, J.H., Becker, S., Ebihara, H., Geisbert, T.W., Johnson, K.M., Kawaoka, Y., Lipkin, W.I., Negredo, A.I., Netesov, S.V., Nichol, S.T., Palacios, G., Peters, C.J., Tenorio, A., Volchkov, V.E., Jahrling, P.B., 2010. Proposal for a revised taxonomy of the family Filoviridae: classification, names of taxa and viruses, and virus abbreviations. Arch Virol 155, 2083–2103.

Laraki, G., Clerzius, G., Daher, A., Melendez-Peña, C., Daniels, S., Gatignol, A., 2008. Interactions between the double-stranded RNA-binding proteins TRBP and PACT define the Medipal domain that mediates protein-protein interactions. RNA Biol 5, 92–103.

Leung, A.K.L., Calabrese, J.M., Sharp, P.A., 2006. Quantitative analysis of Argonaute protein reveals microRNA-dependent localization to stress granules. Proc Natl Acad Sci USA 103, 18125–18130.

Leung, D.W., Ginder, N.D., Fulton, D.B., Nix, J., Basler, C.F., Honzatko, R.B., Amarasinghe, G.K., 2009. Structure of the Ebola VP35 interferon inhibitory domain. Proceedings of the National Academy of Sciences 106, 411–416.

Li, S., Sen, G.C., 2003. PACT-mediated enhancement of reporter gene expression at the translational level. J. Interferon Cytokine Res. 23, 689–697.

Li, W., Li, Y., Kedersha, N., Anderson, P., Emara, M., Swiderek, K.M., Moreno, G.T., Brinton, M.A., 2002. Cell Proteins TIA-1 and TIAR Interact with the 3' Stem-Loop of the West Nile Virus

Complementary Minus-Strand RNA and Facilitate Virus Replication. J Virol 76, 11989–12000.

Lindquist, M.E., Lifland, A.W., Utley, T.J., Santangelo, P.J., Crowe, J.E., 2010. Respiratory Syncytial Virus Induces Host RNA Stress Granules To Facilitate Viral Replication. J Virol 84, 12274–12284.

Lindquist, M.E., Mainou, B.A., Dermody, T.S., Crowe, J.E., Jr, 2011. Activation of protein kinase R is required for induction of stress granules by respiratory syncytial virus but dispensable for viral replication. Virology 413, 103–110.

Linero, F.N., Thomas, M.G., Boccaccio, G.L., Scolaro, L.A., 2011. Junin virus infection impairs stress-granule formation in Vero cells treated with arsenite via inhibition of eIF2 phosphorylation. Journal of General Virology 92, 2889–2899.

Liu, J., Lynch, P.A., Chien, C.Y., Montelione, G.T., Krug, R.M., Berman, H.M., 1997. Crystal structure of the unique RNA-binding domain of the influenza virus NS1 protein. Nat Struct Biol 4, 896–899.

Liu, S., 2006. Insertion and deletion analyses identify regions of non-structural protein 5A of Hepatitis C virus that are dispensable for viral genome replication. Journal of General Virology 87, 323–327.

Lu, L., Chen, J.J., 2002. Molecular cloning and characterization of the promoter of mouse heme-regulated eIF2alpha kinase. Biochim Biophys Acta 1574, 193–199.

Lyakhov, D.L., He, B., Zhang, X., Studier, F.W., Dunn, J.J., McAllister, W.T., 1998. Pausing and termination by bacteriophage T7 RNA polymerase. Journal of Molecular Biology 280, 201–213.

Maggi, L.B.J., Heitmeier, M.R., Scheuner, D., Kaufman, R.J., Buller, R.M., Corbett, J.A., 2000. Potential role of PKR in double-stranded RNA-induced macrophage activation. EMBO J. 19, 3630–3638.

Martini, G.A., 1973. Marburg virus disease. Postgrad Med J 49, 542–546.

Martini, G.A., Siegert, R., 1971. Marburg Virus Disease. Springer, NewYork.

Martínez, M.J., Biedenkopf, N., Volchkova, V., Hartlieb, B., Alazard-Dany, N., Reynard, O., Becker, S., Volchkov, V., 2008. Role of Ebola virus VP30 in transcription reinitiation. J Virol 82, 12569–12573.

Martínez, M.J., Volchkova, V.A., Raoul, H., Alazard-Dany, N., Reynard, O., Volchkov, V.E., 2011. Role of VP30 phosphorylation in the Ebola virus replication cycle. J Infect Dis 204 Suppl 3, S934–40.

Mateo, M., Carbonnelle, C., Martinez, M.J., Reynard, O., Page, A., Volchkova, V.A., Volchkov, V.E., 2011. Knockdown of Ebola Virus VP24 Impairs Viral Nucleocapsid Assembly and Prevents Virus Replication. J Infect Dis 204, S892–S896.

Matthews, J.D., Frey, T.K., 2011. Analysis of subcellular G3BP redistribution during rubella virus infection. Journal of General Virology.

Mazroui, R., Sukarieh, R., Bordeleau, M.-E., Kaufman, R.J., Northcote, P., Tanaka, J., Gallouzi, I., Pelletier, J., 2006. Inhibition of ribosome recruitment induces stress granule formation independently of eukaryotic initiation factor 2alpha phosphorylation. Mol. Biol. Cell 17, 4212–4219.

McCampbell, A., Taylor, J.P., Taye, A.A., Robitschek, J., Li, M., Walcott, J., Merry, D., Chai, Y., Paulson, H., Sobue, G., Fischbeck, K.H., 2000. CREB-binding protein sequestration by expanded polyglutamine. Human Molecular Genetics 9, 2197–2202.

McEwen, E., 2005. Heme-regulated Inhibitor Kinase-mediated Phosphorylation of Eukaryotic Translation Initiation Factor 2 Inhibits Translation, Induces Stress Granule Formation, and

Mediates Survival upon Arsenite Exposure. Journal of Biological Chemistry 280, 16925–16933.

McInerney, G.M., Kedersha, N.L., Kaufman, R.J., Anderson, P., Liljeström, P., 2005. Importance of eIF2alpha phosphorylation and stress granule assembly in alphavirus translation regulation. Mol. Biol. Cell 16, 3753–3763.

Mellor, H., 2010. The role of formins in filopodia formation. Biochim Biophys Acta 1803, 191–200.

Meurs, E., Chong, K., Galabru, J., Thomas, N.S., Kerr, I.M., Williams, B.R., Hovanessian, A.G., 1990. Molecular cloning and characterization of the human double-stranded RNA-activated protein kinase induced by interferon. Cell 62, 379–390.

Modrof, J., Becker, S., Mühlberger, E., 2003. Ebola virus transcription activator VP30 is a zinc-binding protein. J Virol 77, 3334–3338.

Modrof, J., Mühlberger, E., Klenk, H.-D., Becker, S., 2002. Phosphorylation of VP30 impairs ebola virus transcription. J Biol Chem 277, 33099–33104.

Mollet, S., Cougot, N., Wilczynska, A., Dautry, F., Kress, M., Bertrand, E., Weil, D., 2008. Translationally repressed mRNA transiently cycles through stress granules during stress. Mol. Biol. Cell 19, 4469–4479.

Montero, H., Rojas, M., Arias, C.F., Lopez, S., 2008. Rotavirus Infection Induces the Phosphorylation of eIF2 but Prevents the Formation of Stress Granules. J Virol 82, 1496–1504.

Muhlberger, E., 2004. Genome organization replication and transcription of filoviruses, in: Klenk, H.-D., Feldmann, H. (Eds.), Ebola and Marburg Viruses: Molecular and Cellular Biology. Horizon Bioscience.

Muhlberger, E., Lotfering, B., Klenk, H.D., Becker, S., 1998. Three of the four nucleocapsid proteins of Marburg virus, NP, VP35, and L, are sufficient to mediate replication and transcription of Marburg virus-specific monocistronic minigenomes. J Virol 72, 8756–8764.

Muhlberger, E., Sanchez, A., Randolf, A., Will, C., Kiley, M.P., Klenk, H.D., Feldmann, H., 1992. The nucleotide sequence of the L gene of Marburg virus, a filovirus: homologies with paramyxoviruses and rhabdoviruses. Virology 187, 534–547.

Mühlberger, E., 2007. Filovirus replication and transcription. Future Virol 2, 205–215.

Noda, T., Ebihara, H., Muramoto, Y., Fujii, K., Takada, A., Sagara, H., Kim, J.H., Kida, H., Feldmann, H., Kawaoka, Y., 2006. Assembly and budding of Ebolavirus. PLoS Pathog. 2, 864–872.

Noda, T., Hagiwara, K., Sagara, H., Kawaoka, Y., 2010. Characterization of the Ebola virus nucleoprotein-RNA complex. Journal of General Virology 91, 1478–1483.

Nover, L., Scharf, K.D., Neumann, D., 1983. Formation of cytoplasmic heat shock granules in tomato cell cultures and leaves. Molecular and Cellular Biology 3, 1648–1655.

Nover, L., Scharf, K.D., Neumann, D., 1989. Cytoplasmic heat shock granules are formed from precursor particles and are associated with a specific set of mRNAs. Molecular and Cellular Biology 9, 1298–1308.

Ohn, T., Kedersha, N., Hickman, T., Tisdale, S., Anderson, P., 2008. A functional RNAi screen links O-GlcNAc modification of ribosomal proteins to stress granule and processing body assembly. Nat Cell Biol 10, 1224–1231.

Olejnik, J., Ryabchikova, E., Corley, R.B., Mühlberger, E., 2011. Intracellular events and cell fate in filovirus infection. Viruses 3, 1501–1531.

Parker, F., Maurier, F., Delumeau, I., Duchesne, M., Faucher, D., Debussche, L., Dugue, A., Schweighoffer, F., Tocque, B., 1996. A Ras-GTPase-activating protein SH3-domain-binding protein. Molecular and Cellular Biology 16, 2561–2569.

Patel, C.V., 2000. PACT, a Stress-modulated Cellular Activator of Interferon-induced Double-stranded RNA-activated Protein Kinase, PKR. Journal of Biological Chemistry 275, 37993–37998.

Patel, R.C., Sen, G.C., 1998. PACT, a protein activator of the interferon-induced protein kinase, PKR. EMBO J. 17, 4379–4390.

Peters, G.A., Hartmann, R., Qin, J., Sen, G.C., 2001. Modular structure of PACT: distinct domains for binding and activating PKR. Molecular and Cellular Biology 21, 1908–1920.

Peters, G.A., Khoo, D., Mohr, I., Sen, G.C., 2002. Inhibition of PACT-mediated activation of PKR by the herpes simplex virus type 1 Us11 protein. J Virol 76, 11054–11064.

Peters, G.A., Li, S., Sen, G.C., 2006. Phosphorylation of specific serine residues in the PKR activation domain of PACT is essential for its ability to mediate apoptosis. J Biol Chem 281, 35129–35136.

Prins, K.C., Cardenas, W.B., Basler, C.F., 2009. Ebola Virus Protein VP35 Impairs the Function of Interferon Regulatory Factor-Activating Kinases IKK and TBK-1. J Virol 83, 3069–3077.

Qin, Q., Hastings, C., Miller, C.L., 2009. Mammalian Orthoreovirus Particles Induce and Are Recruited into Stress Granules at Early Times Postinfection. J Virol 83, 11090–11101.

Ramanan, P., Shabman, R.S., Brown, C.S., Amarasinghe, G.K., Basler, C.F., Leung, D.W., 2011. Filoviral Immune Evasion Mechanisms. Viruses 3, 1634–1649.

REID, S., CARDENAS, W., BASLER, C., 2005. Homo-oligomerization facilitates the interferon-antagonist activity of the ebolavirus VP35 protein. Virology 341, 179–189.

Rogers, G.W.J., Komar, A.A., Merrick, W.C., 2002. eIF4A: the godfather of the DEAD box helicases. Prog Nucleic Acid Res Mol Biol 72, 307–331.

Ryabchikova, E., Kolesnikova, L., Smolina, M., Tkachev, V., Pereboeva, L., Baranova, S., Grazhdantseva, A., Rassadkin, Y., 1996. Ebola virus infection in guinea pigs: presumable role of granulomatous inflammation in pathogenesis. Arch Virol 141, 909–921.

Ryabchikova, E., Price, B.B.S., 2004. Ebola and Marburg Viruses: A view of Infection Using Electron Microscopy.

Sanchez, A., Kiley, M.P., Klenk, H.D., Feldmann, H., 1992. Sequence analysis of the Marburg virus nucleoprotein gene: comparison to Ebola virus and other non-segmented negative-strand RNA viruses. J. Gen. Virol. 73 ( Pt 2), 347–357.

Schmidt, K.M., Schümann, M., Olejnik, J., Krähling, V., Mühlberger, E., 2011. Recombinant Marburg virus expressing EGFP allows rapid screening of virus growth and real-time visualization of virus spread. J Infect Dis 204 Suppl 3, S861–70.

Schumann, M., Gantke, T., Muhlberger, E., 2009. Ebola Virus VP35 Antagonizes PKR Activity through Its C-Terminal Interferon Inhibitory Domain. J Virol 83, 8993–8997.

Shaner, N.C., Campbell, R.E., Steinbach, P.A., Giepmans, B.N.G., Palmer, A.E., Tsien, R.Y., 2004. Improved monomeric red, orange and yellow fluorescent proteins derived from Discosoma sp. red fluorescent protein. Nat Biotechnol 22, 1567–1572.

Sheth, U., Parker, R., 2003. Decapping and decay of messenger RNA occur in cytoplasmic processing bodies. Science 300, 805–808.

Sheth, U., Parker, R., 2006. Targeting of aberrant mRNAs to cytoplasmic processing bodies. Cell

125, 1095–1109.

Shi, Y., Vattem, K.M., Sood, R., An, J., Liang, J., Stramm, L., Wek, R.C., 1998. Identification and characterization of pancreatic eukaryotic initiation factor 2 alpha-subunit kinase, PEK, involved in translational control. Molecular and Cellular Biology 18, 7499–7509.

Shih, J.D., Waks, Z., Kedersha, N., Silver, P.A., 2011. Visualization of single mRNAs reveals temporal association of proteins with microRNA-regulated mRNA. Nucleic Acids Res. 39, 7740–7749.

Singh, M., Castillo, D., Patel, C.V., Patel, R.C., 2011. Stress-induced phosphorylation of PACT reduces its interaction with TRBP and leads to PKR activation. Biochemistry 50, 4550–4560.

Slenczka, W.G., 1999. The Marburg virus outbreak of 1967 and subsequent episodes. Curr Top Microbiol Immunol 235, 49–75.

Souquere, S., Mollet, S., Kress, M., Dautry, F., Pierron, G., Weil, D., 2009. Unravelling the ultrastructure of stress granules and associated P-bodies in human cells. J. Cell. Sci. 122, 3619–3626.

Srivastava, S.P., Kumar, K.U., Kaufman, R.J., 1998. Phosphorylation of eukaryotic translation initiation factor 2 mediates apoptosis in response to activation of the double-stranded RNA-dependent protein kinase. J Biol Chem 273, 2416–2423.

Tarun, S.Z.J., Sachs, A.B., 1996. Association of the yeast poly(A) tail binding protein with translation initiation factor eIF-4G. EMBO J. 15, 7168–7177.

Teixeira, D., Sheth, U., Valencia-Sanchez, M.A., Brengues, M., Parker, R., 2005. Processing bodies require RNA for assembly and contain nontranslating mRNAs. RNA 11, 371–382.

Tourrière, H., 2003. The RasGAP-associated endoribonuclease G3BP assembles stress granules. J Cell Biol 160, 823–831.

Tourrière, H., Gallouzi, I.E., Chebli, K., Capony, J.P., Mouaikel, J., van der Geer, P., Tazi, J., 2001. RasGAP-associated endoribonuclease G3Bp: selective RNA degradation and phosphorylation-dependent localization. Molecular and Cellular Biology 21, 7747–7760.

Towner, J.S., Paragas, J., Dover, J.E., Gupta, M., Goldsmith, C.S., Huggins, J.W., Nichol, S.T., 2005. Generation of eGFP expressing recombinant Zaire ebolavirus for analysis of early pathogenesis events and high-throughput antiviral drug screening. Virology 332, 20–27.

Towner, J.S., Rollin, P.E., Bausch, D.G., Sanchez, A., Crary, S.M., Vincent, M., Lee, W.F., Spiropoulou, C.F., Ksiazek, T.G., Lukwiya, M., Kaducu, F., Downing, R., Nichol, S.T., 2004. Rapid diagnosis of Ebola hemorrhagic fever by reverse transcription-PCR in an outbreak setting and assessment of patient viral load as a predictor of outcome. J Virol 78, 4330–4341.

Towner, J.S., Sealy, T.K., Khristova, M.L., Albarino, C.G., Conlan, S., Reeder, S.A., Quan, P.-L., Lipkin, W.I., Downing, R., Tappero, J.W., Okware, S., Lutwama, J., Bakamutumaho, B., Kayiwa, J., Comer, J.A., Rollin, P.E., Ksiazek, T.G., Nichol, S.T., 2008. Newly Discovered Ebola Virus Associated with Hemorrhagic Fever Outbreak in Uganda. PLoS Pathog. 4, e1000212.

Valmas, C., Grosch, M.N., Schümann, M., Olejnik, J., Martinez, O., Best, S.M., Krähling, V., Basler, C.F., Mühlberger, E., 2010. Marburg Virus Evades Interferon Responses by a Mechanism Distinct from Ebola Virus. PLoS Pathog. 6, e1000721.

van Hoof, A., Parker, R., 1999. The exosome: a proteasome for RNA? Cell 99, 347–350.

Ward, A.M., Bidet, K., Yinglin, A., Ler, S.G., Hogue, K., Blackstock, W., Gunaratne, J., Garcia-Blanco, M.A., 2011. Quantitative mass spectrometry of DENV-2 RNA-interacting proteins reveals that the DEAD-box RNA helicase DDX6 binds the DB1 and DB2 3' UTR structures.

RNA Biol 8, 1173–1186.

Watanabe, S., Noda, T., Halfmann, P., Jasenosky, L., Kawaoka, Y., 2007. Ebola virus (EBOV) VP24 inhibits transcription and replication of the EBOV genome. J Infect Dis 196 Suppl 2, S284–90.

Weik, M., Modrof, J., Klenk, H.-D., Becker, S., Mühlberger, E., 2002. Ebola virus VP30-mediated transcription is regulated by RNA secondary structure formation. J Virol 76, 8532–8539.

Wek, R.C., Jiang, H.-Y., Anthony, T.G., 2006. Coping with stress: eIF2 kinases and translational control. Biochem. Soc. Trans. 34, 7–11.

White, J.P., Cardenas, A.M., Marissen, W.E., Lloyd, R.E., 2007. Inhibition of Cytoplasmic mRNA Stress Granule Formation by a Viral Proteinase. Cell Host Microbe 2, 295–305.

Wilczynska, A., 2005. The translational regulator CPEB1 provides a link between dcp1 bodies and stress granules. J. Cell. Sci. 118, 981–992.

Williams, B.R., 1999. PKR; a sentinel kinase for cellular stress. Oncogene 18, 6112–6120.

Williams, B.R., 2001. Signal integration via PKR. Sci. STKE 2001, re2.

Yang, W.H., 2006. RNA-associated protein 55 (RAP55) localizes to mRNA processing bodies and stress granules. RNA 12, 547–554.

Yang, W.H., Bloch, D.B., 2007. Probing the mRNA processing body using protein macroarrays and “autoantigenomics.” RNA 13, 704–712.

Yang, Z., 2004. GW182 is critical for the stability of GW bodies expressed during the cell cycle and cell proliferation. J. Cell. Sci. 117, 5567–5578.

Yi, Z., Pan, T., Wu, X., Song, W., Wang, S., Xu, Y., Rice, C.M., MacDonald, M.R., Yuan, Z., 2011. Hepatitis C Virus Co-Opts Ras-GTPase-Activating Protein-Binding Protein 1 for Its Genome Replication. J Virol 85, 6996–7004.

Zhou, C., Arslan, F., Wee, S., Krishnan, S., Ivanov, A.R., Oliva, A., Leatherwood, J., Wolf, D.A., 2005. PCI proteins eIF3e and eIF3m define distinct translation initiation factor 3 complexes. BMC Biol 3, 14.

Zhu, Y., Celebi Cherukuri, N., Jackel, J.N., Wu, Z., Crary, M., Buckley, K.J., Bisaro, D.M., Parris, D.S., 2012. Characterization of the RNA Silencing Suppression Activity of the Ebola Virus VP35 Protein in Plants and Mammalian Cells. J Virol.

# Curriculum vitae


| | |
|---|---|
| Name | Kristina Maria Schmidt |
| Affiliation | Boston University School of Medicine<br>Department of Microbiology<br>72 East Concord street<br>Boston, MA 02118 |
| Phone | 617-638-0337 |
| E-mail | schmidtk@bu.edu |


## SCIENTIFIC EDUCATION

| | |
|---|---|
| *Since 08/ 2008* | Boston University, Boston, USA<br>Continuation of PhD work at Boston University |
| *06/ 2007 - current* | PhD student<br><br>Institute of Virology, Philipps University of Marburg, Germany<br>and<br>Department of Microbiology<br>Boston University School of Medicine, MA<br>Supervisor: Elke Mühlberger, Associate Professor |
| *01/ 2006 – 10/ 2006* | Diploma thesis (equivalent to MSc thesis)<br>“The genomic promoter structure of Ebola and Marburg virus“,<br>Institute of Virology, Philipps University of Marburg, Germany<br>Supervisor: Elke Mühlberger, PD, Dr. |
| *10/ 2001 –10/ 2006* | Diploma in Biology (equivalent to MSc)<br>Majors: Virology, Parasitology, Animal Physiology, Medical Microbiology<br>Philipps University of Marburg, Germany |
| *08/ 1999 – 07/ 2001* | Vocational training,<br>Biological laboratory technician,<br>Vocational College Cologne |

## RESEARCH EXPERIENCE

| | |
|---|---|
| *03/2010 - current* | Special Volunteer<br>Laboratory of Virology, Division of Intermural Research, Rocky Mountain Laboratories, NIAID, NIH<br>Complete training and practical experience in Biosafety Level (BSL) 4, in cooperation with the "National Infectious Diseases Laboratories (NEIDL)" of Boston University<br>Supervisor: Heinz Feldmann, M.D., PhD, Chief |
| *02/ 2007 – 05/ 2007* | Internship, Department of Special Pathogens, Canadian Science Centre for Human and Animal Health, Winnipeg (Manitoba), Canada<br>Supervisor: Heinz Feldmann, M.D., PhD, Chief |
| *11/ 2005 – 02/ 2006* | Research student,<br>Replication and transcription of filoviruses<br>Institute of Cytophatology,<br>Faculty of Medicine, Marburg, Germany |
| *10/ 2002 – 01/ 2003* | Research student,<br>Institute of Developmental Biology<br>Prof. Dr. Renkawitz-Pohl,<br>Faculty of Biology, Marburg, Germany |
| *04/ 2000 – 05/ 2000* | Internship, Biotechnical Microbiology<br>Department of Pharma Operations<br>Bayer AG, Wuppertal |

## PUBLICATIONS

**Schmidt, K. M**., Schümann, M., Olejnik, J., Krähling, V. and Mühlberger, E. (2011) Recombinant Marburg virus expressing EGFP allows rapid screening of virus growth and real time visualization of virus spread. *J Infect Dis* 204 Suppl 3, S861-70

Enterlein, S., **Schmidt, K. M**., Schümann, M., Conrad, D., Krähling, V., Olejnik, J. and Mühlberger, E. (2009) The Marburg virus 3' non-coding region structurally and functionally differs from Ebola virus. *J Virol*. 83, 4508-4519

## ACADEMIC HONORS

| | |
|---|---|
| *06/2010* | FAZIT travel award for the “Negative Strand Viruses (NSV)” conference, Bruges, Belgium |
| *07/2011* | ASV travel award for the American Society of Virology (ASV) meeting, Minneapolis, Minnesota |
| *08/ 2007 – 07/2010* | PhD student scholarship, Jürgen-Manchot foundation, Düsseldorf, Germany |
| *07/2009* | ASV travel award for the American Society of Virology (ASV) meeting, Vancouver, Canada |
| *06/ 2007 – 07/ 2007* | PhD student scholarship, University of Marburg, Marburg |

## LANGUAGES

| | |
|---|---|
| German | First language |
| English | Advanced fluent |
| French | Basic |

Kristina Schmidt Marburg, 30.04.2012